The Selection of DNA Aptamers for the Prevention of Alpha-Synuclein Aggregation as a Therapeutic Tool in Parkinson's Disease

by

Joshua P. Callahan

A thesis submitted to the Faculty of Graduate and Postdoctoral Affairs
in partial fulfillment of the requirements for the degree of

Master of Science

in

Chemistry

Carleton University

Ottawa, Ontario

Abstract

Parkinson's disease is among the most common neurodegenerative disorders with a global rate of incidence of about 17 per 100,000 person-years. While Parkinson's disease research and treatment options continue to grow, there remain many unanswered questions and unexplored potential therapeutics. The addition of improved preventative therapeutic options could greatly benefit the current arsenal of clinical treatments. One proposed mechanism for potential therapeutics has been the prevention of the aggregation of alpha-synuclein. Alpha-synuclein misfolding and aggregation are considered hallmarks for the progression of Parkinson's disease. Aptamer based treatments could be well suited to this application. Aptamers are single stranded oligonucleotides which bind to a specific chemical target with high affinity and specificity. Aptamers have demonstrated their capacity to inhibit the aggregation of proteins implicated in other neurogenerative disorders. Aptamer sequences are discovered through a process known as SELEX (the systematic evolution of ligands by exponential enrichment). Here, starting pools of aptamer candidates are derived from a 2010 SELEX by Tsukakoshi et al. in which aptamers were selected for affinity towards alpha-synuclein. These pools, coupled with a novel SELEX method which employs the aggregation of alpha-synuclein, has yielded promising results towards the use of aptamers for the prevention of alpha-synuclein aggregation. Based on the combination of sequencing data, the probability of forming a G-quadruplex structure, and preliminary *in vitro* aggregation prevention assays, the aptamer ASYN2 has been selected as an introductory candidate for *in vivo* testing. Comparisons of sequence distributions among various SELEX pool by MiSeq sequencing has revealed that ASYN2 likely holds the capacity to inhibit alpha-synuclein aggregation. G-quadruplex secondary structure prediction software predicted a strong possibility of G-quadruplex formation within ASYN2. Within a preliminary *in vitro* alpha-synuclein aggregation inhibition assay,

ASYN2 out-performed the other candidates and the established M5-15 aptamer by producing the smallest set of alpha-synuclein morphologies with the smallest diversity in sizes.

Acknowledgements

I would like to start by sincerely thanking my thesis supervisor and long time science idol, Dr. Maria DeRosa. As a teenager out of high school without much direction, I remember reading though several of your lab group's publications and finding my interest in chemistry and bionanotechnology there. Without your work, I never would have entered into chemistry, and would probably be an engineer today. Words cannot express my gratitude. When as an undergraduate you accepted me into your lab, you made my four years infinitely more rewarding. You found the perfect project for me to take on, combining my interests in a way far better than anything I could have imagined. When to my surprise, you took me on as a Master's student, it was undoubtedly the single greatest achievement of my academic carrier before today. For my Master's degree, you once again handed me a perfect project and it has been unbelievably rewarding. I know my words reflect the entire lab group's sentiment when I say that you truly are a perfect role model and mentor. Your patience, knowledge, and determination are often awe inspiring.

Next, I would like to thank my long-time mentor, lab partner, and constant source of motivation, Dr. Erin McConnell. You have single-handedly taught me more practical lab knowledge than the rest of my education combined. Your contribution to all of my work, this project, and this thesis cannot be overstated. Your determination, selflessness, and ability to solve any problem have inspired and changed me over the past three years. Your work ethic is second to none, and after three years of trying, I am still unable to keep up. You are truly an irreplaceable part of the DeRosa lab, and I cannot thank you enough for all that you have done for me.

To all the members of the DeRosa lab I would like to express my appreciation. You have all been unbelievably welcoming and accommodating. To our PhD candidates Emily, Eman, Annamaria, Christopher, Phepa, and Selvan, I would like to especially thank all of you. You have all contributed your

knowledge, insight, and help to this project in one way or another. Since the day, I started in the lab, you have all been both great friends and colleagues. To our older generation of Master's students McKenzie, Dan, and Dylan, I would like to thank you all for being such great friends and some of the most interesting people I know. Between Dylan's knitting, Dan's hunting, and McKenzie's cats, this degree was made much more fun by going through it with you all. You are all so talented, and I'm proud to be your peer. To our newer generation of Master's students, I wish you the best in all your DeRosa lab endeavors. May your aptamers bind and your assays work the first time. To Vernon and Louis, I want to thank you two especially for taking on this project where I leave off. It may not be the easiest project, but I promise it is especially rewarding. With you two watching over the project I am sure our aptamer payloads will reach their destination. I would also like to give special thanks to Dr. Velu and Nana, whose contributions to my other project helped me pursue my passion with this one.

Within the Carleton community I would like to acknowledge and thank the staff and faculty of the Chemistry Department. Special thanks to Chantelle for helping navigate this degree, to Natalie and Mastaneh for being the best lab coordinators, and to JJ and Carlos for helping us handle an endless supply of TEM and mass spectroscopy samples. I would also like to thank my teachers in both the Chemistry and Neuroscience departments who made learning some of the hardest disciplines easy.

I would like to offer a very special thank you to my thesis committee of Dr. Chee and Dr. Willmore who also put a great deal of time and effort into helping me with ultracentrifugation. The great effort you both put in made the defence of this thesis a fond memory for me.

I owe a great deal of gratitude to my family and friends who made this Master's degree possible. To my parents whose boundless effort and commitment ensured I could not fail, I owe you much more than my thanks. To my aunt Liz, I want to acknowledge just how much your struggle served as a driving

force and my daily determination to succeed with this project. The late nights were made easy by the idea that I had an opportunity to make some real difference.

To my best friends Charles, Ermanno, Kostya, and Jori I want to thank you all for always being there when I needed a chaperone during the many late nights that went into this project. I really appreciate the time you took to help me keep going in the lab after everyone else had gone home. A special thanks to Jori who was the witness to the longest lab night I ever took on.

To my girlfriend Emilie, I cannot thank you enough for always being there to keep me going, and for encouraging me when I needed it most. You have helped keep me sane and healthy through what have been some of the hardest years of my life and I thank you for each day.

And finally, I would like to thank the Michael J. Fox Foundation for Parkinson's Research which contributed vital funding towards this project. Hopefully this backing and partnership can be extended towards the future work of this ongoing project.

Table of Contents

List of Figures

List of Tables

List of Abbreviations

A: adenine

AADC: aromatic amino acid decarboxylase

AD: Alzheimer's disease

Aβ: amyloid beta

BBB: blood brain barrier

C: cytosine

CaM: calmodulin

CPG: controlled pore glass

DBS: deep brain stimulation

EDS: energy dispersive spectroscopy

G: guanine

HD: Huntington's disease

LAS: lysosomal autophagy system

L-Dopa: levodopa

MAOB: Monoamine oxidase type B

mHTT: mutant variant of the huntingtin protein

MRI: magnetic resonance imaging

NSF: N-ethylmaleimide sensitive fusion protein

PAGE: poly acrylamide gel electrophoresis

PCR: polymerase chain reaction

PEG: polyethylene glycol

PET: positron emission tomography

PHAC: The Public Health Agency of Canada

POHEM: population health model

PrPC: normal cellular prion protein subtype

PrPSC: abnormal cellular prion protein subtype

SDD: elemental silicon drift detector

SNARE: soluble NSF attachment protein receptor

TAN I: tanshinone I

TAN IIA: tashinone IIA

TBE: tris(hyrdroxymethyl)aminomethane, boric acid, ethylenediaminetetraacetic acid

TEM: transmission electron microscopy

TEMED: tetramethylethylenediamine

TSE: transmissible spongiform encephalopathies

VTA: ventral tegmental area

1 Introduction

1.1 What is Parkinson's Disease?

Parkinson's disease is most commonly known by its effects over a patient's motor coordination. These effects result in a series of motor-related symptoms that include resting tremors, bradykinesia, disorders of gait and balance, and muscular rigidity.[1] It has also been noted that these primary motor symptoms often express themselves in less obvious ways, such as the apparent dulling of a patient's facial expressions, a stooped posture, speech problems, difficulty swallowing, sexual dysfunction, and micrographia.[1]

In the time since its original observation by James Parkinson, a series of non-motor related symptoms have also been identified and studied. The non-motor symptoms of Parkinson's disease include many of those associated with the central nervous system. These symptoms include cognitive defects such as impaired memory retrieval, dementia, hallucinosis, depression, disorders in sleep patterns, and hyposmia. Other symptoms are more related to the autonomic nervous system and include orthostatic hypotension, constipation, urogenital dysfunction, and hyperhidrosis. These symptoms can vary dramatically form one patient from the next, and the emergence of many of the symptoms are linked to the further progression of the illness. While less used as a diagnostic tool, the non-motor symptoms of Parkinson's disease can appear prior to the onset of motor symptoms in some cases.[1]

1.1.1 Implications to quality of life

In recent years, it has been recognised through patient reports that a great deal of the quality of life impedances for those suffering with the illness have drawn from the non-motor related symptoms of the disease. Of these symptoms, it has been reported that depression, postural instability, and cognitive

impairment have the greatest influence.[2,3,4] This is partly an effect of the relative advances made in the treatment of the primary motor related symptoms. Moving forward, administration of medication to mitigate the effects of non-motor related symptoms will likely become more common place as these symptoms are better understood and their prevalence is better tracked.[5]

1.2 Disease Incidence and Global Implications

While the numbers often vary between studies, due in part to non-unified diagnostic criteria, it has been shown that the global rate for the incidence for Parkinson's disease is about 17 per 100,000 person-years.[6] In males over the age of 40, we see an incidence rate of about 61 per 100,000 person-years, while females over 40 produce a rate of about 38 per 100,000 person-years.[7] These rates jump to 258 and 103 respectively for populations over the age of 80, making age the greatest risk factor towards the development of Parkinson's disease.[7] A 2013 study which looked at the 5 most populous European countries coupled with the 10 most globally populous countries has estimated that the total number of individuals above the age of 50 with Parkinson's disease within these countries was between 4.1 and 4.6 million in 2005. The study also predicted that this number would grow dramatically by the year 2030 to between 8.7 and 9.3 million.[8]

Statistics Canada via a self report survey indicated a prevalence of about 0.2% among the household population in 2011.[9] Another analysis by Statistics Canada assumed an incidence rate at 60 per 100,000 person-years and modeled, by POHEM (Population Health Model by Statistics Canada), the increase in patients over the next twenty years accounting for the aging population. The results indicated that by the year 2021, the incidence would increase to 70 per 100,000 and to 90 per 100,000 by 2031 (with respect to the assumed 60 per 100,000 person-years starting point). This predicts that the number of patients would increase from the 10,400 in 2011 to 18,600 in 2031.[4]

The Public health Agency of Canada (PHAC) estimated that between the years 2000-2001, the direct cost of Parkinson's disease to Canada was estimated to be $202 million CAD, with an additional indirect cost of $245 million CAD.[10] Of Canadians with Parkinson's disease between the ages of 18 and 64, only 17% held jobs, while 42% were not currently employed, and 41% reported being permanently unable to work (2011-2012).[4]

1.3 A Brief History of Parkinson's Disease and Alpha-Synuclein

James Parkinson first identified the set of motor symptoms which has collectively come to be known as Parkinson's Disease, in an 1817 publication titled "An Essay on the Shaking Palsy". In 1919, the distinct loss of pigment of the substantia nigra as well as the spread of Lewy bodies around the brainstem was discovered by K. Tretiakoff.[1] Lewy bodies are now known to be large aggregates of protein associated with alpha-synuclein aggregation.[11] Next, several important discoveries were made about the chemical nature of the disease.[1]

Notably, the neurotransmitter dopamine was discovered, and in particular its abundance in the striatum was noted.[1] It was then discovered that those suffering from Parkinson's disease had reduced levels of dopamine, and that the introduction of levodopa (the natural dopamine precursor, L-3,4-dihydroxyphenylalanine) served to increase its levels. It wasn't until 1970 that over a century of work was able to produce L-Dopa (levodopa) as a treatment for patients.[1]

Alpha-synuclein was not discovered until Goedert and Spillantini of Cambridge characterized two proteins (alpha-synuclein and beta-synuclein) fortuitously labeled by the anti-tau antibody 11.57. In 1997, alpha-synuclein was finally implicated when it was shown that in the brains of Parkinson's patients the Lewy bodies formed were very immunoreactive for alpha-synuclein.[12]

1.4 Structural Significance of Alpha-Synuclein

The amino acid sequence of alpha-synuclein is determined to be MDVFMKGLSKAKEGVVAAAEKTKQGVAEAAGKTKEGVLYVGSKTKEGVVHGVATVAEKTKEQVTNVGGAVVTGVTAVAQKTVEGAGSIAAATGFKKKDQLGKNEEGAPQEGILEDMPVDPDNEAYEMPSEEGYQDYEPEA.[13] Alpha-synuclein is transcribed from the gene locus Chromosome 4 SNCA.[14]

At its N-terminal (residues 1-87), alpha-synuclein possesses seven repetitions of an 11-residue sequence, which is understood to form an amphipathic alpha-helix. This sequence is a highly conserved KTKEGV hexameric motif.[15] It has been noted that all known mutant human forms of the protein possess their deviations within this N-terminal domain. These repetitions generate a three-turn helix and supports the protein's capacity to interact directly with a membrane's surface at multiple helical sites. The native structure and function of the alpha-synuclein protein is not well understood. In fact, conflicting theories exist in the literature. Work has shown that *in vitro*, pure alpha-synuclein exists in a natively unfolded state. However, there is some literature to suggest that this is a product of denaturation steps which occur during purification, and is not representative of the structure native to recombinant production by bacteria or that which exists in the human brain. Interestingly, unfolded alpha-synuclein, when introduced to artificial membranes, has been shown to undergo a structure switch to an alpha-helix to accommodate membrane binding.[16]

The core domain of alpha-synuclein (residues 61-95) is referred to as the amyloid-binding central domain. It is this domain that is strongly associated with the capacity for alpha-synuclein to aggregate and form more structured amyloid and fibril morphologies. This capacity has been recognized as a function of the domain's capacity to form cross beta-structures.[15]

The C-terminal of alpha-synuclein (residues 96-140) contains 10 Glu and 5 Asp residues resulting in the formation of an acidic random coil structure due to low hydrophobicity and high net negative charge.[15]

Due to studies *in vitro* which showed enhanced aggregation rates of alpha-synuclein in systems with lower pH, it is theorized that the C-terminal might be responsible for aiding the prevention of aggregation *in vivo*. The reduced pH could serve to neutralize the net negative charge of the coil and impede the C-terminal's regulatory interaction with the core domain. The core domain when uninhibited assumes a low energy "pro-aggregation" (cross beta) structure. The necessity of this inhibitory interaction was further studied when Al^{3+} was shown to generate enhanced aggregation in the system through binding to the C-terminal. This effect has also been shown when researchers dephosphorylated the residue serine 129 of the C-terminal and noted enhanced aggregation.[15]

1.5 Alpha-Synuclein's Intended Function in the Brain

While the intended neuronal function of alpha-synuclein is still under review, researchers have produced several strong theories. From what is known, in the brains of healthy individuals, the proper function and degradation of alpha synuclein is in part overseen by the lysosomal autophagy system (LAS) and in part by the ubiquitin-proteasome system.[17] It should be noted that the unique sequences of amino acids found within alpha-synuclein have only been detected within vertebrates. Organisms such as flies, worms and yeast possess no homologues for the protein, indicating that the protein's function does not appear universally fundamental to systems like synaptic transmission or membrane trafficking.[16] One studied function of alpha-synuclein is its capacity to supress the apoptosis mechanism of kinase C which is often triggered by oxidative stress in dopaminergic neurons.[18] Evidence indicates that alpha-synuclein produces this effect by down regulating the expression of kinase C. It has been demonstrated that alpha-synuclein monomer has potent functions which prevent apoptosis when

presented with an oxidative stressor (peroxide for example). However, the underlying mechanism is still under debate .[15]

There is some evidence to indicate that alpha-synuclein may play a role in glucose regulation. It has been shown that in pancreatic beta-cells, alpha-synuclein interacts with KATP channels of insulin-secretory granules and inhibits insulin release.[19]

A 2003 study showed that by interacting with alpha-synuclein, calmodulin (CaM) shifts its function from an inhibitor to an activator for G-protein-coupled receptor kinase 5 to which synucleins are substrates. This study also suggested that the introduction of Ca^{2+} to an alpha-synuclein-CaM system induces fibrillation.[20] CaM is a messenger protein activated by Ca^{2+}.[15]

The role of alpha-synuclein as a presynaptic exocytosis aid has been well studied. On-membrane binding, alpha-synuclein has been shown to multimerize and mediate the assembly of the “soluble NSF (N-ethylmaleimide sensitive fusion protein) attachment protein receptor” (SNARE) complex.[21]

Alpha-synuclein has also been shown to have a high affinity for lipid bilayers and readily binds to small vesicles. Through this affinity, alpha-synuclein has been shown to generate an inhibitory effect over the volume and speed at which vesicles function in the presynaptic area.[22] In dopaminergic cells, alpha-synuclein has also been a shown to function as an indirect down regulator for dopamine production via an interaction with protein phosphatase 2A.[23]

Alpha-synuclein has been shown to function as a molecular chaperone in that it helps to stabilize other proteins as they form correct structures, as well as to help correct the structure of those that are incorrectly folded.[24] In a related manner, Alpha-synuclein has been shown to modulate the function of the acyl-coA-6 isoform responsible for incorporating arachidonic acid (a n-6 fatty acid) into phospholipids. Through this it in fact may influence the polyunsaturated fatty acid (PUFA) levels in the brain. The incorporation of PUFAs into the membrane is vital to membrane permeability and fluidity.[25]

1.6 Mechanism of Alpha-Synuclein Aggregation

The formation of large protein aggregates highly composed of alpha-synuclein (Lewy bodies) is considered universal among all patients with Parkinson's disease.[1] Alpha-synuclein's aggregation is deemed primarily to be the product of misfolding. Once the misfolded protein reaches a critical concentration, the initial oligomerization events can occur (also referred to as seed nucleation). This is quickly followed by the growth phase during which the oligomer continually acquires misfolded monomeric protein and grows in size. This stage brings seeds to form prefibrillar amyloid structures and in turn full amyloid fibrils. It should be noted that, this stage can in some cases end with the formation of prefibrillar oligomers which do not further progress. It is believed that from the formation of full fibrils, interaction and amassing of other neighboring protein structures take place to form what is known as Lewy bodies. Alternatively, amyloid fibrils can fragment, producing more seeds for fibrilization.[26] This is noted as the reversibility of the amyloid fibril formation presented in Figure 1.

The presence of Lewy bodies typically begins in the cholinergic and monoaminergic neurons of the brainstem as well as within neurons of the olfactory system. Later with disease progression, these Lewy bodies begin to appear in the limbic and neocortical regions.[27]

1.7 Mechanism of Dopaminergic Decay and Alpha-Synuclein Toxicity

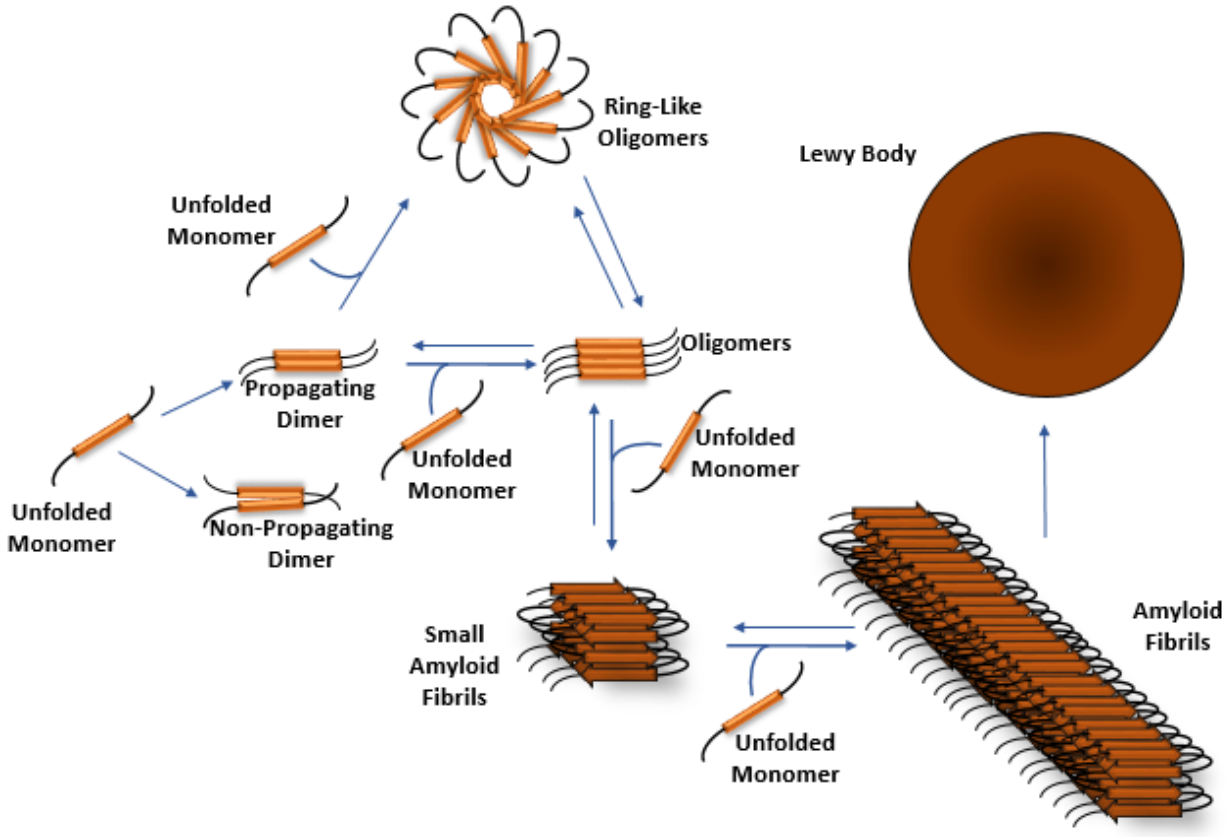

Figure 1. Propagation of alpha-synuclein aggregation. While Lewy bodies and amyloid plaques are often characterized as accumulation alpha-synuclein, they can be made up of, in varying proportions, other aggregating proteins such as amyloid beta.[81,1]

Despite a growing number of theories and findings the prevailing mechanism behind the toxicity of alpha-synuclein is still unresolved. There is evidence to suggest that the toxicity of the aggregation process is encompassed by smaller, still soluble oligomeric states as opposed to the larger fibrillar formations of alpha-synuclein associated with the disease.[28]

One idea that has been repeatedly established is the notion that alpha-synuclein aggregation generates decay of dopaminergic systems and generates impaired motor function. One 2015 paper simply injected chemical species that they observed to dramatically enhance alpha-synuclein

aggregation into the brains of mice and tested for motor defects and subsequently alpha-synuclein fibrillation in brain tissue. They found that alpha-synuclein positive mice demonstrated a huge impairment in sensory motor systems when provided with an aggregation accelerator (a ring-fused 2-pyridone, FN075), while alpha-synuclein knock-out mice showed no related impairment.[29]

Other studies focus on the neurotoxic effects of alpha-synuclein as a monomer, and relate neuronal decay to increased intracellular concentration. One recent study illustrated the capacity for alpha-synuclein to boost cellular cadmium intake and accumulation, leading to mitochondrial mediated apoptosis due to oxidative stress.[30] Another recent study discovered that alpha-synuclein can disrupt the critical tethering of the endoplasmic reticulum and mitochondria, resulting in disrupted Ca^{2+} exchange and ATP production.[31]

One proposed model of aggregate formation is the continuous decrease in the function of the LAS and ubiquitin-proteasome system in the aging brain. As mentioned before, these systems aid in the normal degradation of alpha-synuclein and a reduction in their function could yield increased elevated concentrations of alpha-synuclein and in turn enhance its capacity for aggregation. It has been shown that alpha-synuclein gradually increases in dopaminergic nigral neurons in both healthy and Parkinson's patients. This increased alpha-synuclein concentration has been shown to be specifically coordinated to neurons with reductions in tyrosine hydroxylase which relates to dopamine production.[32] Additionally, a 2011 paper showed that in the presence of dopamine, alpha synuclein takes on a resistant oligomeric state, which is then secreted from the neurons at a rate that is proportional to local dopamine concentration. Monomer secretion remained unchanged.[33]

1.8 Neurodegeneration is Localized in Parkinson's Disease

It has been suggested that nigral dopaminergic neurons are highly susceptible to metabolic and oxidative stress based on unique features of the neurons and their positioning with regard to neighboring neuronal systems. These neurons are noted to consume a great deal of energy to sustain themselves. This is attributed to their huge spans of unmyelinated axon (stretching up to 4.5 meters) and the density of their synapses (up to 2.4 million on a single neuron).[1] Another popular theory is that high levels of dopamine and its metabolites can lead to enhanced levels of toxic oxidative stress.[1,34] It should be noted that the neighboring dopaminergic neurons in the ventral tegmental area (VTA) do not experience this stress and are quite resilient. It was also noted that the dopaminergic neurons in the VTA exhibit autonomous pacemaking by oscillating intracellular calcium extrusion. The contrasts between the resilience of these neuronal groups was explored in a 2010 study by Mosharov et al.[34] The results noted that the administration of concentrated L-DOPA to each neuronal group generated neurotoxicity through elevated dopamine levels. However, the neurons of the VTA demonstrate a 2-3-fold resilience to this neurotoxicity based on the functioning of their dihydropyridine-sensitive Ca^{2+} channels. They also noted that in neurons lacking alpha-synuclein expression were resistant to L-dopa induced neurotoxicity despite observing no change in intracellular dopamine levels.[34]

1.9 Diagnosis of Parkinson's Disease

For modern clinical diagnostic purposes, Parkinson's disease is defined by the presence of bradykinesia, at least one more additional Parkinson's related motor symptom, as well as special attention to other supporting or exclusionary criteria. This diagnostic criterion for Parkinson's disease is organized by the International Parkinson and Movement Disorder Society, who also prescribe the relative weighting of each of the established supporting and exclusionary criteria.[35]

Imaging can be used to observe the depletion of dopaminergic activity in the substantia nigra. Live imaging was initially performed by administering ^{18}F-labeled L-DOPA and observing its interaction and uptake using positron emission tomography (PET) in the 1980's.[1] More modern imaging methods like magnetic resonance imaging (MRI) are now capable of resolving differences between Parkinson's disease and other similar forms of neurodegeneration through a range of post-processing procedures. Another interesting method of discerning between Parkinson's disease and similar illnesses has been to assess myocardial sympathetic denervation via PET or SPECT by administering noradrenergic tracers.[1] Another studied imaging method of note is transcranial ultrasonography to observe enhanced echogenicity in the substantia nigra of Parkinson's patients.[36]

At this time, genetic testing does not see much use as a diagnostic tool in Parkinson's, but genetic predisposition has been associated with a small fraction of cases in clinical practice.[1] This small fraction however could be under represented since the list of discovered mutations causing monogenic types of Parkinson's disease continues to grow. As a diagnostic tool, genetic testing is typically only used in situations where there is a strong familial link or the condition is early-onset. Early-onset cases are common among individuals with one of several recessive genes.[1]

The potential for application of sensors to test patient fluids such as serum, urine, and cerebrospinal fluid for various diagnostic biomarkers has been a topic of a great deal of research. Today, sensors for these biomarkers have been seen as either too insensitive or lacking in the necessary specificity for use with biological samples. This may be a domain in which improved aptamers for alpha-synuclein may find a well-suited application.[1]

1.10 Current and Future Treatments for Parkinson's Disease

Current methods of drug based treatment for Parkinson's disease can be separated into two categories: those that treat for the depleted dopaminergic activity of the brain, and those that target

secondary afflicted systems. Those medicines that treat for depleted dopaminergic activity have served as the front-line treatment for symptom prevention. For the last half century, L-DOPA has been the prevailing treatment for Parkinson's disease. It functions as a rapidly converted precursor for dopamine. As a treatment, it has been proven to have a limited span of efficacy which ends in either motor response oscillation or drug-induced dyskinesias. Continuous use of L-DOPA is associated with a 30% increase in the incidence of the aforementioned motor complication within 2-3 years of administration. This statistic increases to 50% for use beyond the 5-year mark. The underlying mechanism behind this effect is still not entirely understood but appears to be a combination of neuronal maladaptations. The nature of these maladaptations appear to be linked to the oscillating dopamine concentrations that the administration of L-DOPA induces.[37] This effect has been attributed to the short half-life of L-DOPA, as well as the variability of the capacity for gastrointestinal drug uptake and blood brain barrier (BBB) transport. Modern research supports the possibility that enhanced delivery vectors may mitigate these maladaptive effects.[38] A less direct method for improving dopaminergic activity currently in use along side L-DOPA administration is inhibitors of aromatic amino acid decarboxylase (AADC). This cuts off a primary pathway for the metabolism of L-DOPA allowing it to retain a longer half-life.[1] Even greater steps to this end are undergoing clinical use such as the application of catechol-O-methyltransferase inhibitors. These inhibitors serve to cut off a secondary metabolic pathway for L-DOPA which takes over when the AADC pathway is properly inhibited.[39] Another inhibitor related method used for the elevation of cortical dopamine levels is the administration of Monoamine oxidase type B (MAOB) inhibitors. This method cuts off one of the primary clearance methods of dopamine within the synapse resulting is an increased potency of dopamine upon release.[40] Another category of dopaminergic activity enhancing drug is simple dopamine and dopamine receptor agonists. These drugs tend to have a much greater half life than L-DOPA allowing for a more controlled rate of dopaminergic activity with less of the pulsed effect seen with L-DOPA.[41] The complications from dopamine agonists come from the agonists limited

effect size when compared to L-DOPA, and their potential interaction with D3 receptors which can produce hypoactivity in the ventral striatum. These interactions can present themselves as impaired impulse control in the patients by influencing reward circuitry.[42]

The targeting of secondary non-dopaminergic systems in Parkinson's treatment is a quite modern concept. Non-dopaminergic (non-motor) symptoms of Parkinson's are often influenced by chemical oscillations of non-motor areas of the brain.[43] These oscillations are thought to result from the dopaminergic oscillations of the motor areas of the brain largely generated by dopamine replacement therapies. However, the symptoms generated typically do not respond to forms of dopamine replacement therapies and are can be aggravated by the continued use of these therapies. As such, these treatment for non-motor symptoms are often administered in addition to dopamine replacement therapies and are typically used to combat specific symptoms on a case by case basis. One example of this are cholinesterase inhibitors, which have been shown to be effective on mitigating cognitive impairment for Parkinson's patients suffering from dementia. Other examples include the administration of a noradrenaline precursor to treat orthostatic hypotension, or anti-muscarinic drugs for urinary incontinence.

Another increasing popular form of Parkinson's treatment is deep brain stimulation (DBS), which has demonstrated its efficacy though application at the subthalamic nucleus in treating motor fluctuations and dyskinesia.[44] However, it should be noted that the efficacy of DBS is positively correlated to the effectiveness of treating the same patient with L-DOPA. The greatest result of DBS may be that L-DOPA drug dose post surgery is reduced by 31%-58%. This produces a dramatic decrease in the prevalence of motor-related dopaminergic fluctuations.[45] The effectiveness of DBS treatment is likely to increase as the related technology improves over the coming years.[1]

The use of cellular implantation to replace the lost neuronal density of the dopaminergic system in the substantia nigra in Parkinson's patients is an ongoing field of research. So far, results have been varied and the capacity to track long term implication of the treatment in clinic tests has been limited. One study has gone so far as to perform implantation of fetal ventral mesencephalic tissue which is rich in dopaminergic neuroblasts. While the study was limited to the analysis of two participants (one 15 and one 18 years post implantation), the results indicated that both patients had become, and stayed free from pharmacological dopaminergic therapy post implantation, with enduring symptomatic relief.[46] Another study from 2014, generated functioning and transplantable dopamine neurons from human embryonic stem cells. When implanted in a rat model for Parkinson's disease, the results indicated their efficacy in the restoration of motor neurons. The study went on to demonstrate that the cells generated could accommodate the length needed for use in humans and acquire the correct form and structure.[47]

Another form of potential treatments that have reached human clinical trials now are the PD01A and PD03A vaccines. These vaccines use small peptides that mimic specific regions of the alpha-synuclein molecule which can be conjugated to carriers to initiate antibody responses. So far the vaccines have been shown functional in selective recognition of alpha-synuclein, generating alpha-synuclein antibodies, and preventing alpha-synuclein related neurodegeneration in animal models. Further results are expected during 2017.[48,49]

1.10.1 Potential Drugs Based on Alpha-Synuclein Aggregate Prevention

While the vast majority of treatments under development or in current practice are primarily targeted towards the mitigation of symptoms while minimizing side effects, a few studies have begun assessing the capacity for more preventative treatments. While there have been a variety of proposed target mechanisms, the prevention of alpha-synuclein aggregation has been one of great interest.[12] While this project has proposed the use of DNA aptamers as the best tool to this end, a wide range of

other methods have been proposed. For example, nicotine consumption has been associated with a reduced risk of Parkinson's development.[50] As such nicotine has been investigated and proven to produce a dose-dependant inhibition of alpha-synuclein fibril formation, as well as a destabilization of preformed fibrils *in vitro*.[51]

Traditional Chinese medicines have incorporated tanshinone I (TAN I) and tashinone IIA (TAN IIA) for centuries. A 2016 study demonstrated that both these compounds are capable of disaggregating preformed fibrils and inhibiting the formation of new fibrils by prolonging the lag phase of fibril growth. The study also demonstrated the capacity for TAN I and TAN IIA administration to improve the longevity of transgenic Cainorhabditis elegans producing human alpha-synuclein.[52]

A 2012 study tested a novel curcumin derivative, curcumin-glucoside, for its capacity to prevent alpha-synuclein aggregation. The results indicate that it has the capacity to prevent the formation of oligomer and inhibits fibril formation in a dose-dependant manner. Micro-calorimetry indicated curcumin-glucoside has limited affinity for monomer, but strong binding with oligomers.[53]

A 2009 study assessed the chemical chaperone, sodium 4-phenylbutyric acid, for its capacity to prevent Parkinson's progression in human alpha-synuclein producing transgenic mice (double mutations A30P + A53T). The results of administration were the reduced rate of motor deteriorations, reduced loss of tyrosine hydroxylase-positive neurons, and reduced levels of phosphorylated alpha-synuclein in the substantia nigra. The outcome was that the study reported no loss of striatal dopamine content in the treated mice.[54]

Another interesting method of alpha-synuclein control comes in the form of a specialized protein from yeast, Hsp104. This protein possesses strong disaggregase activity and functions by coupling ATP hydrolysis with the disassembly and reactivation of proteins trapped in a wide range of oligomeric formations.[55] The administration of Hsp104 was shown to supress alpha-synuclein toxicity in

yeast, eliminate aggregates, as well as suppress dopaminergic neurodegeneration in a Parkinson's model using transgenic Caenorhabditis elegans.[56]

1.11 Aptamers

1.11.1 What are Aptamers

Aptamers are typically short single stranded pieces of DNA or RNA which interact with a target of interest with high affinity, and selectivity. Aptamers typically range from 40 to 100 bases and have been shown to recognize a wide range of targets such as amino acids, antibodies, proteins, bacteria, viruses, and small molecules.[57] In addition to the diverse range of targets, there exists an ever-growing series of applications. These include medicine and diagnosis in clinical settings, sensors, reaction mediators, functional nanomachines, targeted delivery vectors, and imaging applications.[58,59] Interactions with targets are governed by intermolecular forces such as hydrogen bonding, van der Waals forces, electrostatic interactions and base stacking.[57] Because of their similarities, aptamers are often compared to antibodies, to which they have several advantages within the broad scope of applications. Aptamer production is scalable and done chemically which eliminates the potential for viral or bacterial contamination. The modification of aptamers is made easy during synthesis or afterwards through a series of simple chemical reactions with typically produce high yields.[60] Aptamers can also be used in applications where a reversible structure switch is desired.[57]

1.11.2 How Aptamers are Generated

The primary method for the production of aptamers today is SELEX (Systemic Evolution of Ligands by EXponential enrichment), although other methods are the topic of continued research.[57] The SELEX method incorporates selective evolution, in which an extremely diverse candidate pool (typically randomized DNA sequences) is repeatedly partitioned based on a desired aptamer capacity specific to

the individual SELEX experiment. Those members of the candidate pool that demonstrate the desired capacity are retained and replicated once partitioned from those members of the candidate pool which do not. While each candidate likely only exists as a singular, unique sequence within the starting pool, the repeated partitioning and replication quickly results in the overrepresentation of strong candidates within the produced "enriched" candidate pool. Those strong candidates can then be identified through sequencing of the enriched pool. The candidate sequences which demonstrate the greatest degree of overrepresentation within the enriched pool are typically selected for analysis with assays that evaluate candidates specifically for the capacity of interest.[57]

1.11.3 Application of Aptamers in Neurodegenerative Disease

Aptamers are especially comparable to antibodies within clinical applications. Because of their small size (typically less than 30 kDa) when compared to traditional antibodies (about 150 kDa), aptamers demonstrate improved permeability though biological tissues, allowing them better access to intracellular targets.[57,61] Aptamers are not inherently immunogenic, while antibodies often are, making them suitable for a wider range of diseases.[57,60] Unlike antibodies, aptamers can undergo reversible structure switching which makes them resistant to thermal denaturing. This is a key feature for storage and application in medicine.[62] Aptamers also have the capacity to select against specific targets including undesired cell surface targets.[60] Despite the numerous advantages, aptamer applications in clinical settings are often limited by their short half-life in the body. This is the result of susceptibility to blood borne nucleases and vulnerability to renal filtration due to their small size. Several strategies have been identified to overcome these limitations. Common strategies so far have been the conjugation of the aptamer to species such as polyethylene glycol (PEG) or cholesterol, or the modification of the phosphodiester backbone to improve nuclease resistance.[57,63] Another strategy to improve aptamer half-life has been the incorporation or encapsulation of the aptamer within a protective delivery vector.[59]

With regards to protein targets, it is common to find that aptamers inhibit the function of the target protein upon binding.[60] This is associated with the idea that the active sites of a protein tend to have more exposed sites for hydrogen bonding or other desirable aptamer-target interactions. Another possible explanation for the commonly observed inhibition is the increased probability that aptamers which fit themselves into the clefts of a protein are more likely to be resilient through SELEX partition stages. The availability of these crevices is often very important for a protein's functionality, and as such, aptamers targeting these sections are more likely to be inhibitory to this functionality.[60]

1.11.4 Existing Aptamer Work for Neurodegenerative Diseases Centered Around Protein Aggregation

To date, a great deal of work has been put into aptamer development towards applications in neurodegenerative disease treatment and research. The most prevalent of these diseases are largely attributed to the accumulation of misfolded protein within the central nervous system. Aptamer work done in this field often seeks to produce sequences which have the capacity to inhibit aggregation of the related proteins. Neurodegenerative diseases to which related aptamers have been generated include Parkinson's disease, Alzheimer's disease (AD), transmissible spongiform encephalopathies (TSE or prion diseases), and Huntington's disease (HD).[57]

As mentioned before, Parkinson's disease is hallmarked by the misfolding and aggregation of the protein alpha-synuclein.[57] The first aptamer SELEX for alpha-synuclein was conducted by Tsukakoshi et al. in 2010. This selection led to the initial discovery of the M5-15 aptamer. This 2010 aptamer selection and the M5-15 aptamer, in many ways, served as a launching point for the work conducted in this project. This selection used alpha-synuclein monomer free in solution as the target. In this selection, partitioning of alpha-synuclein bound from unbound aptamer candidates is accomplished using native PAGE. Aptamers which appeared higher in the gel were identified as those bound to monomer by

colocalization of fluorescence from the aptamer pool and Coomassie Brilliant Blue staining of the monomeric protein. After four rounds of SELEX, the aptamer pool was sequenced and M5-15 was identified. In vitro testing by a blotting assay revealed M5-15 had a significantly greater affinity towards oligomeric morphologies than monomeric alpha-synuclein.[64]

Tsukakoshi et al. produced a new selection in 2012. In this new selection, they generated aptamers capable of binding selectively to both the smaller oligomeric morphologies of alpha-synuclein and amyloid beta. This second selection incorporated oligomeric alpha-synuclein as the target. This oligomeric protein was generated by lyophilization of monomeric protein stock followed size exclusion chromatography. To produce fibrils for counter selection, the generated oligomers underwent a 120 hour incubation in phosphate buffered saline at pH 7.3 and 37 °C. The partitioning of oligomer bound aptamer candidates from those which were unbound, was performed by agarose gel electrophoresis. This partitioning was used for SELEX rounds 1 and 2 before a new partitioning method was incorporated in its place. The second partitioning method employed used nitrocellulose membrane retention. Three separate membranes were used in this stage. One membrane was mounted with monomeric alpha-synuclein, the second was mounted with oligomeric alpha-synuclein, and the third was mounted with fibrillated alpha-synuclein. Aptamer pool was then introduced to each membrane. The aptamer pool which demonstrated retention by the oligomeric alpha-synuclein mounted membrane was extracted and amplified for use in the following round. Three SELEX rounds were performed using this partitioning method. Samples from each of the pools that were retained by the various nitrocellulose filters were extracted for analysis by sequencing. This sequencing yielded eight final aptamer candidates all of which generate G-quadruplex domains. The capacity for the aptamer candidates to inhibit the aggregation of alpha-synuclein was not explored.[65]

The hallmarks of Alzheimer's disease (AD) are the misfolding and aggregation of the protein amyloid beta (Aβ). To date, two different aptamers have been produced which target this aggregation of

Aβ by attempting inhibit Aβ production.[57] These sequences target the BACE1 enzyme necessary for Aβ production.[57] The first of these two aptamers is a DNA aptamer referred to A1. This aptamer was selected by mounting wells with a BACE1 extracellular domain as a target. Then the aptamer pool was introduced to the well. The partitioning of binding aptamer candidates from non-binding candidates was accomplished by washing the system repeatedly with buffer. The resulting DNA aptamer demonstrated the capacity to reduce Aβ production in a model cell line.[66] The second aptamer selection performed towards this goal implemented a RNA library. This selection incorporated the entire cytoplasmic domain of the BACE1 protein immobilized on Sepharose as the target. Partitioning of binding candidates from non-binders was done by washing away non-binders from the Sepharose substrate.[67]

Two more aptamers were generated for AD treatment which instead target the toxic Aβ oligomeric protein morphology itself.[57] An RNA aptamer was selected by immobilized a 40-residue variant of Aβ. Binding versus non-binding aptamers were partitioned by washing with Tris-buffered saline.[68] The second aptamer was DNA based, and was selected using same 40-residue variant of Aβ as a target. In this selection, the target protein was affixed to a substrate the partitioning of binding candidates from non-binding candidates was accomplished using G-50 columns.[69]

TSE is a neurodegenerative disorder characterized by the accumulation of the abnormal subtype of the cellular prion protein (PrP^{SC}).[57] A 2003 selection by James et al., produced the RNA based SAF-93 aptamer which binds to both PrP^{SC} and the normal protein subtype, PrP^{C} (from which PrP^{SC} is produced). SAF-93 demonstrated the capacity to inhibit for conversion of PrP^{C} to PrP^{SC}. The selection was performed using treated fibril morphologies generated in the brains of hamsters. The partitioning of bound and unbound candidates was performed by centrifugation and pelleting of the resulting fibril-aptamer complexes.[70]

Huntington's disease has been associated with the misfolding and aggregation of the mutant variant of the huntingtin protein (mHTT).[57] A 2006 study by Skogen et al. revealed that a 20 base DNA sequence of exclusively guanine bases can effectively inhibit mHTT aggregate formation.[71]

1.12 Thesis Objectives

The primary aim of the research encompassed in this thesis is the discovery of DNA aptamers with the capacity to inhibit the aggregation of alpha-synuclein. Towards this goal, the established M5-15 aptamer for alpha-synuclein is tested, and a new SELEX method is proposed and implemented. The method proposed necessitates that the aptamers selected, not only bind to alpha-synuclein with high affinity and selectivity, but also inhibit alpha-synuclein aggregation. Other SELEX methods have selected aptamers with high affinity for aggregating proteins, and for a couple, their testing has proven the capacity to prevent aggregation. However, no study to date has gone so far as to embed this aptamer functionality within the selection itself. While binding to a toxic oligomerized morphology of alpha-synuclein might impede its toxicity, preventing the initial formation of these toxic oligomers would naturally be preferred. A novel SELEX method proposed here would have monomeric protein introduced to the SELEX pool and made to aggregate until no free monomer remains. Any remaining monomeric alpha-synuclein must be bound to aptamer candidates which prevent their monomer's capacity to aggregate. Because oligomeric morphologies of the protein are inherently larger and denser then monomeric forms, it is simple to partition the aptamer bound monomer from the other, larger morphologies and unbound aptamer pool. This work employs ultracentrifugation to accommodate this partitioning. A lighter fraction containing unbound monomer and aptamer candidates is considered a negative selection pool. A mid gradient fraction containing aptamer bound monomer is considered the positive selection pool. A lower fraction containing aptamer candidates bound to aggregated alpha-synuclein morphologies is considered the counter selection pool. Implementing a second partitioning

stage to the SELEX method serves to improve the stringency with which aptamer candidates are selected. For this second partitioning step, nitrocellulose filtration is employed in this work. Nitrocellulose filtration serves to remove aptamer candidates which have become detached from their monomeric protein and retains aptamers based on their affinity for the protein. By amplifying the resulting aptamer pool and repeating this process several times it is believed that aptamers with the capacity to inhibit alpha-synuclein aggregation would be overrepresented in the final pool. Sequencing the aptamer pool from various stages within the SELEX provides information about the progression of the pool, and the behaviour of the aptamer candidates within it. Secondary analysis of random region of individual sequences provides additional insights into each aptamer's potential functionality and unique capacities. Beyond selection, a preliminary *in vitro* assay designed to mimic the SELEX conditions, shows the varying capacity of each candidate to inhibit alpha-synuclein aggregation.

2 Materials and Methods

2.1 Statement of Contribution

Pre-SELEX aggregation assays were performed by Dr. Erin McConnell and Josh Callahan. Original pool and primer designs were generated by Tsukakoshi et al. (2012).[65] Novel pool synthesis and clean-up was performed by Dr. Erin McConnell. Mutant pool synthesis and clean-up was performed by Emily Mastronardi. SELEX rounds 1 and 2 were performed by Dr. Erin McConnell and Josh Callahan. SELEX rounds 3, 4, and 5 were performed by Josh Callahan. Non-denaturing PAGE assay for SELEX round 1 was performed by Dr. Erin McConnell and Josh Callahan. Ultracentrifugation steps were completed with help from Dr. Bill Willmore. TEM imaging for SELEX round 2 was conducted by Dr. Erin McConnell, Dr. Jianqun Wang, and Josh Callahan. TEM imaging for SELEX rounds 3 and 4 was conducted by Dr. Jianqun Wang and Josh Callahan. Elongated primer tail designs by Illumina Inc. MiSeq analysis was performed by Dr.

Erin McConnell, Dr. Alex Wong, and Josh Callahan. Alpha-synuclein aggregation assay with aptamer candidates under SELEX conditions was performed by Josh Callahan with help from Dr. Jianqun Wang. Direction and guidance provided by Dr. Maria DeRosa. Experiments designed by Dr. Maria DeRosa, Dr. Erin McConnell, and Josh Callahan.

2.2 Aggregation Test 1-Incubation of Alpha-synuclein

This incubation was initiated for by dissolving a dry 0.5 mg aliquot of alpha-synuclein (common human variant expressed in E. coli and purchased from rPeptide, Bogart, GA, USA) in a minimal volume of deionized water. Six different 100 µL samples were made up with three being diluted further in deionized water while the remaining three were diluted with a PBS buffer (0.137 M NaCl, 2.7 mM KCl, 8.1 mM Na2HPO4, 1.8 mM KH_2PO_4, pH of 7.27). Each three sample group was made up of one sample at 15 µM alpha-synuclein, one at 25 µM alpha-synuclein, and another at 50 µM alpha-synuclein. The incubation was performed on an orbital shaker and incubator (Innova 40 by New Brunswick Scientific) at 180 RPM and 37 °C for 16 hours. Once the incubation was complete, each of the six samples were further split into three fractions (One receiving 20 µL, the second receiving 30 µL, and the third receiving 40 µL). This allowed for the assessment of the required number of moles a sample needed in order to be properly visually stained.

2.3 Aggregation Test 1 -Alpha-Synuclein Testing Via Native Polyacrylamide Gel Electrophoresis

Non-denaturing poly-acrylamide gels were prepared at a density of 12% acrylamide. This was done by mixing 14 mL of deionized water, 15 mL of concentrated TBE buffer (Tris, boric acid, EDTA), and 23.5 mL of acrylamide stock (containing acrylamide/bis-acrylamide 40% purchased from Bioshop, Burlington, Ontario, Canada). This mixture was then stirred while heating to 37°C. Once the temperature

had a chance to stabilize, the solution was then filtered though a filter paper into a fresh beaker. 0.5 mL of a fresh 10% ammonium persulfate solution, as well as 35 µL of TEMED (Tetramethylethylenediamine) were then added to the mixture to initiate the polymerization. Once the two gels were poured into the mold (Hoefer Inc.), the system was then allowed to sit for 30 minutes. While the poured gels polymerized, a running buffer of 1:5 diluted TBE buffer was prepared. At this point the gel apparatus was mounted with a water cooling system. Once suspended in running buffer, the gels were pre-run for 30 minutes at 250 V supplied by a Fisher Scientific FB1000. Alpha-synuclein samples of varying concentration and volume were weighed down with 50% water-glycerol solutions and then loaded. Once loaded, a running ladder (Precision Plus Protein All Blue Standard from Bio-Rad, Hercules, California, USA) was loaded into a secondary well. Loaded gels were then run at 250 V for 4 hours. Once running was complete, the gels were placed in a basin to be stained over night (Stains-All, Sigma-Aldrich, St. Louis, Missouri, USA). Once de-stained, images were captured of the gels.

2.4 Aggregation Test 2- Incubation of Alpha-synuclein

This incubation was initiated by dissolving a dry 0.5 mg aliquot of alpha-synuclein in a minimal volume of deionized water. From here, two separate 200 µL samples were diluted in PBS buffer to concentrations of 25 µM and 50 µM respectively. The incubation was performed on an orbital shaker and incubator (Innova 40 by New Brunswick Scientific) at 180 RPM and 37 °C for 16 hours. After incubation, the samples were placed at 4 °C for 24 hours. Finally, 20 µL aliquots were drawn from each sample to be assessed by gel electrophoresis.

2.5 Aggregation Test 2 -Alpha-Synuclein Testing Via Native and Denaturing Polyacrylamide Gel Electrophoresis

For this experiment two different gels were prepared. One non-denaturing poly-acrylamide gel was prepared at a density of 5% acrylamide. This was done by mixing 27.2 mL of deionized water, 15 mL of concentrated TBE buffer, and 9.8 mL of acrylamide stock (containing acrylamide/bis-acrylamide 40%). Next, one urea based denaturing poly-acrylamide gel was prepared at a density of 10% acrylamide. This was done by mixing 31.5 g of urea, 17.4 mL of deionized water, 15 mL of concentrated TBE buffer, and 19.6 mL of acrylamide stock (containing acrylamide/bis-acrylamide 40%). Each mixture was then stirred while heating to 37°C. Once the temperature had a chance to stabilize, the solutions were then filtered though a filter papers into fresh beakers. 0.6 mL of a fresh 10% ammonium persulfate solution, as well as 35 µL of TEMED were then added to each mixture to initiate the polymerization. Once the two gels were poured into their respective mold (Hoefer Inc.), the system was then allowed to sit for 30 minutes. While the poured gels polymerized, a running buffer of 1:5 diluted TBE buffer was made up. At this point the non-denaturing gel apparatus was mounted with a water cooling system. Once suspended in running buffer, the gels were pre-run for 30 minutes at 250 V supplied by a Fisher Scientific FB1000. Alpha-synuclein samples of varying concentration and volume were weighed down with 50% water-glycerol solutions and then loaded. Once loaded, a running ladder (Precision Plus Protein All Blue Standard, Bio-Rad, Hercules, California) was loaded into a secondary well. The loaded gels were then run at 250 V. Once running was complete, as indicated by ladder progression, the gels were placed into basins and stained over night (Stains-All purchased from Sigma-Aldrich). Once de-stained, images were captured of the gels.

2.6 Pre-SELEX Preparation Procedures

2.6.1 General Handling and Sterilization Procedures for SELEX and Pre-SELEX work

All repeated-use materials that came into direct and indirect contact with SELEX pool samples, were either bleached and washed repeatedly with deionized water or wiped down well with ethanol and irradiated for 25 minutes before use. These included all tube racks, pipettes, nitrocellulose filter mount, cuvettes, gel apparatus, and any secondary glassware used in the generation of buffers or other solution. For the most part, any materials that were allowed direct contact with the pool were typically disposable and intended for one-time use. If a length of time existed between experiments, any sample containing DNA was dried down if possible and stored at -20 °C. For periods lasting longer than two weeks, these samples would be transferred to a -80 °C freezer. Any samples of DNA coming out of a frozen state would be allowed to thaw at room temperature before being heated to 95 °C and allowed to cool to room temperature before use, to generate a more consistent secondary structure.

2.6.2 Pool Design

This SELEX used two individual pools (named mutant and novel) which initially ran independently before eventually becoming partially mixed. The mutant and novel pools were based on the previously identified aptamer M5-15.[64] Both mutant and novel pools utilized entirely identical primer domains as M5-15 (18 bases on either end of the sequence) and replicated the M5-15 aptamer with a central random region size of 30 bases. The mutant pool took the M5-15 aptamer and incorporated a 30% rate of randomization within the random region of the strand with respect to M5-15. This means that, for any given strand, up to 100% of the random region could differ from M5-15, but the most prevalent

degree of variation is firmly at the 30% mark. The novel pool operated in the same way but with the most prevalent degree of variation from the random region of M5-15 at 75%.

The resulting pools all used the following template sequence where N represents a randomized base:

5'-ATAGTCCCATCATTCATTNNNNNNNNNNNNNNNNNNNNNNNNNNNNNNNAGATATTAGCAAGTGTCA-3'

2.6.3 Pool Synthesis

The pool was synthesized on a BioAutomation Mermade 6 oligonucleotide synthesis system. Synthesis ran 3' to 5' originating from a 1000 Å controlled pore glass (CPG) column (produced by BioAutomation). The silica beads making up the 6 columns used were primed with a mounted initial adenine base by the manufacturer. On the 5' end, a single fluorescein modifier (produced by Glen Research) was added to each sequence. The stock protected phosphoramidites were purchased from Glen Research. Other materials such as deblock, activator, acetonitrile, cap A, cap B, and oxidizer were also purchased from Glen Research.

After primary synthesis, the columns were removed and the CPG beads were extracted, each into tubes containing 1mL of ammonium hydroxide. The synthesized oligonucleotides were then removed from the beads by allowing them to rest for 18 hours at 55°C. The solution was then centrifuged for 10 minutes at 10,000 RPM. The supernatant free of beads could then be moved to a new tube. The pellet of silica beads was then resuspended in deionized water, vortexed, and centrifuged again. This supernatant was then placed in a new tube. From here the samples could be dried down on a speed-vac (New Brunswick INNOVA 40). Once these samples were dried down, they could then be re-suspended in a smaller solution of 1:1 deionized water and formamide.

2.6.4 Gel Electrophoresis for Purification of Pools

Urea based denaturing poly-acrylamide gels were prepared at a density of 12% acrylamide. This was done by mixing 31.5 g urea, 14 mL deionized water, 15 mL concentrated TBE buffer, and 23.5 mL acrylamide stock (containing acrylamide/bis-acrylamide 40%). This mixture was then stirred while heating to 37°C. Once the temperature had a chance to stabilize, the solution was then filtered though a filter paper into a fresh beaker. Next, 0.5 mL of a fresh 10% ammonium persulfate solution, as well as 35 µL of TEMED were then added to the mixture to initiate the polymerization. Once poured into the mold (Hoefer Inc.), the system was then allowed to sit for 30 minutes. This process produced two gels. As such, it was repeated two more times to produce the six gels required to purify the products of six columns. While the poured gels polymerized, a running buffer of 1:5 diluted TBE buffer was made up. Once suspended in running buffer, the gels were pre-run for 30 minutes at 250 V supplied by a Fisher Scientific FB1000. Synthesized DNA samples in water-formamide solutions were then heated to 95°C for 10 minutes prior to loading. Once loaded, a running ladder (Precision Plus Protein All Blue Standard, BioRad) was loaded into a secondary well. Loaded gels were then run at 250 V for 2.5 hours. Once running was complete, the gels were placed on an imaging plate and photographed under UV-light (using an Alpha Innotech AlphaImager EC). The various sizes of synthesized DNA appeared as dark bands as they absorbed UV light. The band containing the purified, full-length product was determined by relative location on the gel with respect to the ladder and other bands. The product band was then cut from the gel and broken into tiny pieces before being submerged into a small volume of deionized water (~3 mL). These samples were then placed onto an orbital shaker and incubator (Innova 40 by New Brunswick Scientific) set to 37°C and 170 RPM for 24 hours. Once the purified DNA had diffused into the deionized water, the system could be filtered to remove the polyacrylamide gel fragments. This was performed using a 10 mL syringe mounted with a 0.22 µM PEG filter (produced by Celltreat). Once filtered into a new tube the samples were ready for desalting.

2.6.5 Purified Pool Clean-Up Via Desalting

Desalting was carried out using 3K NMWL cellulose centrifugal filters by Amicon ultra. Samples were introduced to the desalting filters in aliquots of 0.4 mL. The system was spun at 10,000 RPM for 20 minutes to pull the salt rich solution through the filter, leaving the DNA behind. Once the entirety of the starting samples had been aliquoted into the system, the DNA was washed with four 0.4 mL aliquots of deionized water. Once washed, the filters were flipped and the retained DNA was centrifuged into a clean tube.

2.6.6 Purified Pool Quantification

Quantification of these samples was performed using a Varian Cary 300 Bio UV-Visible Spectrophotometer. By using DNA's absorption of light at 260 nm, coupled with a calculated extinction coefficient of 721000 L mol^{-1} cm^{-1}, a rough estimation of the samples concentration was determined.

2.7 SELEX Targeting the Inhibition of Alpha-Synuclein Aggregation

The following steps were completed once with the novel pool alone, and then repeated four more times with the mutant pool in tandem.

2.7.1 Alpha-synuclein and Pool Incubation

This stage was varied slightly between SELEX rounds. To begin, the desired quantity of each system (Alpha-synuclein or SELEX pool) was dissolved to a desired concentration in PBS buffer (0.137 M NaCl, 2.7 mM KCl, 8.1 mM Na_2HPO_4, 1.8 mM KH_2PO_4, pH=7.269). This buffer was altered for SELEX round 4 in which the pH of the incubating system was tuned to a pH of 6.5 with HCl. For each round, the volume and concentration of alpha-synuclein (target) was always matched 1:1 with the amount of DNA (aptamer pool). DNA-free controls were also generated for each round, matching the alpha-synuclein system with an equal volume of PBS. For round 1 this amount was 3.6 nmol in 120 µL (30 µM). For round

2 it was 2.8 nmol in 170 µL (16.5 µM). It should be noted that a small amount of mutant pool and M5-15 was introduced during this incubation in round 2. For rounds 3, 4, and 5 this amount was 1.4 nmol in 170 µL (7 µM). The dissolved pool was then mixed with the matched alpha-synuclein sample. In the cases of rounds 1,2, and 3, the mixed sample was flash-frozen with liquid nitrogen and then placed on a lyophilizer (Labconco FreeZone 4.5) overnight to dry down. The dry solution was then suspended to their original volume with deionized water. Having undergone this step or not, the samples were then placed on an incubator at 180 RMP and 37 °C. Duration of this incubation phase varied round to round. During round 1 this incubation lasted 42 hours. Round 2 used a 126 hour incubation. Round 3 used a 122 hour incubation. Round 4 used a 106 hour incubation. Round 5 used a 317 hour incubation.

2.7.2 Ultracentrifugation of Incubated System to Partition Alpha-Synuclein Morphologies

Five millilitre thermal sealing ultracentrifuge tubes (Beckman) were carefully loaded with density gradient layer by layer. The layers for the gradient were produced by combining OptiPrep (Sigma-Aldrich) with PBS buffer and deionized water in varying ratios. The resulting layers contain 40% PBS buffer with a varying percent iodixanol. The gradient layers used varied between the rounds of SELEX. Round 1 used three layers (0.71 mL of 35%, 2.14 mL of 25%, 2.4 mL of 2.5%). Round 2 had six layers (1.0 mL of 35%, 1.0 mL 25%, 1.0 mL of 12%, 1.0 mL of 6%, 1.0 mL of 2.5%, 0.6 mL of 1%). Rounds 3, 4, 5 had six layers again (1.0 mL of 35%, 1.0 mL 25%, 1.0 mL of 20%, 1.0 mL of 12%, 1.0 mL of 6%, 0.6 mL of 2.5%). Each tube was then loaded with the relevant sample. In order to reduce the amount of air in the tubes, as well as for balancing purposes, the tubes were topped off with a small amount of the lightest density layer employed in that system. Once balanced, the tubes were thermal sealed using a Beckman Tube Sealer. The tubes were then mounted in to an angled mount Type 100 Ti rotor head (Beckman, serial number 97U 442)) and placed in an ultracentrifuge (Beckman Optima LE-80K). Once the

system was sealed and a vacuum was reached, the tubes were spun. Round 1 spun at 50,000 x g for 1 hour. Round 2 spun at 100,000 x g for 20 hours. Round 3 spun at 100,000 x g for 7 hours. Round 4 spun at 100,000 x g for 5.5 hours. Round 5 spun at 100,000 x g for 6 hours. Once the run was finished the system was depressurized and the tubes were removed from the rotor head. The top of a tube could then be removed with a fresh razor blade. Layers each were carefully removed from the surface of the gradient and placed into individual tubes. For round 1 and 2 these layers were 200 µL in volume, while rounds 3,4, and 5 drew layers of 250 µL. Most trials (rounds 2, 3, and 4 as well as optimization round) involving the ultracentrifuge ran a control tube containing an 80 µL aliquot of protein ladder to generate an estimation of the location of the various DNA-Protein systems within the gradient post-ultracentrifugation. Of the layers/fractions extracted from the tube, some would go on to have their DNA pool extracted and purified. These select layers were used as the positive (+), negative (-), and counter (X) selections for the round. The layers pertaining to each of these designations varied with each alteration to the density gradient.

Prior to conducting this ultracentrifuge step during round 3, an optimization round was carrier out in order to assess the resolution generated by a newly proposed ultracentrifugation density gradient and run time. This optimization round tested the new density gradient found in rounds 3,4 and 5 (1.0 mL of 35%, 1.0 mL 25%, 1.0 mL of 20%, 1.0 mL of 12%, 1.0 mL of 6%, 0.6 mL of 2.5%). This run lasted 6 hours at 100,000 x g. After running, the tubes were labeled at the locations where bands of the protein ladder were present. Layers of 250 µL were then drawn from the surface of the density gradient. Layers that coordinated with labels marked on the tubes were noted.

2.7.3 Analysis of Ultracentrifugation by Fluorescence

This analysis tracked the movement of our labeled DNA through the density medium via fluorescent analysis of our extracted layers. This analysis method was carried out for rounds 1,2 and 3.

The samples were loaded into a standard quartz cuvette and the fluorescence was read by a Fluorolog spectrophotometer (by Horiba Jobin Yvon). An excitation wavelength of 494 nm was coupled with an emission wavelengths of 520 nm, corresponding to the excitation and emission of fluorescein.

2.7.4 Analysis of Ultracentrifugation via Non-denaturing PAGE

Non-denaturing poly-acrylamide gels were prepared at a density of 5% acrylamide. This was done by mixing 27.2 mL of deionized water, 15 mL of concentrated TBE buffer, and 9.8 mL of acrylamide stock (containing acrylamide/bis-acrylamide 40%). This mixture was then stirred while heating to 37°C. Once the temperature had a chance to stabilize, the solution was then filtered though a filter paper into a fresh beaker. 0.5 mL of a fresh 10% ammonium persulfate solution, as well as 35 µL of TEMED were then added to the mixture to initiate the polymerization. This procedure was repeated twice to accommodate 4 gels (2 gels per batch). Once four gels were poured into the mold (Hoefer Inc.), the system was then allowed to sit for 30 minutes. While the poured gels polymerized, a running buffer of 1:5 diluted TBE buffer was made up. At this point the gel apparatus was mounted with a water cooling system. Once suspended in running buffer, the gels were pre-run for 30 minutes at 250 V supplied by a Fisher Scientific FB1000. Ultracentrifuge fraction samples of were then weighed down with 50% water-glycerol solutions and loaded. Once loaded, a running ladder (Precision Plus Protein All Blue Standard purchased from BioRad) was loaded into a secondary well. Loaded gels were then run at 250 V for 4 hours. Once running was complete, the gels were placed in a basin to be stained over night (Stains-All purchased from Sigma-Aldrich). Once de-stained images were captured of the gels. This assay was run for SELEX round 1, prior to the implementation of TEM imaging. The assay for round 1 included samples from all density gradient fractions taken, while round 2 only included only select fractions.

2.7.5 Analysis of Ultracentrifugation via TEM

In order to assess the protein morphologies present in different layers from the density gradient, transmission electron microscopy (TEM) images were taken for select fractions. This was carried out for rounds 2, 3, and 4. Samples were deposited on carbon coated copper TEM grids (manufactured by Electron Microscopy Sciences, Model CF300-Cu). Standard deposition was done by initial introduction of 4 µL of sample followed by a 10-minute settling period. After this period, the 4 µL samples were drawn from the grid and disposed of. The analysis of TEM samples was performed with a FEI Tecnai G2 F20 TEM. Elemental analysis by energy dispersive spectroscopy (EDS) was performed using an Oxford AztecTEM with 80mm elemental silicon drift detector (SDD). A TEM beam voltage of 120kV was used to observe protein and DNA formations. The EDS employed a take off angle of 20 degrees.

2.7.6 Nitrocellulose Filtration of Select Ultracentrifuge Gradient Fractions to Remove Aptamer Candidates Which Released Their Monomer

To begin, a nitrocellulose filter (produced by Millipore) was soaked in 1 mL of 0.5 M KOH for 20 minutes while gently vortexed. The filter was then washed by replacing the ambient solution four times with 2 mL aliquots of deionized water (vortexing for 2 minutes in the fresh water each time). Then 100 µL from a pair of selected adjacent fractions were combined to form a new, larger pool. The fluorescence of selection pool could then be measured on a Fluorolog spectrophotometer. Using a Millipore Swinnex filter mount and a 1 mL syringe, the pool was passed over the prepared membrane. The sample that passed through the membrane was retained as a negative selection. Then the filter was removed from the mount and placed in a new tube containing 1 mL of urea elution buffer (7 M urea, 0.05 M HEPES, pH=7.506). This was then vortexed for 20 minutes and subsequently heated to 95 °C on a heat block for 15 minutes. The filter was then removed and placed in a new tube.

2.7.7 Phenol Chloroform Extraction and Ethanol Precipitation to Extract Aptamer Pool From Bound Alpha-Synuclein

One milliliter of phenol:chloroform:isoamyl alcohol (25:24:1) was then added to the urea elution buffer which now contained the desired DNA pool. This solution was then vortexed and centrifuged at 12,000 x g for 5 minutes. The aqueous phase produced by the elution buffer was then removed and placed in a new tube. This extraction was performed two more times with fresh aliquots of phenol:chloroform:isoamyl alcohol. Finally, an extraction with pure chloroform was performed in the same manner in order to extract residual phenol from the aqueous phase. The ethanol precipitation was started by adding 100 µL of sodium acetate to the aqueous phase and vortexing. 2.75 mL of pre-chilled ethanol was then added to the solution and the solution was vortexed. This solution was then placed on ice for 20 minutes before being immediately placed on a centrifuge for 15 minutes at 12,000 x g. The supernatant was then removed from the solution, leaving only a small pellet and volume of solution at the bottom of the tube. The pellet was then resuspended in 500 µL of deionized water and transferred to a desalting tube. While in the desalting tube, the sample was centrifuged at 12,000 x g for 25 minutes. The remaining 100 µL solution that had not passed though the filter contained the pool and was transferred to a new tube. The fluorescence of the sample could then be testing using a Fluorolog spectrophotometer in order to assess yield (pool retention rate) of the process.

2.7.8 Polymerase Chain Reaction of Selection Pools

Each round the selection pools progressing onto the next round underwent a 60 reaction PCR (polymerase chain reaction) as well as a 3 reaction negative control PCR. Rounds 1 and 2 also incorporated a 3 reaction positive control pcr using a sample of the original R0 pool. To start, forward and reverse primer sequences were diluted to a concentration of 0.2 mM with deionized water. Five master mix solutions were then formed in order to generate enough material for 75 reactions (15

reactions per master mix). The master mix solutions were each composed of 750 µL of 2xFlumag Buffer (100 mM KCl, 200 mM Tris, 2% triton x-100, pH of 9.0), 555 µL of deionized water, 120 µL of $MgCl_2$, 30 µL of dNTPs (BioShop Canada Inc.), 7.5 µL of the each of the 0.2 mM primer solutions. Once combined, these master mix solutions were vortexed briefly. To activate the mixture, 15 µL of Taq DNA Polymerase (BioShop Canada Inc.) was added to each master mix solution and mixed by pipetting the solution up and down. The master mix solutions were then distributed among PCR reaction tubes in aliquots of 99 µL each. To 60 of the PCR reaction tubes the 1 µL of the desired pool was added. In the case of the negative control reactions, 1 µL of deionized water was added. The tubes were then placed on an Authorized Thermal Cycler (Eppendorf No. 5341 K 011688). This system used the following thermal program: 94.0 °C for 10 minutes, 30 repetitions of [94.0 °C for 1 minute, 47.0 °C for 1 minute, 72 °C for 1 minute], 72.0 °C for 10 minutes, 4.0 °C for 10 minutes. Once the thermal program had run its course the contents of the positive reaction tubes were combined and placed on a speedvac to dry down. The samples were then resuspended in a 1:1 deionized water and formamide mixture.

Table 1: Primers used to amplify pools during SELEX

Primer	Sequence	Notes
5' Primer	5’- RATAGTCCCATCATTCATT	"R" refers to a Fluorescein modification
3' Primer	5’- AAAAAAAAAAAAAAAAAAAANTGACACTTGCTAATATCT	"N" refers to a Spacer Phosphoramidite 18 modification

2.7.9 Purification of PCR Product by Gel Electrophoresis

Urea based denaturing poly-acrylamide gels were prepared at a density of 12% acrylamide. This was done by mixing 31.5 g urea, 14 mL deionized water, 15 mL concentrated TBE buffer, and 23.5 mL acrylamide stock (containing acrylamide/bis-acrylamide 40% purchased from Bioshop, Burlington, Ontario, Canada). This mixture was then stirred while heating to 37°C. Once the temperature had a

chance to stabilize, the solution was then filtered though a filter paper into a fresh beaker. Next, 0.5 mL of a fresh 10% ammonium persulfate solution, as well as 35 µL of TEMED were then added to the mixture to initiate the polymerization. Once poured into the mold, the system was then allowed to sit for 30 minutes. This process produced 2 gels. While the poured gels polymerized a running buffer of 1:5 diluted TBE buffer was made up. Once suspended in running buffer, the gels were pre-run for 30 minutes at 250 V supplied by a Fisher Scientific FB1000. PCR produced DNA samples in water-formamide solutions were then heated to 95°C for 10 minutes prior to loading. The products of the negative PCR were loaded into a secondary well. Once all samples were loaded, a running ladder was loaded into another secondary well. Loaded gels were then run at 250 V for 2.5 hours. Once running was complete, the gels were photographed under UV illumination. The various sizes of produced DNA appeared as dark bands as they absorbed UV light. The band containing the purified, full-length PCR product was determined by relative location on the gel with respect to the ladder and other bands. The product band was then cut from the gel and broken into tiny pieces before being submerged into a small volume deionized water (~2 mL). These samples were then placed onto an incubator set to 37°C and 170 RPM for 24 hours. Once the purified DNA had diffused into the deionized water, the system could be filtered to remove the polyacrylamide gel fragments. This was performed using a 10 mL syringe mounted with a 0.22 µM PEG filter. Once filtered into a new tube the samples were ready for desalting.

2.7.10 Enriched Pool Clean-Up Via Desalting

Samples were introduced to the desalting filters in aliquots of 0.4 mL. The system was spun at 10,000 RPM for 20 minutes to pull the salt rich solution through the filter, leaving the DNA behind. Once the entirety of the starting samples had been aliquoted into the system, the DNA was washed with four 0.4 mL aliquots of deionized water. Once washed, the filters were flipped and the retained DNA was centrifuged into a clean tube. This sample was then quantified via UV-visible spectroscopy using an extinction coefficient of 721000 L mol^{-1} cm^{-1}.

2.8 MiSeq Sequencing

The following preparation and analysis process was carried out for SELEX rounds 4 and 5 of the novel pool. The mutant pool never reached this stage, with the exception of that which had been spiked into the novel pool.

2.8.1 PCR for Sequence Elongation for MiSeq Pool Preparation

To start, special forward and reverse primer sequences containing elongated tails for MiSeq recognition (ordered from Integrated DNA Technologies, tails designed by Illumina) were diluted to a concentration of 0.2 mM in deionized water. A Master mix solutions was then formed with enough solution to generate 15 reactions. The master mix solution was each composed 750 µL of 2xFlumag Buffer (100 mM KCl, 200 mM Tris, 2% triton x-100, pH of 9.0), 555 µL of deioinized water, 120 µL of $MgCl_2$, 30 µL of dNTPs, 7.5 µL of the each of the 0.2 mM primer solutions. Once combined, the master mix solution was vortexed briefly. To activate the mixture, 15 µL of Taq polymerase was added to the master mix solution and mixed by pipetting the solution up and down. The master mix solution was then distributed among PCR reaction tubes in aliquots of 99 µL each. To 12 of the PCR reaction tubes, the 1 µL of the desired pool was added. In the case of the 3 negative control reactions, 1 µL of deionized water was added. The tubes were then placed on an Authorized Thermal Cycler (Eppendorf No. 5341 K 011688). This system used the following thermal program: 94.0 °C for 10 minutes, 17 repetitions of [94.0 °C for 1 minute, 58-60 °C for 1 minute, 72 °C for 1 minute], 72.0 °C for 10 minutes, 4.0 °C for 10 minutes. Once the thermal program had run its course the contents of the positive reaction tubes were combined and placed on a speedvac to dry down. The samples were then resuspended in a 1:1 deionized water and formamide mixture.

Table 2. Elongating MiSeq Primers Used to Sequence Each Pool.

Pool	Primer Name	Primer Sequence
Original Novel	F1	AATGATACGGCGACCACCGAGATCTACACTCTTTCCCTACACGACGCTCTTCCGATCTRATAGTCCCATCATTCATT
	R1	CAAGCAGAAGACGGCATACGAGATCGTGATGTGACTGGAGTTCAGACGTGTGCTCTTCCGATCTTGACACTTGCTAA TATCT
Round 2 Novel Fractions 8+9 (Positive) + Nitrocellulose Retained (Positive) (+,+)	F2	AATGATACGGCGACCACCGAGATCTACACTCTTTCCCTACACGACGCTCTTCCGATCTNRATAGTCCCATCATTCATT
	R3	CAAGCAGAAGACGGCATACGAGATGCCTAAGTGACTGGAGTTCAGACGTGTGCTCTTCCGATCTNTGACACTTGCTA ATATCT
Round 4 Novel Fractions 10+11 (Positive) + Nitrocellulose Retained (Positive) (+,+)	F4	AATGATACGGCGACCACCGAGATCTACACTCTTTCCCTACACGACGCTCTTCCGATCTNNNRATAGTCCCATCATTCA TT
	R5	CAAGCAGAAGACGGCATACGAGATCACTGTGTGACTGGAGTTCAGACGTGTGCTCTTCCGATCTNNTGACACTTGCT AATATCT
Round 4 Novel Fractions 4+5 (Negative) + Nitrocellulose Retained (Positive) (-,+)	F4	AATGATACGGCGACCACCGAGATCTACACTCTTTCCCTACACGACGCTCTTCCGATCTNNNRATAGTCCCATCATTCA TT
	R4	CAAGCAGAAGACGGCATACGAGATTGGTCAGTGACTGGAGTTCAGACGTGTGCTCTTCCGATCTNTGACACTTGCTA ATATCT
Round 4 Novel Fractions 16+17 (Counter) + Nitrocellulose Retained (Positive) (x,+)	F4	AATGATACGGCGACCACCGAGATCTACACTCTTTCCCTACACGACGCTCTTCCGATCTNNNRATAGTCCCATCATTCA TT
	R6	CAAGCAGAAGACGGCATACGAGATATTGGCGTGACTGGAGTTCAGACGTGTGCTCTTCCGATCTNNTGACACTTGCT AATATCT
Round 5 Novel Fractions 4+5 (Negative) + Nitrocellulose Failed (Negative) (-,-)	F3	AATGATACGGCGACCACCGAGATCTACACTCTTTCCCTACACGACGCTCTTCCGATCTNNRATAGTCCCATCATTCATT
	R8	CAAGCAGAAGACGGCATACGAGATTCAAGTGTGACTGGAGTTCAGACGTGTGCTCTTCCGATCTNNNTGACACTTG CTAATATCT
Round 5 Novel Fractions 4+5 (Negative) + Nitrocellulose Retained (Positive) (-,+)	F3	AATGATACGGCGACCACCGAGATCTACACTCTTTCCCTACACGACGCTCTTCCGATCTNNRATAGTCCCATCATTCATT
	R7	CAAGCAGAAGACGGCATACGAGATGATCTGGTGACTGGAGTTCAGACGTGTGCTCTTCCGATCTNNNTGACACTTG CTAATATCT
Round 5 Novel Fractions 10+11 (Positive) + Nitrocellulose Retained (Positive) (+,+)	F3	AATGATACGGCGACCACCGAGATCTACACTCTTTCCCTACACGACGCTCTTCCGATCTNNRATAGTCCCATCATTCATT
	R2	CAAGCAGAAGACGGCATACGAGATACATCGGTGACTGGAGTTCAGACGTGTGCTCTTCCGATCTTGACACTTGCTAA TATCT
Round 5 Novel Fractions 16+17 (Counter) + Nitrocellulose Retained (Positive) (x,+)	F3	AATGATACGGCGACCACCGAGATCTACACTCTTTCCCTACACGACGCTCTTCCGATCTNNRATAGTCCCATCATTCATT
	R6	CAAGCAGAAGACGGCATACGAGATATTGGCGTGACTGGAGTTCAGACGTGTGCTCTTCCGATCTNNTGACACTTGCT AATATCT

2.8.2 Purification of Elongated MiSeq Pool by Gel Electrophoresis

Urea based denaturing poly-acrylamide gels were prepared at a density of 12% acrylamide. This was done by mixing 31.5 g urea, 14 mL deionized water, 15 mL concentrated TBE buffer, and 23.5 mL acrylamide stock (containing acrylamide/bis-acrylamide 40%). This mixture was then stirred while heating to 37°C. Once the temperature had a chance to stabilize, the solution was then filtered though a filter paper into a fresh beaker. Next, 0.5 mL of a fresh 10% ammonium persulfate solution, as well as 35 µL of TEMED were then added to the mixture to initiate the polymerization. Once poured into the mold, the system was then allowed to sit for 30 minutes. This process produced two gels so it could accommodate the purification of two elongated pool purifications simultaneously. While the poured gels polymerized a running buffer of 1:5 diluted TBE buffer was made up. Once suspended in running buffer, the gels were pre-run for 30 minutes at 250 V supplied by a Fisher Scientific FB1000. PCR produced DNA samples in water-formamide solutions were then heated to 95°C for 10 minutes prior to loading. The products of the negative PCR was loaded into a secondary well. Once all samples were loaded, a running ladder was loaded into another secondary well. Loaded gels were then run at 250 V for 6.5 hours. Once running was complete, the gels were placed on an imaging and photographed under UV-light. The various sizes of produced DNA appeared as dark bands as they absorbed UV light. The band containing the purified, full-length PCR product was determined by relative location on the gel with respect to the ladder and other bands. At this point it was determined whether the primers or PCR reagents had been contaminated with pool by overserving the bands produced by then negative PCR. The product band was then cut from the gel and broken into tiny pieces before being submerged into a small volume deionized water (~1 mL). These samples were then placed onto an incubator set to 37°C and 170 RPM for 24 hours. Once the purified DNA had diffused into the deionized water, the system could be filtered to remove the polyacrylamide gel fragments. This was performed using a 10 mL syringe mounted with a 0.22 µM PEG filter. Once filtered into a new tube the samples were ready for desalting.

2.8.3 Elongated MiSeq Pool Clean-Up Via Desalting

Samples were introduced to the desalting filters in aliquots of 0.4 mL. The system was spun at 10,000 RPM for 20 minutes to pull the salt rich solution through the filter, leaving the DNA behind. Once the entirety of the starting samples had been aliquoted into the system, the DNA was washed with four 0.4 mL aliquots of deionized water. Once washed, the filters were flipped and the retained DNA was centrifuged into a clean tube.

2.8.4 Quantification of Elongated MiSeq Pool by Nano-Drop Analysis

For this stage quantification of DNA was achieved through Nano-Drop Analysis (Thermo NanoDrop 1000 Spectrophotometer) due to the necessity for minimization of sample loss. After quantification, a small sample from each pool prepared for MiSeq could be combined to form a 5 µL sample of 4 nM DNA with each pool in equal representation.

2.8.5 MiSeq Sequencing

To begin the MiSeq reagent cartridge (purchased from Illumina Inc.) was thawed to room temperature. Then the 4 nM combined pool sample prepared before was mixed with 5 µL of fresh 0.2 N NaOH. The solution was mixed and places on a centrifuge at 280 x g for 1 minute. It was then allowed to sit at room temperature for 5 minutes. 990 µL of chilled HT1 (hybridization buffer provided by Illumina) was then added to the DNA solution. From this new 20 pM solution, 120 µL were drawn and placed into a new tube. The 120 µL aliquot then received 480 µL of HT1 to produce a 4 pM DNA solution.

Next, a PhiX control was made up. This was done by diluting a 2 µL sample of a 10 nM PhiX with 3 µL of 10 nM Tris pH 8.5 and 5 µL of 0.2 N NaOH. This solution was then mixed and allowed to sit at room temperature for 5 minutes. This solution was then mixed with 990 µL of HT1 and mixed. From this new 20 pM stock 120 µL was drawn and mixed with 480 µL of HT1 to produce 4 pM PhiX stock. Next,

480 µL of the 4 pM DNA solution was then mixed with 120 µL of the 4 pM PhiX stock. This solution was then injected into a the MiSeq reagent cartridge and loaded into an Illumina MiSeq.

Raw data was uploaded to Illumina Basespace for cloud storage and then extracted to a desktop terminal. Here Aptacluster software sorted and grouped the data while reducing it to sequences corresponding to the pools of interest with intact primer domains. The sorted data was then processed for meta-analysis via AptaGUI.[72,73] This meta-analysis sorted similar sequences into groups and assessed trends appearing among individual sequences and the groups over several selection pools. AptaGUI also provided measures of pool diversity and disparities among random region sizes.

2.9 Preliminary Assessment of Aptamer Candidates Via Alpha-Synuclein Aggregation Assay Under SELEX Conditions and TEM

Five final aptamer candidates selected through screening of the MiSeq data underwent this assay.

2.9.1 Incubation of Alpha-Synuclein Aggregation Assay with Under SELEX Conditions

To begin, the desired quantity of each system (Alpha-synuclein or SELEX pool) was dissolved to a concentration of 7 µM in PBS buffer. Aptamer sequences were then quantified by UV-Vis spectroscopy using absorption at 260 nm and an extinction coefficient specific to each sequence. For each aptamer candidate, a sample of was 1.4 nmol in 170 µL (7 µM) was prepared. Each was then mixed with an equal volume of diluted alpha-synuclein (7 µM). The mixed samples were then placed on an incubator at 180 RMP and 37 °C for 125 hours.

2.9.2 Ultracentrifugation

Five milliliter thermal sealing ultracentrifuge tubes were carefully loaded with density gradient layer by layer. The layers for the gradient were produced by combining OptiPrep (Sigma-Aldrich) with PBS buffer and deionized water in varying ratios. The resulting layers contain 40% PBS buffer with a varying percent iodixanol. The gradient layers used had six layers (1.0 mL of 35%, 1.0 mL 25%, 1.0 mL of 20%, 1.0 mL of 12%, 1.0 mL of 6%, 0.6 mL of 2.5%). Each tube was then loaded with the relevant sample. These samples included 5 novel aptamer candidates, a M5-15 sample run in parallel and a DNA-free alpha-synuclein control. In order to reduce the amount of air in the tubes, as well as for balancing purposes, the tubes were topped off with a small amount of the 2.5% OptiPrep solution. Once balanced, the tubes were thermal sealed using a Beckman Tube Sealer. The tubes were then mounted in to an angled mount Type 100 Ti rotor head (Beckman serial no. 97U 442) and placed in an ultracentrifuge (Beckman Optima LE-80K). Once the system was sealed and a vacuum was reached, the tubes were spun. The system spun at 100,000 x g for 6 hours. Once the run was finished the system was depressurized and the tubes were removed from the rotor head. The top of a tube could then be removed with a fresh razor blade. Layers of 1 mL each were carefully removed from the surface of the gradient and placed into individual tubes.

2.9.3 Alpha-Synuclein Aggregation Assay with Aptamer Candidates Under SELEX Conditions -Analysis of Ultracentrifuge Gradient Layers Through TEM

In order to assess the morphologies present in different layers from the density gradient, transmission electron microscopy (TEM) images were taken for select fractions. Samples were deposited on carbon coated copper TEM grids (manufactured by Electron Microscopy Sciences, Model CF300-Cu). Standard deposition was done by initial introduction of 4 µL of sample followed by a 10-minute settling period. After this period, the 4 µL samples were drawn from the grid and disposed of. The analysis of

TEM samples was performed with a FEI Tecnai G2 F20 TEM. Elemental analysis by energy dispersive spectroscopy (EDS) was performed using an Oxford AztecTEM with 80mm elemental silicon drift detector (SDD). A TEM beam voltage of 120kV was used to observe protein and DNA formations. The EDS employed a take off angle of 20 degrees.

2.10 Tabulated Summary of SELEX

Table 3. Summary of incubation protocol by SELEX round.

SELEX Round	Pools Involved	Incubation Concentration (Each Component)	Incubation Time (Hours)	Special Incubation Notes
1	-Novel	15 µM	42	Lyophilized to start incubation
2	-Mutant -Spiked Novel [Spiked with mutant and M5-15]	8.25 µM	126	Lyophilized to start incubation
3	-Mutant -Spiked Novel	3.5 µM	122	Lyophilized to start incubation
4	-Mutant -Spiked Novel	3.5 µM	106	pH tuned to 6.5
5	-Spiked Novel	3.5 µM	317	-

Table 4. Summary of ultracentrifugation, analysis and retained fraction by round.

SELEX Round	Ultra-centrifugation Gradient Used	Ultra-centrifugation Speed and Duration	Post Round Analysis Methods	Positive Fractions Used to Proceed
1	0.71 mL of 35% 2.14 mL of 25% 2.4 mL of 2.5%	50,000 x g for 1 hour	-Native PAGE -Fluorescence of ultracentrifuge layers	15+16
2	1.0 mL of 35% 1.0 mL 25% 1.0 mL of 12% 1.0 mL of 6% 1.0 mL of 2.5% 0.6 mL of 1%	100,000 x g for 20 hours	-TEM -Fluorescence of ultracentrifuge layers	8+9
3	1.0 mL of 35% 1.0 mL 25% 1.0 mL of 20% 1.0 mL of 12% 1.0 mL of 6% 0.6 mL of 2.5%	100,000 x g for 7 hours	-TEM -Fluorescence of ultracentrifuge layers	10+11
4	1.0 mL of 35% 1.0 mL 25% 1.0 mL of 20% 1.0 mL of 12% 1.0 mL of 6% 0.6 mL of 2.5%	100,000 x g for 5.5 hours	-TEM -MiSeq of Novel Pool Trial 1 -MiSeq of Novel Pool Trial 2	10+11
5	1.0 mL of 35% 1.0 mL 25% 1.0 mL of 20% 1.0 mL of 12% 1.0 mL of 6% 0.6 mL of 2.5%	100,000 x g for 6 hours	-MiSeq of Novel Pool	10+11

3 Results and Discussion

3.1 Statement of Contributions

Analysis of pre-SELEX aggregation assay was performed by Dr. Erin McConnell and Josh Callahan. Selection and assessment of within SELEX TEM images for rounds 2,3 and 4 was performed by Dr. Erin McConnell, Dr. Maria DeRosa and Josh Callahan. Analysis of MiSeq sequencing results was performed by Dr. Erin McConnell and Josh Callahan with help from Eman Hassan and Jan Hoinka. G-Quadruplex analysis by Dr. Erin McConnell and Josh Callahan. Alpha-synuclein aggregation assay with aptamer candidates under SELEX conditions TEM analysis by Dr. Erin McConnell and Josh Callahan.

3.2 Pre-SELEX Alpha-Synuclein Aggregation Assay and Gel Electrophoresis Observed the Loss of Monomeric Protein

The very first experiment conducted here was a preliminary test to assess alpha-synuclein under varied conditions, in order to estimate incubation parameters that would eliminate monomeric protein with a high level of confidence. In this experiment, alpha synuclein was introduced to PBS buffer or water (depending on experimental group) at concentrations of 15 μM, 25 μM, and 50 μM and allowed to incubate at 37 °C at 180 RPM for 16 hours. These were then administered to non-denaturing PAGE gels in varying aliquots sizes. This is illustrated by Table 5.

Table 5. Pre-SELEX Alpha-Synuclein Incubation Test 1 Gel Electrophoresis Lanes

Gel Lane:	Concentration of Alpha-Synuclein (μM)	Volume Added (μL)	Alpha-Synuclein Administered to Lane (nmol)
3	15	20	0.30
4	15	30	0.45
5	15	40	0.60
7	25	20	0.50
8	25	30	0.75
9	25	40	1.00
11	50	20	1.00
12	50	30	1.50
13	50	40	2.00

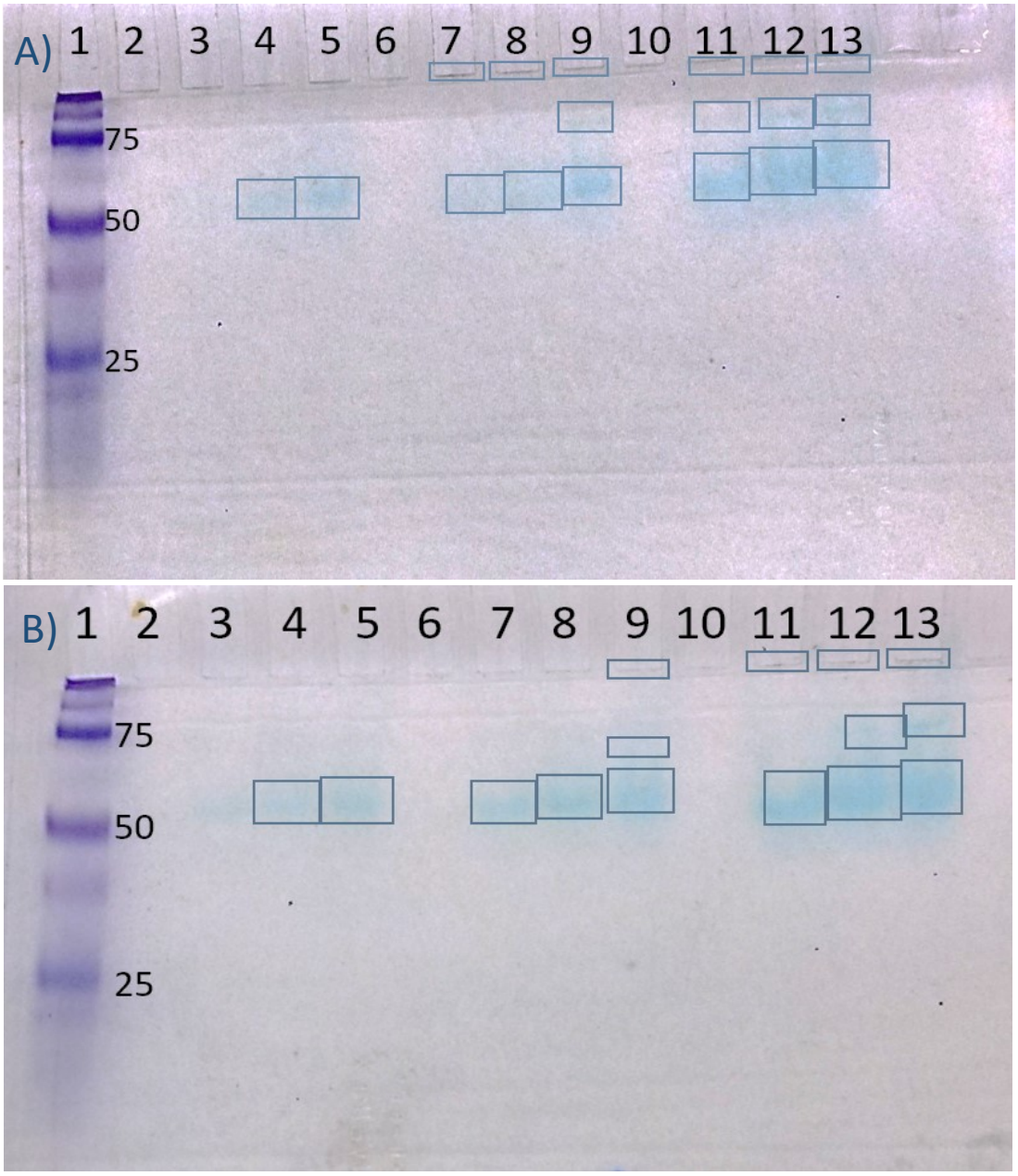

Figure 2. Gel Images for Pre-SELEX Alpha-Synuclein Aggregation Test 1. A) Non-denaturing PAGE. Deionized water as incubation solvent for alpha-synuclein. Lanes here are as depicted in Table 5. B) Non-denaturing PAGE. PBS buffer as incubation solvent for alpha-synuclein. Lanes here are as depicted in Table 5. Stains-all used to stain protein for imaging. Locations containing stained protein are indicated by boxes. Precision Plus All Blue Protein ladder appears in lane 1.

This initial test was done to assess the state of the aggregating alpha-synuclein system after the short incubation period of 16 hours. The approximate masses of stained protein morphologies (as determined by relative gel progress with respect to protein ladder) were estimated to be around the 55 kDa and 75 kDa ranges in both incubation conditions. Both gels also indicated some staining at the basins of select wells, presumably either larger aggregated morphologies or simply well boundary retention. It was also noted that no staining appeared in the area expected to yield monomeric protein (14.46 kDa). This indicated that within the 16 hour incubation, the monomeric protein had likely all undergone some level of oligomerization. Based on a 2011 paper, the prominent ~55 kDa band likely represented a stable helically folded tetramer at a mass of 57.84 kDa.[74] Less prominent bands located slightly above in the range of 75 kDa were more curious, potentially indicating the presence of a more progressive oligomerization or a potential, stable pentameric state of alpha-synuclein seldom described in literature which would have a mass of 72.3 kDa.[75] If staining seen around the lower well boundaries indicated the presence of large aggregate morphologies, they would appear to be greater than 100 kDa in mass. Because the appearance of bands around the 75 kDa mark appeared to correlate better to number of mols administered to the well, as opposed to incubation concentration, it could not be said whether the incubation concentration at 15 uM demonstrated reduced aggregation. Between the groups reflecting incubation buffer differences, no significant change was apparent. This might have been a product of the short incubation time allowed. With respect to the SELEX, this test primarily indicated that within short incubation periods, the loss of monomer in pure alpha-synuclein solutions was profound. If the literature incubation time of 120 hours was to be applied it would likely mean the oligomerization of all unprotected alpha-synuclein monomer.

The next assay was extremely similar to the first. The purpose for this assay was to assess the stability or reversibility of the oligomerization though introducing a cooling stage to the incubation and analyzing the system under both non-denaturing PAGE and urea based denaturing PAGE. The incubation

processes employed started with a 16 hour incubation of protein in PBS buffer at 37 °C and 180 RPM. The solution was then placed at 4 °C for 24 hours. Two incubation concentrations (25 and 50 uM) were used and 20 uL were administered to each lane.

Table 6. Pre-SELEX Alpha-Synuclein Incubation Test 2 Gel Electrophoresis Lanes

Gel Lane:	Concentration of Alpha-Synuclein (µM)	Volume Added (µL)	Mols of Alpha-Synuclein Administered to Lane (nMol)
3	25	20	0.50
5	50	20	1.00

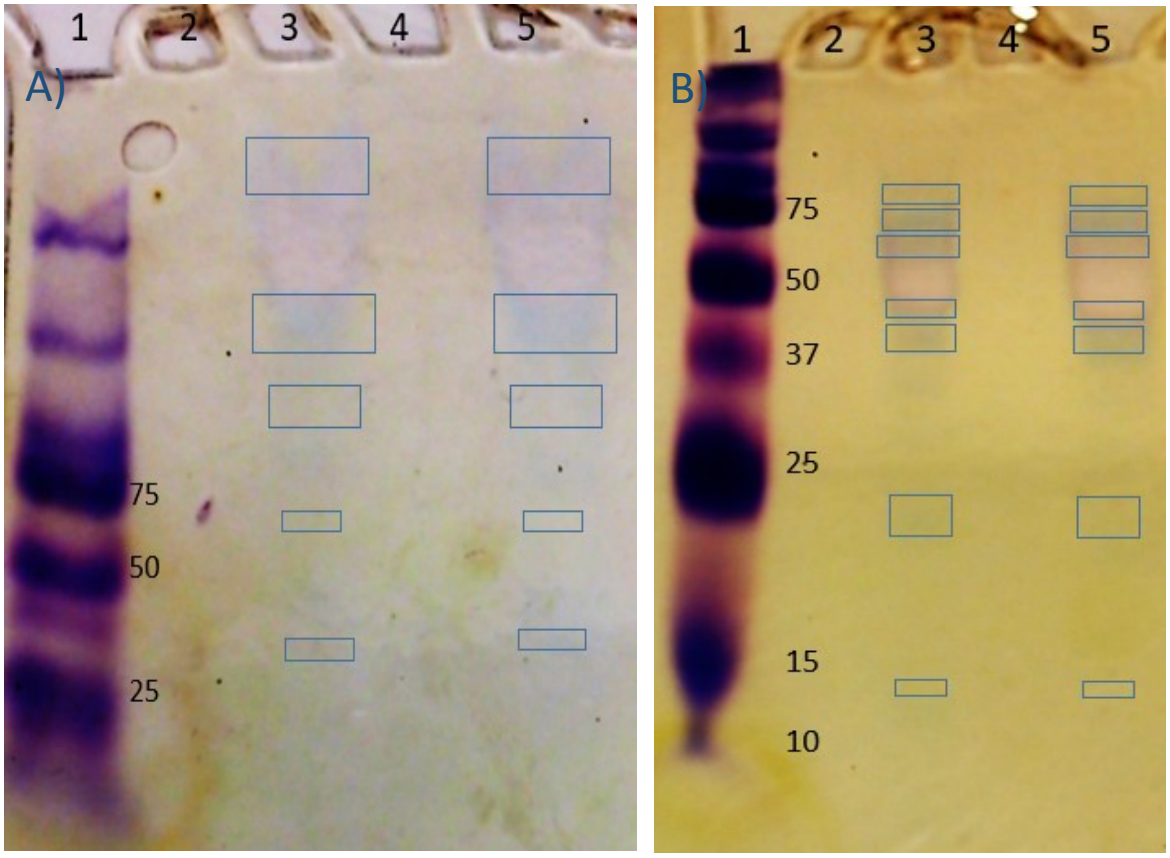

Figure 3. Gel Images for Pre-SELEX Alpha-Synuclein Aggregation Test 2. A) Non-denaturing PAGE. B) Urea based denaturing PAGE. Lanes here are as depicted in Table 6. Stains-all used to stain protein for imaging. Protein appears blue likely due to a capacity for alpha-synuclein to accommodate Ca^{2+} binding. Locations containing stained protein are highlighted by boxes. Precision Plus All Blue Protein ladder appears in lane 1.

In the non-denaturing gel, (Figure 3 A) bands appeared near 35 kDa, 58 kDa, 120 kDa, 160 kDa, and one at 300+ kDa. The urea-based denaturing PAGE yielded bands at about 14 kDa, 23 kDa, 39 kDa, 46 kDa, 58 kDa, 68 kDa, 74 kDa, and 80 kDa. These results indicate that, by using a urea based denaturing gel, a small fraction of the oligomerized protein can return to a monomeric state represented by the band appearing at the 14 kDa mark in Figure 3.2 B) (monomer mass of 14.46 kDa). These results also indicated that by introducing a cooling phase to the incubation, a more diverse series of morphologies emerged likely though oligomeric growth and subsequent fragmenting. Allowing the protein to permeate further into the gel, allowed for the resolution of larger morphologies in Test 2 than with Test 1. Overall, this test indicated that SELEX incubations and methods of morphology partitioning should be free of denaturing compound due to the theory that, if the system were to generate new monomer during the partitioning phase, it could allow for new targets for aptamer binding that can accommodate aptamer retention based solely on monomer binding. This form of retention could undermine the goal of the SELEX, which required aptamers selected to not only bind to small alpha-synuclein morphologies (monomer as an ideal), but also prevent their assimilation into growing oligomeric bodies. Aptamers that simply bound to small alpha-synuclein morphologies after the incubation phase, would not have to demonstrate the capacity to prevent aggregate growth in order to be retained in the enriched pool.

3.3 Development of New SELEX Method Towards Aptamers Which Inhibit Alpha-Synuclein Aggregation

After the pair of preliminary pre-SELEX aggregation assays provided a basic understanding of the alpha-synuclein aggregation system and its potential limitation, a novel SELEX method could be developed. The SELEX method developed would employ the aggregation of alpha-synuclein while ensuring that aggregation was not undone by denaturing agents.

At its core, this novel SELEX method functions by slowly eliminating the target of the positive selection (monomeric alpha-synuclein), while it is replaced by the counter selection target (aggregated alpha-synuclein morphologies). As the target of the positive selection is slowly eliminated, aptamers must bind with high affinity while preventing their bound target (monomeric alpha-synuclein) from undergoing aggregation. Only by accommodating this feat can they be retained though a partitioning by size stage (ultracentrifugation applied in this work). The fraction limited to aptamer candidates which managed to retain intact monomer then undergoes a second partitioning stage based on target affinity (nitrocellulose filtration applied in this work). By applying next generation sequencing (MiSeq) and modern data sorting software, strong aptamer candidates can be studied and chosen through common meta analysis parameters.

Naturally, this core method was supplemented by additional processing steps, optimization, and within SELEX pool tracking and testing, in order to form the full SELEX experiment conducted. The full process behind each SELEX round is described below in Figure 4.

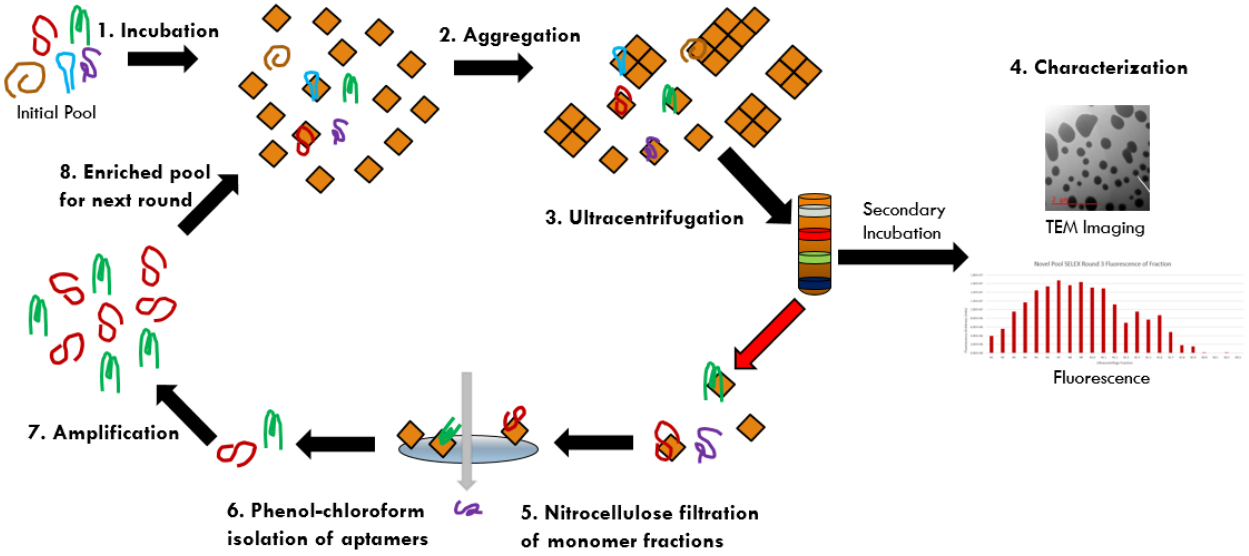

Figure 4. SELEX Method Developed and Employed. Here, monomeric synuclein units are represented by brown squares. Step 1 combines alpha-synuclein monomer with DNA aptamer pool. Step 2 allows monomer to aggregate. Step 3 partitions the various morphologies of alpha-synuclein and aptamer-protein complexes by ultracentrifugation. Step 4 is the analysis of the morphologies of alpha-synuclein and DNA aptamer concentrations in each ultracentrifuge gradient fraction. Step 5 is the partitioning of bound from unbound (to protein) aptamers. Step 6 is phenol-chloroform extraction and ethanol precipitation reactions to remove protein from the aptamer pool. Step 7 is the PCR amplification of the retained pool of aptamers. Step 8 illustrates this amplified pool entering the next SELEX round at step 1.

The SELEX experiment conducted here contained nine steps, with the ninth being MiSeq sequencing. The other eight steps were conducted in a repeating cyclic circuit five times. Each cycle of the first eight steps was referred to as a SELEX round.

Starting with step 1, incubation, a pool of randomized sequences was introduced to an equal quantity of alpha-synuclein monomer. As this incubation progressed step 2, aggregation, began. Here alpha-synuclein monomer was converted to larger oligomeric forms, also known as aggregates. This stage always includes an extended period of time where the incubating system was placed at 37 °C and

shaken in PBS buffer to represent the relevant physiological conditions of the final therapeutic application of the aptamers. Rounds 1, 2, and 3 all incorporated lyophilization to initiate the incubation step and accelerate aggregation. Round 4 produced accelerated aggregation though the acidifying of the incubating solution. Once sufficient time had passed that all the free monomer (those not bound to an aptamer) had likely been removed by aggregation, the process moved onto step 3.

Step 3 was the first partitioning step to the SELEX round. Here, an ultracentrifuge density gradient was made up by using OptiPrep, and then loaded with the incubated samples. Once spun at 100,000 x g for several hours, the density gradient was carefully divided up into fractions. Each fraction was unique with regards to the types of DNA and alpha-synuclein systems present within it. Monomeric alpha-synuclein and unbound aptamer candidates were expected to appear in the upper, less dense fractions (typically fractions 1-5). A piece of these upper fractions was used to as the negative (-) selection. Below this, mid-gradient fractions were expected to hold a combination of the desired monomeric alpha-synuclein-aptamer complexes, as well as dimerized alpha-synuclein (fractions varied by gradient employed, but fractions 10 and 11 were used in rounds 3 through 5). A piece of these mid-gradient fractions was used as the positive (+) selection. Lower fractions were expected to contain larger oligomeric protein formations and aptamer candidates with high affinity for them (fractions 15-25). A piece of these lower gradient fractions was used as the counter (X) selection.

Step 4 took the various ultracentrifuge fractions and characterized them for the different alpha-synuclein morphologies and the quantity of DNA present after a second secondary incubation. Characterization of alpha-synuclein morphologies was performed by either non-denaturing PAGE (SELEX round 1) or TEM imaging (SELEX rounds 2, 3, and 4). TEM imaging following a secondary incubation provided within SELEX evidence of the functioning of enriched aptamer pools to prevent further aggregation of alpha-synuclein. After ultracentrifugation, the morphologies of alpha-synuclein present in any given fraction of the pool containing sample should be roughly the same size as those present in the

alpha-synuclein control. However, after a secondary incubation, new aggregation is observed and the differences (observed by TEM) between the pool containing sample and the alpha-synuclein control become dramatically enhanced.

Determination of the quantity of DNA aptamers present was conducted during rounds 1, 2, and 3 via fluorescence spectroscopy (aptamers within the pool were labelled at the 5' end with fluorescein). Once these results were assessed, and the fraction containing monomeric alpha-synuclein bound aptamers was determined, this fraction progressed to step 5. For rounds 1 and 2, this determination was used as a method by which Optiprep density gradient was optimized. What started as a density gradient containing only three layers of varying density, quickly became a gradient of six layers. The added layers were strategically placed to accommodate enhanced partitioning in the areas where the system of interest migrated to. This ensured that the partitioning by ultracentrifugation was as selective as possible.

Step 5 of the SELEX made up the second partitioning step. Here, a primed nitrocellulose membrane was used to separate the aptamers candidates in the fraction of interest which remained bound to their monomeric protein, from those which were no longer bound. Because of the affinity for proteins for the membrane, aptamers which were protein bound were retained by the membrane. Because DNA does not have a high affinity for the membrane, the unbound aptamers passed right through. Therefore, those aptamers which were now unbound from their monomeric protein were not retained by the membrane. After being heat shocked and bathed in a urea based denaturing buffer, the aptamers were released from the membrane and moved on to step 6.

Step 6 entailed the combination of a standard phenyl-chloroform extraction and a subsequent ethanol precipitation reaction. This step simply served to remove the monomeric alpha-synuclein from

the aptamer pool. Completion of this step meant that the monomeric protein would not interfere with the aptamer pool during the next step of the round (PCR).

Step 7 was a simple PCR consisting of 60 reactions. This step amplified the pool, replicating each successful aptamer candidate many times over. This provided enough aptamer pool to accommodate the following round of SELEX.

Step 8 was simply the clean-up of the PCR products via urea based PAGE and desalting, as well as the quantification of the aptamer pool via UV-vis spectroscopy. Once this step was completed, the resulting enriched pool was ready to enter the next SELEX round starting back at step 1.

Once sufficient rounds had passed, MiSeq sequencing was conducted for various pools of interest. MiSeq sequencing is a form of next-generation sequencing developed by Illumina Inc. The process is broken down into four steps. The first step is to add special tails to the ends of the aptamers that require sequencing. These tails contain two domains: one domain which allows the aptamer sequences to be tethered down, and a second domain which contains a special barcode to identify which pool the aptamer was taken from. These tails are added though PCR to form elongated aptamers. The second stage is the administration of the elongated aptamers to a MiSeq flow chip. The elongated aptamers become tethered to the chips surface through binding to small DNA fragment complementary to the tail mounted to the aptamers. Here each sequence is then replicated several times while bound to the surface. All the replicates of the sequence remain bound locally to form a cluster. The third step is the sequencing of the clusters. This is done by sequencing through synthesis, where the complementary version of the aptamer is built up along the aptamer itself using special fluorescent nucleotides. Each time a new base is added, the instrument detects the unique colour of light emitted from the base and determines the aptamer's nucleotide base sequence as the complement is built. Once each aptamer sequence has been determined, the MiSeq's software groups the reads into the different aptamer pools

using the barcode on each aptamer, and exports the data as the final step.[76] This data is then further treated using AptaCluster software, and AptaGUI software.[73,72]

This SELEX method provides several benefits over some traditional methods. In this method, the aptamer-target interaction occurs free in solution, opening all potential binding domains of the target and preventing potential deviations in target morphology that could accompany target immobilization. SELEX conditions attempt to mimic those of the final application as closely as possible in order to eliminate the possibility of generating aptamers whose affinity is specific to unrelated ambient conditions (pH, salinity, etc.). On this basis, accommodating a target that is free in solution is often preferred. Unlike more traditional SELEX method where counter SELEX steps are run separate to the positive selection, this SELEX method provides direct competition between the two targets. In many cases, this direct competition is likely better related to the conditions within the aptamer's final application. This is because counter section targets are often similar chemical species found ambient to the primary target. Another benefit to this method is the capacity to tune the stringency of each SELEX round without necessarily altering the concentrations of the target and aptamer pools, which is often preferred. In this SELEX, to increase the stringency for a given round, one must simply allow the system to incubate for an increased amount of time or introduce practices to accelerate aggregation. By accelerating aggregation or providing more time for aggregation to occur, it is possible to selectively retain stronger aggregation inhibiting aptamers. In the case of this SELEX, varied incubation times were coupled with rounds using lyophilization to induce aggregate seeding, or others which tuned the ambient pH to accelerate aggregation. However, once again, it is important to avoid incorporating methods which may cause the selection conditions to deviate too far from what is relevant to the final application.

While this SELEX incorporated ultracentrifugation and nitrocellulose filtration as the partitioning methods, a huge variety of alternative methods exist. Ultracentrifugation could in theory be replaced by

any number of size or mass based partitioning procedures such as high performance liquid chromatography, gel electrophoresis, or size exclusion filtration techniques. Nitrocellulose filtration could in theory be replaced with anything within an ever-growing range of interesting SELEX partitioning methods. However, nitrocellulose often a preferred method when working with protein targets for its effectiveness, speed, and efficacy.[77]

3.4 Within SELEX Analysis:

SELEX rounds 1, 2 and 3 employed analysis of the extracted ultracentrifugation fractions via fluorescence spectroscopy. These rounds of SELEX were significant because they each represented a significantly varied ultracentrifugation gradient and centrifuge run duration. This analysis, coupled with a quick assessment of the relative ladder positioning in a control ultracentrifuge gradient (used in rounds 2, 3, and 4), allowed for the tracking of the labelled DNA and determination of which fractions contained aptamer bound protein systems. Figures 5, 8, and 10 represent the fluorescent data acquired for each of the three rounds.

SELEX round 1 also employed the use of non-denaturing PAGE to assess the relative placement of the generated alpha-synuclein morphologies within the gradient and coordinated these results with a fluorescent analysis of labeled DNA within the ultracentrifuge gradient fractions.

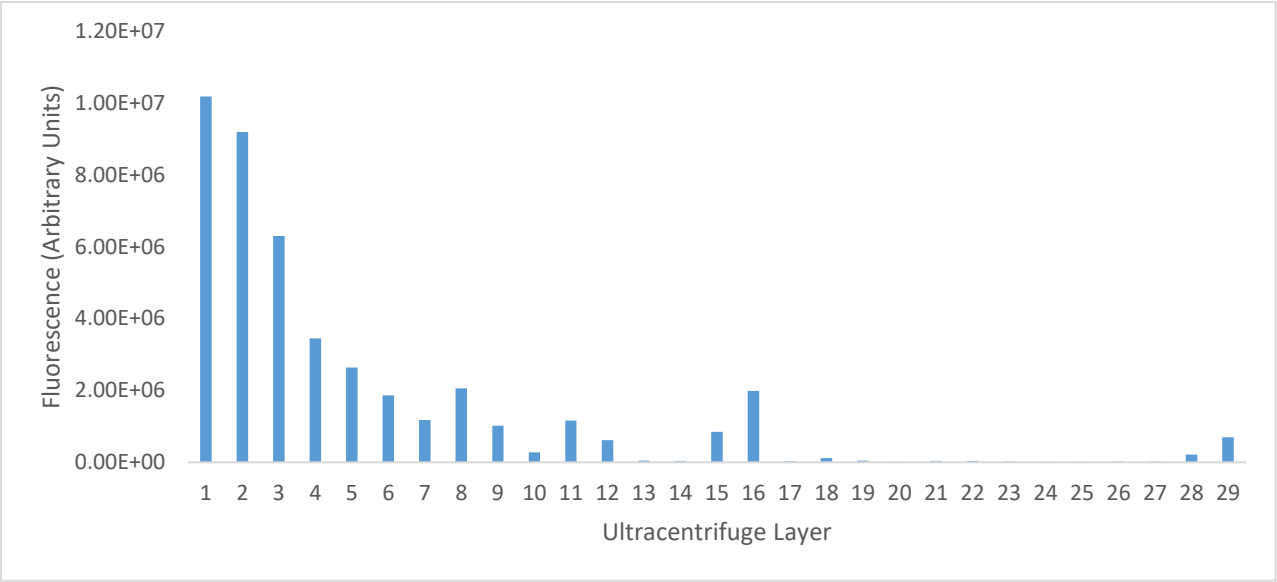

Figure 5. Fluorescent analysis of novel pool's ultracentrifuge fractions for SELEX round 1. Fraction 1 represents the upper most layer of the ultracentrifuge gradient containing systems with the smallest molecular mass (monomeric alpha-synuclein and unbound DNA sequences).

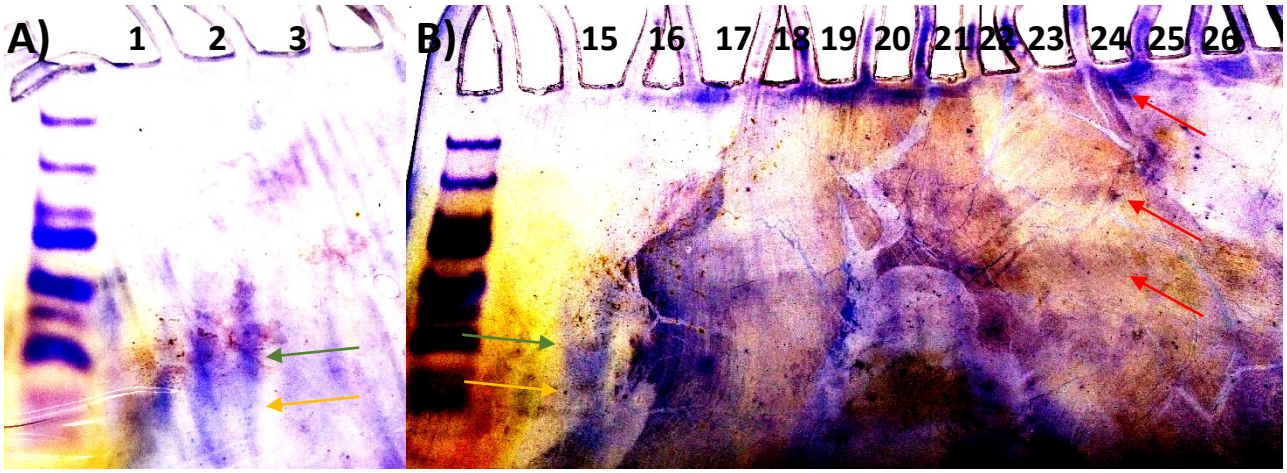

Figure 6. Non-denaturing PAGE of density gradient fractions from novel pool SELEX round 1. A) Monomeric protein (yellow arrow) and DNA bands (green arrow) in fractions 1, 2, and 3. B) Monomeric protein (yellow arrow) and DNA bands (green arrow) from fractions 15 and 16. Potentially less resolved bands of higher masses in later fractions (red arrows).

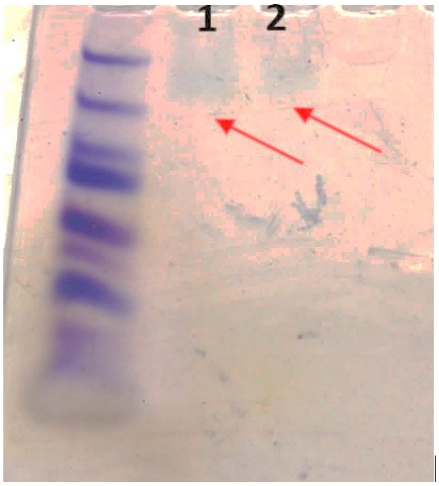

Figure 7. Non-denaturing PAGE of density gradient fractions from uninhibited alpha-synuclein control for SELEX round 1. Red arrows indicate locations of the staining of a small amount of a large oligomerized alpha-synuclein morphology present in fractions 1 and 2.

For round 1, no protein ladder was run as an ultracentrifuge gradient control. Instead, samples of fractions taken from the ultracentrifuge were analyzed by non-denaturing gel electrophoresis to assess the species present in the fraction. For this round, fractions 15 and 16 were selected as the

round's positive pool based on the premise that those fractions indicated a strong presence of fluorescent DNA outside of the clear abundance of unbound DNA in fractions 1, 2, and 3. The only manner with which DNA in the pool should be able to progress that far into the ultracentrifuge gradient is upon target binding. This assessment was also backed up by the non-denaturing gel electrophoresis (Figure 7) which took place after an 18 hour time period at 4 °C. The non-denaturing PAGE assay demonstrated the presence of a great deal of monomer in upper pool fractions (fractions 1 and 2), as well as the retention of monomer in pool fractions 15 and 16. Other fractions failed to reveal monomer through staining. These results, coupled by the total disappearance of monomer from a control run in parallel containing no DNA, indicated that fractions 15 and 16 must contain DNA generating inhibition of aggregation of the bound alpha-synuclein monomer.

The analysis of the non-denaturing PAGE (Figures 6 and 7), yielded an intricate profile of the SELEX incubation and the efficiency of the ultracentrifugation. Post ultracentrifugation, monomer alone existed in the upper fractions (1 and 2) of both the pool containing sample and the alpha-synuclein control. In the pool containing fractions 15 and 16 two separate systems existed, one being tetrameric oligomers and the other being pool bound monomer. After 16 hours at 4 °C, the small amount of monomeric protein in the upper fractions (1 and 2) of the alpha-synuclein control underwent some degree of oligomerization. After 16 hours at 4 °C, the small amount of tetrameric protein in fractions 15 and 16 of the alpha-synuclein control quickly underwent aggregation as a seeded system removing itself from the scope of the gel with its high molar mass. Alpha synuclein monomer present in the pool containing fractions resisted aggregation. Much of the small oligomeric alpha-synuclein morphologies located in fractions 15 and 16 containing pool likely aggregated as it was unprotected by DNA as restricted by the mass limits present in these layers of the ultracentrifuge gradient. These small protein morphologies also likely did not appear clearly in the gel as an effect of the poor gel staining or its limited presence following initial incubation in the presence of pool DNA. In addition to some poorly

resolved tetramer, some later (heavier) fractions containing pool appear to yield what appears to be larger aggregate formation around the 125 kDa mark. Also of note is the sporadic staining of the injections wells, primarily in those of the later fractions of the pool containing samples, could indicate the presence of larger aggregates. The alpha-synuclein control sample only generated what appeared to be large aggregates within the upper most gradient fractions. These large aggregate morphologies likely formed after ultracentrifugation from monomer, as a result of the secondary, post-ultracentrifuge incubation. Protein within other fractions of the control system likely aggregated to such a degree they could not be observed within the gel.

Several issues existed with this original method of aggregate tracking. The distinct shape of the alpha-synuclein band within the pool containing gel's lighter fractions was likely the result of DNA presence. DNA can confound the staining of this protein by interacting with Stains-all to become blue. While the "monomer" band spans from the 12 kDa to 22 kDa range, it is likely that the portion making up the upper region of the band may fall within the range where we might expect DNA (20.5 kDa range). This is the last time that Stains-all is used for applications containing both DNA and alpha-synuclein. Because OptiPrep demonstrates a high capacity for absorbance through the 260 nm domain, UV imaging of these gels were impossible. Because this assay takes place after ultracentrifugation, the two samples are differentiated by altered rates of aggregation. The control versus pool systems contained very different relative quantities of monomer, oligomer, and fibrils. The effect of the short 16 hour incubation time is likely exaggerated by these varied concentrations. Poor staining and de-staining of the gels was likely related to the presence of OptiPrep, as the indicated by the unusual staining of the running path of many of the wells used.

Just as round 1 did, SELEX round 2 also employed fluorescent analysis of its ultracentrifuge gradient layers as a method for tracking the aptamer pool Figure 8). However, in place of non-

denaturing PAGE, round 2 incorporated transmission electron microscopy (TEM) as the method of tracking the various alpha-synuclein morphologies within the ultracentrifuge gradient.

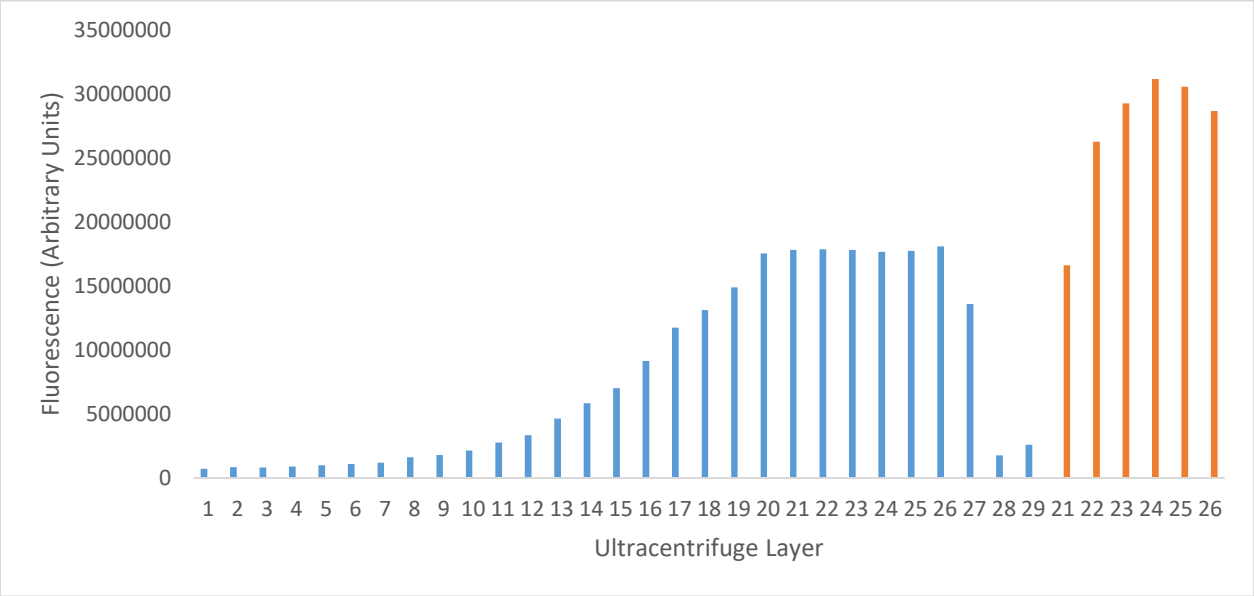

Figure 8. Fluorescent analysis of the M5-15 control's ultracentrifuge fractions for SELEX round 2. Fraction 1 represents the upper most layer of the ultracentrifuge gradient containing systems with the smallest molecular density. Bands in orange indicate a re-examination of select fraction to accommodate for suspected detector maximization.

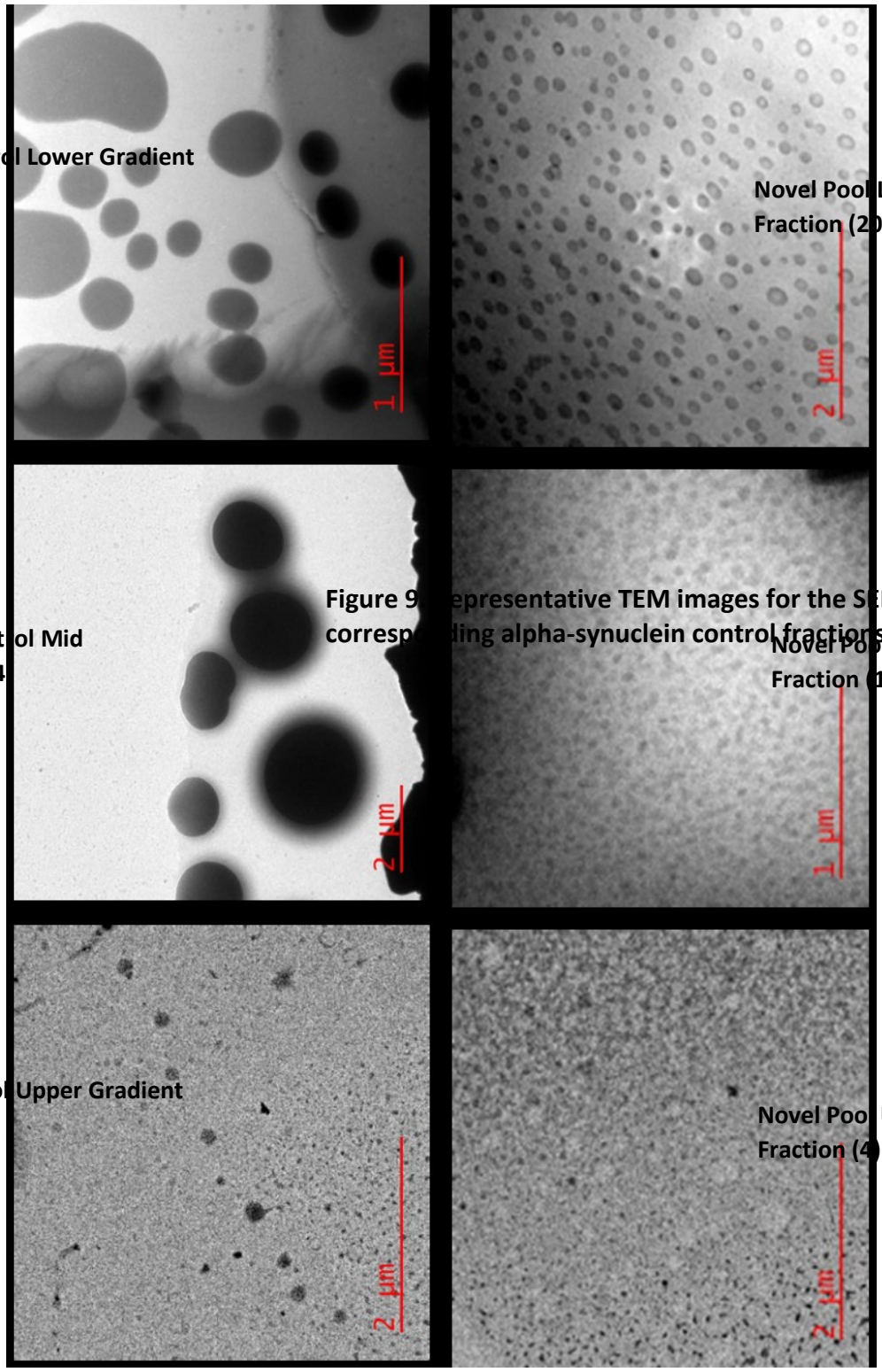

Figure 9 epresentative TEM images for the SELEX round 2 novel pool's ult
corresp ding alpha-synuclein control fractions. Additional images provide

SELEX round 2 incorporated several new components. In addition to a switch from gel electrophoresis to TEM imaging (Figure 9) for protein morphology profiles, the mutant pool was added to the SELEX, and the established M5-15 aptamer was tested for its potential capacity to prevent aggregation (results discussed in section 3.7). It was also during this round that our novel aptamer pool was spiked with both mutant pool and M5-15. As noted before, this round also brought with it a new ultracentrifugation protocol and new less concentrated incubation system. This new less concentrated incubation system sought to improve the stringency of the SELEX round by forcing potential aptamers to have stronger affinity towards their target in order to be retained. TEM images of the various fractions from the given incubation systems reveal that the density gradient and ultracentrifuge parameters are generating the desired result with larger morphologies distinctly more abundant in lower (heavier) fractions. It should be noted that a 130 hour incubation took place at 4 °C prior to the deposition of the TEM samples. This incubation may have served to enhance the differences between pool containing and fractions. TEM images indicate the greatest degree of aggregation within the alpha-synuclein control as expected.

A couple of factors impeded the full capacity for TEM's in this assay. First was the overwhelming presence of dry OptiPrep (iodixanol) on the surface of grid which formed a thick sheet. This made it quite difficult to image systems properly, and especially in later (heavier) fractions which contained a much higher level of iodixanol. In some cases, the only locations capable of accommodating images were between the cracks in the iodixanol film. Another issue arose from the limited capacity to use EDS. Relevant elements for detection of DNA are typically phosphorus and on occasion nitrogen. In this system, both of these signals are confounded. First by the presence of phosphorus in the incubation's buffer and then by nitrogen found within iodixanol. The only thing remaining as a viable target for EDS is the sulphur found in several of the amino acids making up the alpha-synuclein protein.

As noted by Figure 8, this round saw a shift towards the heavier fractions with respect to the relative abundance of fluorescent DNA in each fraction. However, this data was drawn from M5-15 ultracentrifuge fractions analysis in an effort to retain as much of the pool fractions as possible. It was only later discovered that M5-15 had a distinct affinity for larger morphologies of alpha-synuclein. This affinity would explain the apparent shift in the fluorescent profile for the round. This effect seemed to correct itself in round 3 where novel pool fractions were used to generate the fluorescent profile (Figure 10).

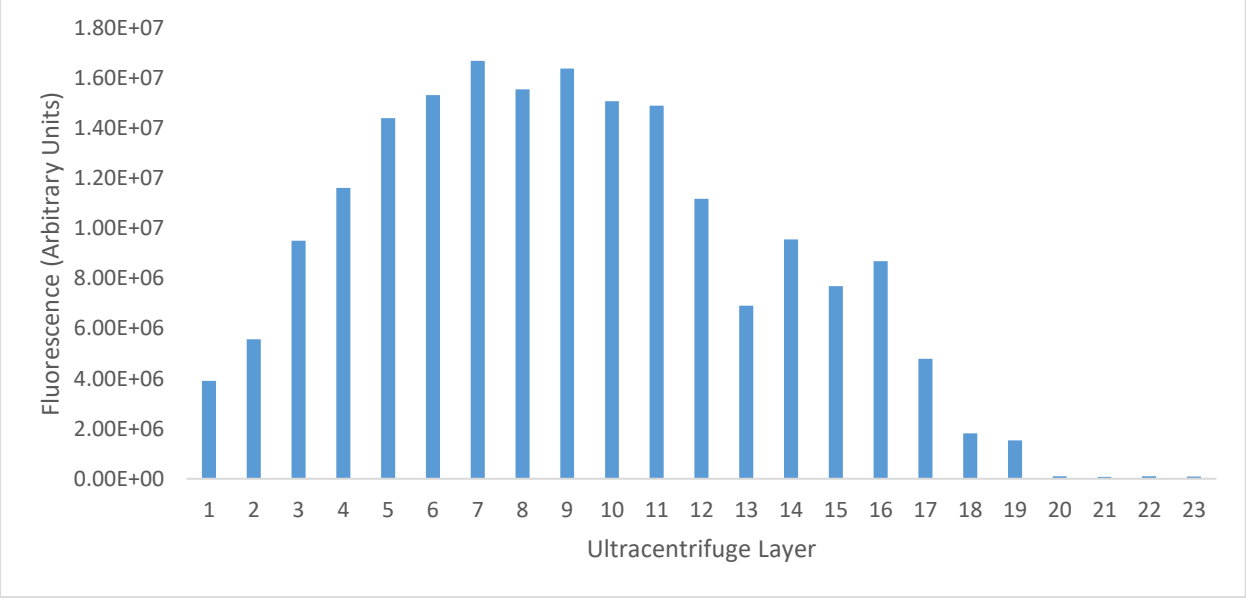

Figure 10. Fluorescent analysis of the novel pool's ultracentrifuge fractions for SELEX round 3. Fraction 1 represents the upper most layer of the ultracentrifuge gradient containing systems with the smallest molecular density.

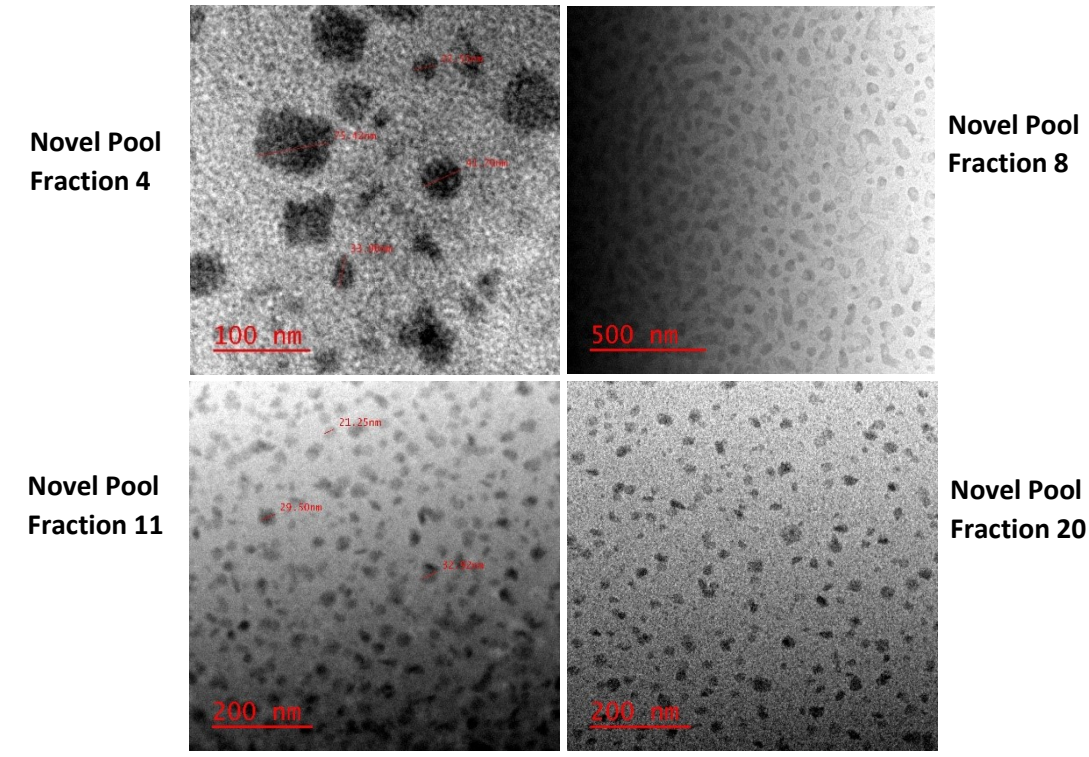

Figure 11. TEM images for select density gradient fractions from SELEX round 3's novel pool. Selected images are representative of the collection of images taken.

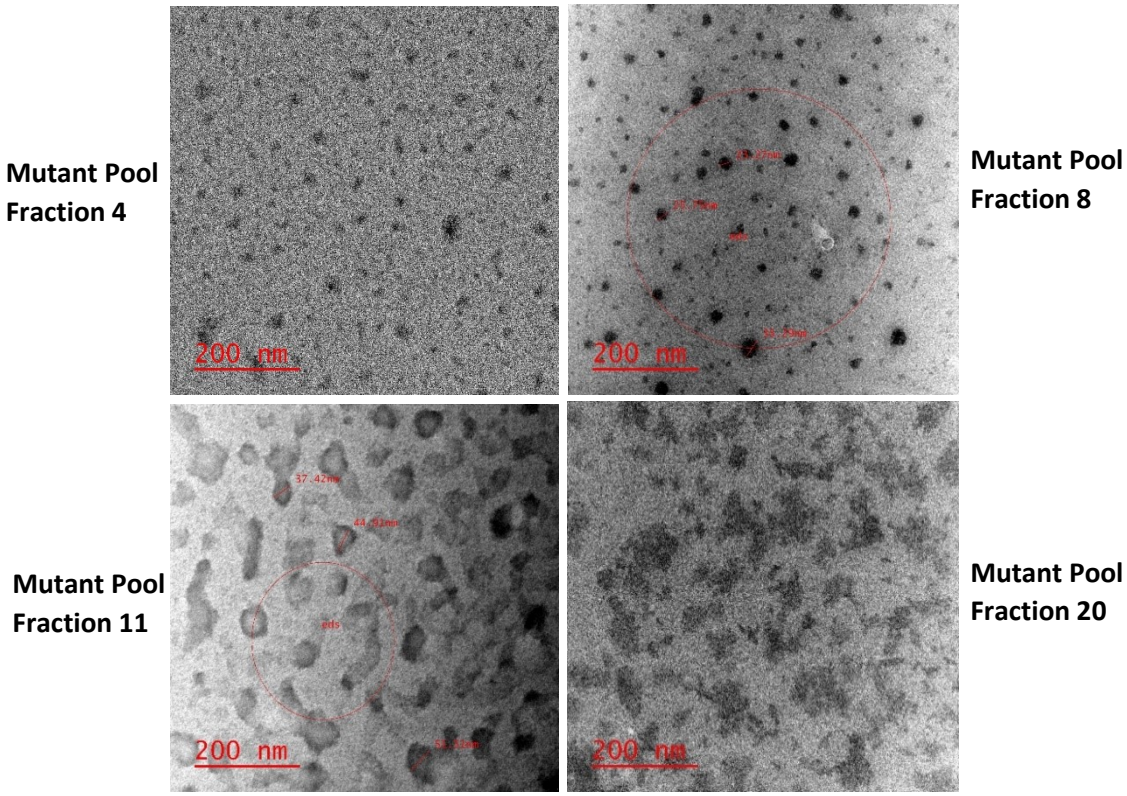

Figure 12. TEM images for select density gradient fractions from SELEX round 3's mutant pool. Selected images are representative of the collection of images taken.

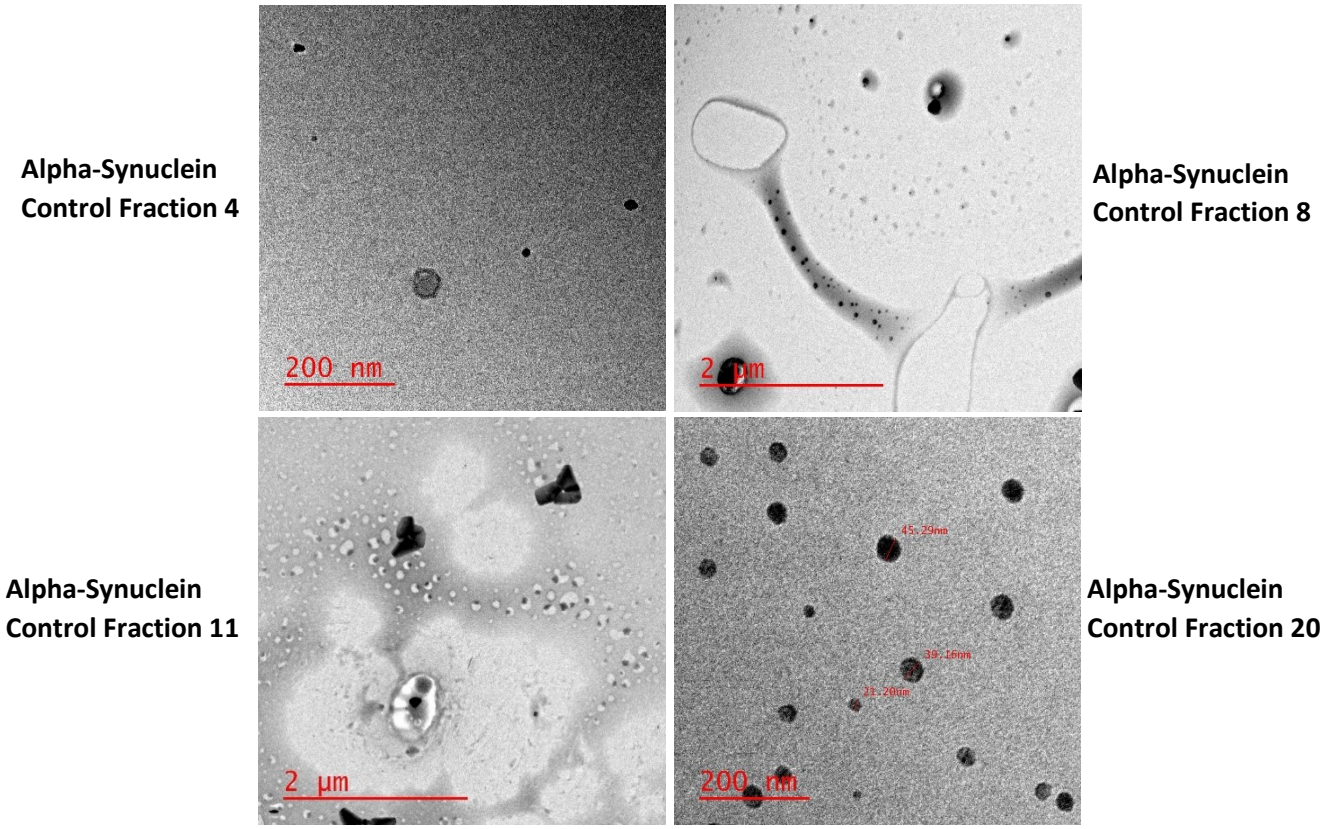

Figure 13. TEM images for select density gradient fractions from SELEX round 3's alpha-synuclein control. Selected images are representative of the collection of images taken.

SELEX round 3 introduced a new ultracentrifuge gradient as well as more stringent incubation conditions in which the concentration of both SELEX pool and alpha-synuclein were reduced. These results demonstrate what was to be expected from the ultracentrifugation with the exception of the samples from the heavy fractions. Unlike round 2 where the samples had an extended secondary incubation period, these samples were plated for TEM shortly following partitioning by ultracentrifugation. The TEM images (Figures 11,12, and 13) illustrate what was expected, with very small formations present in the lighter ultracentrifuge fractions. The only exception to the expected results was the odd lack of large morphologies in the heavier fraction. The most plausible explanation for the apparent lack of large aggregate formations within the heavy density gradient fractions (20) is the limited capacity for imaging that results from the high level of Optiprep film coverage in these very dense later fractions. The imaging space on these samples is usually limited to domains where the

Optiprep film has cracked and receded during drying. This process may create a bias towards revealing smaller alpha-synuclein morphologies by better holding larger morphologies within the film. It is also possible that the mechanical energy produced by the film cracking might be enough to generate some fragmentation of aggregate morphologies. This film cracking is illustrated in Figure 14.

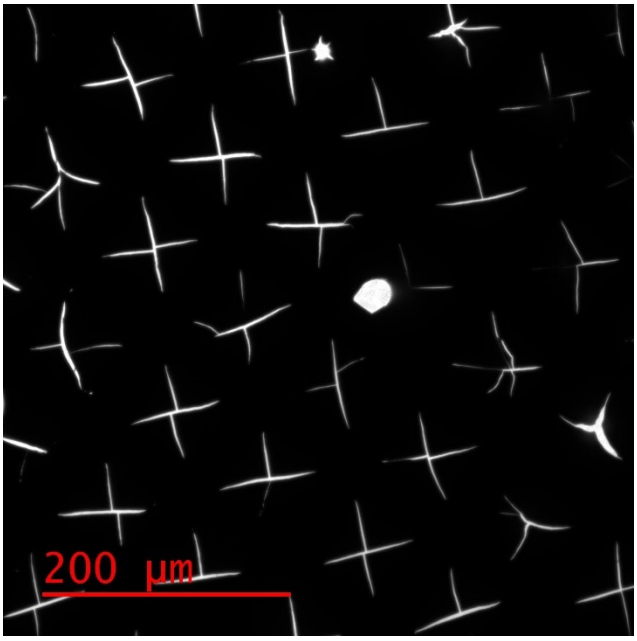

Figure 14. TEM Image of TEM grid deposited with SELEX round 4 novel pool's density gradient fraction 16 (counter fraction). Optiprep film appears black at this distance, while the locations available for imaging are the white cracks in the film. The surface of the TEM grid is divided into small windows which are visible via the overarching pattern of squares.

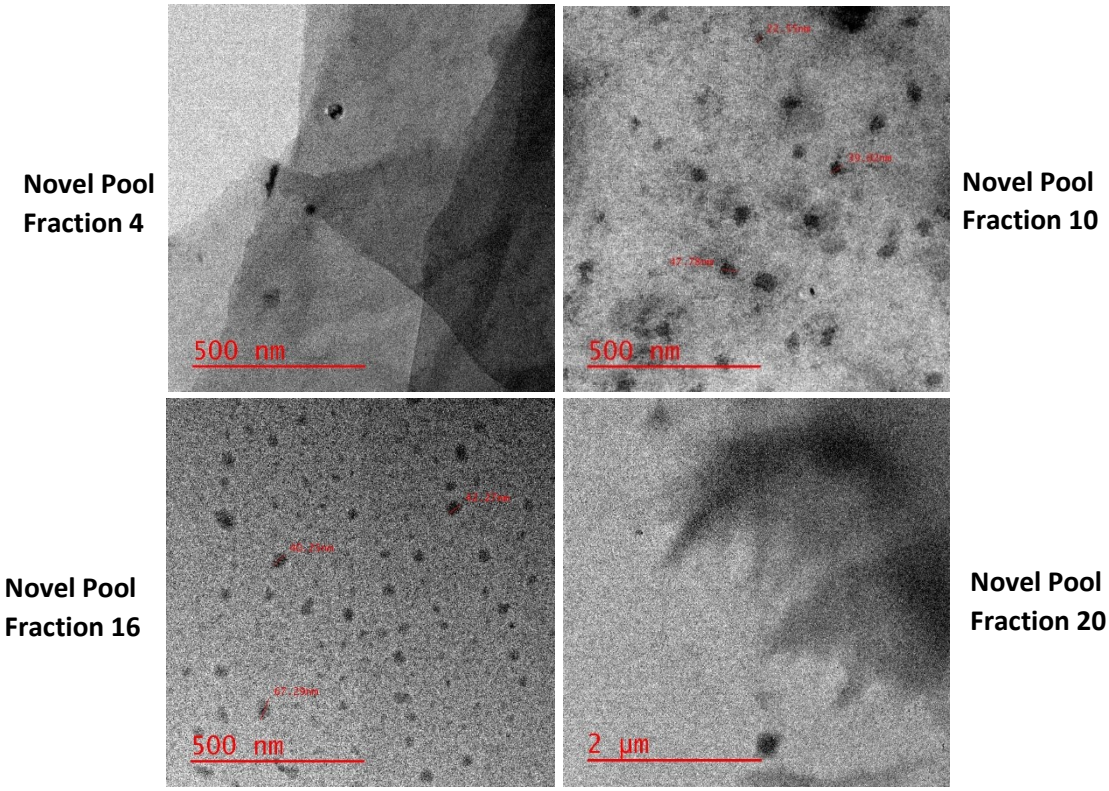

Figure 16. TEM images for select density gradient fractions from SELEX round 4's novel pool.

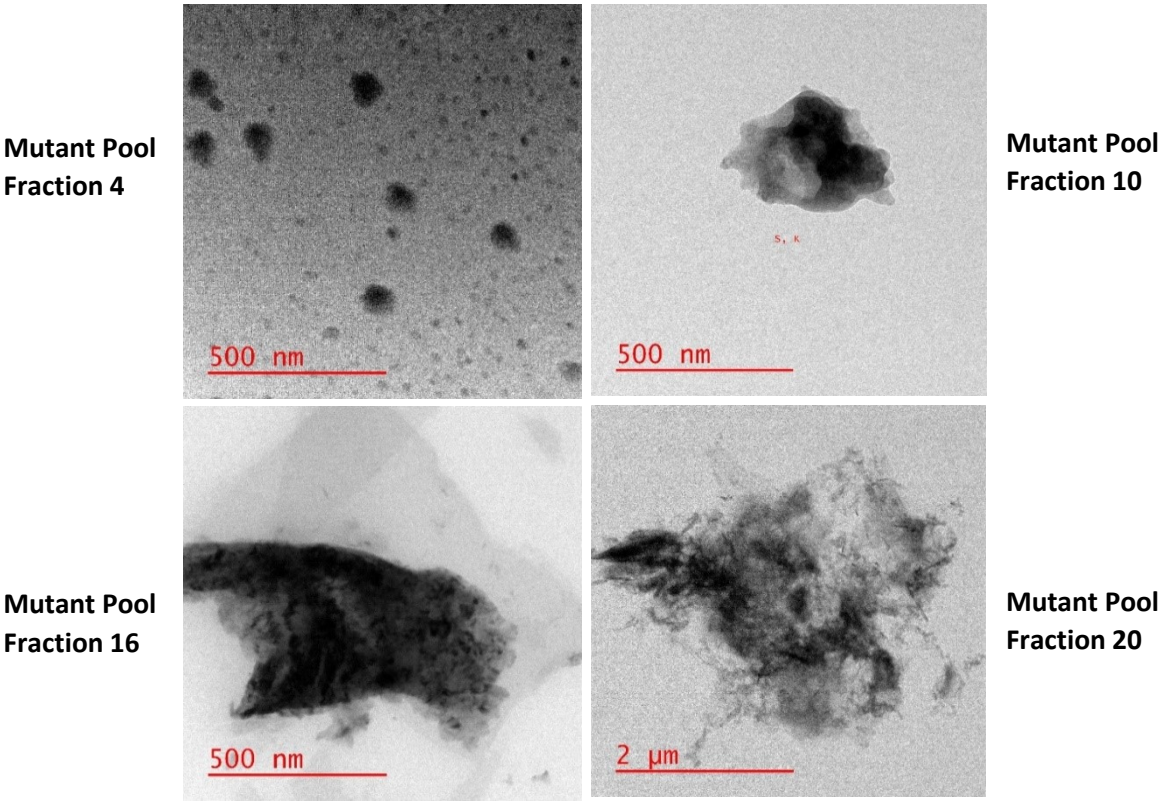

Figure 15. TEM images for select density gradient fractions from SELEX round 4's mutant pool.

Alpha-Synuclein Control Fraction 4

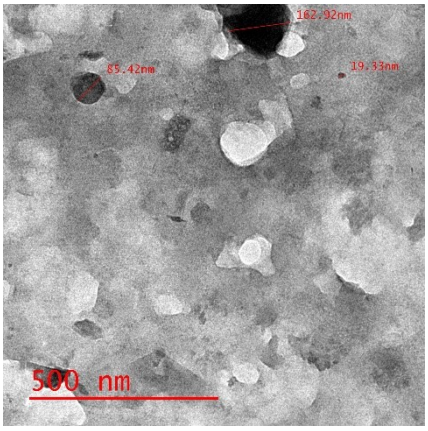

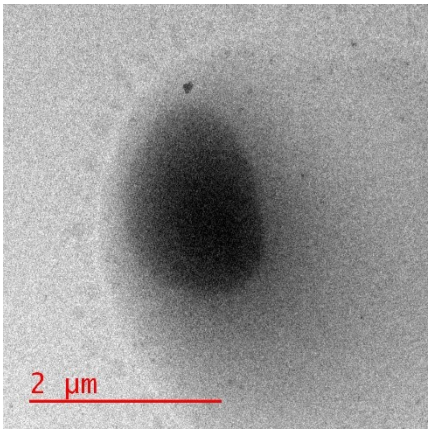

Alpha-Synuclein Control Fraction 10

Alpha-Synuclein Control Fraction 16

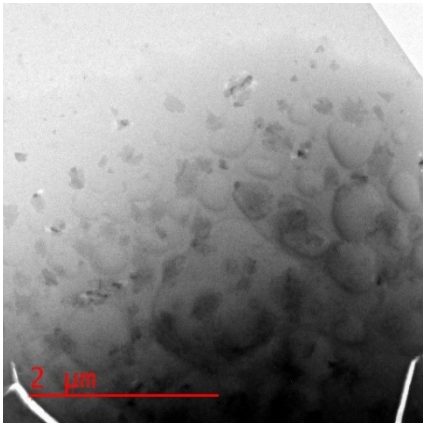

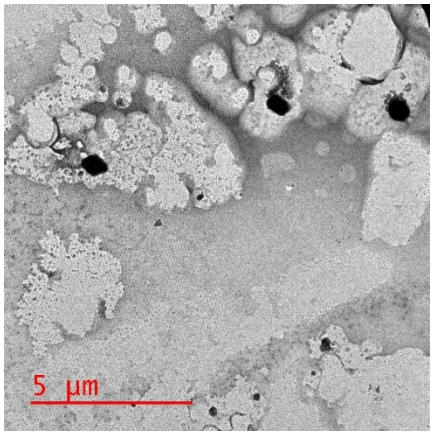

Alpha-Synuclein Control Fraction 20

Figure 17. TEM images for select density gradient fractions from SELEX round 4's alpha-synuclein control.

TEM imaging (Figures 15, 16 and 17) of heavier fractions in SELEX round 4 posed difficult just as it did in round 3. However, it appears that gradient fractions from round 4 may have been able to produce varying degrees of aggregation before they could be deposited on TEM grids. This is especially apparent when comparing the larger morphologies seen in fractions 10 and 16 of the alpha-synuclein control sample with those respective fractions from the novel pool. It should be noted that imaging of the fraction 20 TEM sample grids for each group was extremely limited. In the case of the novel pool, the image selected to represent fraction 20 was one of only two reasonable images generated.

Based on these results, it was decided that a MiSeq sequencing analysis would be conducted for the SELEX round 4 novel pools. The original attempt at this analysis (trial 1) was disrupted by high levels

of contamination from non-elongated aptamer sequences. Trial 2 was conducted and generated much clearer results. However, analysis of the produced data failed to yield a set of clearly dominant aptamer candidates. It was at this point that SELEX round 5 was conducted and its pools were assessed by MiSeq sequencing.

3.5 Analysis of MiSeq Sequencing Data

MiSeq sequencing took place on three occasions; twice following round 4, and a final time after round 5. As the last round of the SELEX, aptamer candidates identified from round 5 took precedent over the previous rounds. For the purposes of MiSeq sequencing, only novel pool fractions and rounds were analyzed largely due to the increased number of SELEX rounds the novel pool underwent. In total, nine different pools were analyzed via MiSeq. These pools were composed of the R0 (original pool), round 2 (R2) positive, R4 positive, R4 negative-positive (negative fraction from ultracentrifuge, positive retention by nitrocellulose filtration), R4 counter, R5 positive, R5 counter, R5 negative-positive (negative fraction from ultracentrifuge, positive retention by nitrocellulose), R5 negative-negative (negative fraction from ultracentrifuge, unretained by nitrocellulose). The source of each of the sequenced pools within the greater scope of the SELEX is illustrated in Figure 18.

AptaGui software properly sorted and grouped the data provided Aptacluster. The relevant processed data appears primarily as counts for each sequence in the pool as well as the total counts of sequences in each pool. From here, fraction values were generated by dividing the count for the given sequence (raw counts are provided in Appendix B) within a pool by the total cumulative sum of sequences in the respective pool. Fraction values are typically converted by a factor of 10^7 to produce a better interpreted score. From here, enrichment scores are generated by dividing the fraction score of a

sequence for a given pool by the fraction score of the same sequence from the positive pool of the prior SELEX round.

It should be noted that while the tables below (Tables 7, 9, 10, 11, and 12) provide the results from all three MiSeq experiments conducted, the lower row of frequency and enrichment pertaining to each respective pool derives from the largely disregarded round 4 MiSeq trial 1. Due to high levels of labeled pool impurity within round 4 MiSeq trial 1, each pool sequenced generated insufficient data for analysis, as well as, highly unbalanced relative representations of each pool. When referring to treated sequencing data associated with any pools within R4, R2, or R0, the data from round 4 MiSeq trial 2 is considered the authority. This newer data appears as the upper row of data for each of these respective pools.

3.5.1 Example Calculations of Treated Data:

$$Fraction = \frac{Raw\ Count * 10^7}{Total\ Counts\ Within\ Pool}$$

$$= \frac{Raw\ Count_{ASYN1\ Round\ 5\ Positive\ Pool} * 10^7}{Total\ Counts\ Within\ Round\ 5\ Positive\ Pool} = \frac{11 * 10^7}{612142} = 179.7 \cong 180$$

$$Enrichment = \frac{Frequency\ of\ Aptamer\ in\ Pool\ From\ Later\ Round}{Frequency\ of\ Aptamer\ in\ Positve\ Pool\ of\ Earlier\ Round}$$

$$Enrichment = \frac{Frequency_{ASYN5\ Round\ 5\ Counter\ Pool}}{Frequency_{ASYN5\ Round\ 4\ Positive\ Pool}} = \frac{27.9}{22.3} = 1.25$$

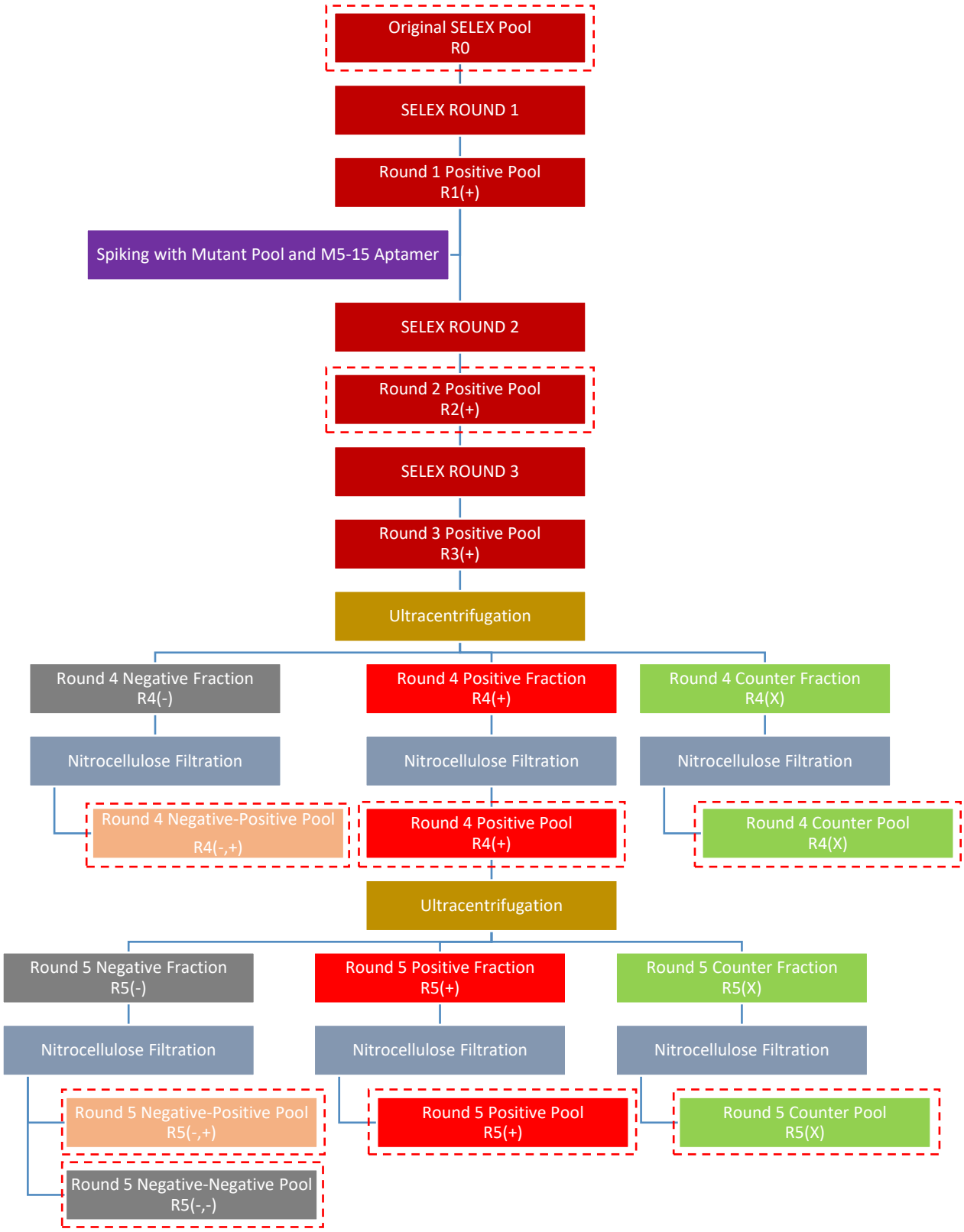

Figure 18. Illustration of the overall SELEX scheme and the source of sequenced pools. Sequenced pools are indicated by a dashed red box.

It should be noted that, due to nature of the fact that each step of the SELEX did not incorporate the total sum of the sample from which it was drawn, the base space is naturally reduced even outside of intended partitioning stages of SELEX. An example of this is the drawing of a sample of the synthesized round 0 pool to be used in the round 1 incubation. Due to the immensity of the base space, a vast quantity of the possible variations of the pool's sequences are immediately lost by this seemingly inconsequential step. This effect becomes less and less dramatic as the SELEX progresses and each sequence exists as a series of clones created through PCR. Having multiple clones makes a sequence naturally more robust to random removal. The progressive, random shrinking of pool diversity generates a natural degree of observed enrichment. An example experiment is to simply take 100 µL of a perfectly diverse set of sequences, remove a 10 µL sample, shake and spin the drawn sample, and then PCR the sample by using 1 µL of the 10 µL drawn. Sequencing the resulting "enriched pool" would identify a 99% decrease in sequence diversity with respect to the starting set of unique sequences. This decrease in sequence diversity would express itself as a 100 fold "enrichment score". In a more complex example experiment where each sequence in the initial pool has 100 copies of itself, the generated artificial enrichment is drastically lower. To accurately determine the degree to which this factor artificially inflates the enrichment scores presented here would be impossible. Therefore, the minimum enrichment value required for a pool to be considered "positively enriched" is placed at 1.10, or 10% enrichment.

Based on the relative appearance of a given sequence in each pool, five aptamer candidates were chosen. Based on the relative frequency with which a sequence appears in various select pools each aptamer candidate was provided a score out of 5. The first point is allotted to aptamer candidates that showed a positive enrichment within the R5 positive pool with respect to the R4 positive pool. This point represents that the sequence agreed with the SELEX conditions during round 5 and as such could potentially be useful in preventing aggregation of alpha-synuclein.

The second point is given to candidates that showed a positive enrichment within the R4 positive with respect to the R2 positive. This point represents the sequence's agreement with the SELEX conditions during rounds 3 and 4, and therefore could potentially be useful in preventing aggregation of alpha-synuclein.

The third point is given to candidates that showed a negative enrichment within the R5 counter with respect to the R4 positive. This point represents the capacity for a sequence to resist binding to large oligomeric protein formations or to resist allowing bound monomer to oligomerize.

The fourth point is given to candidates that showed a negative enrichment within the R5 negative-negative with respect to the R4 positive. This point is designed to remove sequences that show little affinity for alpha-synuclein when partitioned by ultracentrifugation as well as nitrocellulose filtration.

The fifth point is given to candidates that showed a negative enrichment within the R4 counter with respect to the R2 positive. Just as the second point, this point represents the capacity for a sequence to resist binding to large oligomeric protein formations or to resist allowing bound monomer to oligomerize.

Special considerations are given to candidates that showed a negative enrichment within the R5 negative-negative with respect to the R4 positive, coupled with a positive enrichment within the R5 negative-positive. Comparing these terms provides insight into how an aptamer candidate was able to bind to free monomer in the upper fractions after ultracentrifugation. Those that bound to free monomer were retained by nitrocellulose filtration and appeared in the negative-positive pool. Those that failed in competing for free monomer binding sights were not retained and appeared in the negative-negative pool. This measure could have just as easily been done by comparing fraction values as was done with enrichment. By comparing the enrichment of the R5 negative-positive with the R5

negative-negative we can create a measure that might be predictive of later on-off rates of target binding for the aptamer candidates chosen. The results of this measure for each candidate is provided in Table 8. This measure was not used as a primary criterion for aptamer candidate selection as simple binding does not necessarily represent the primary objective of the SELEX.

Based on these criteria, five final aptamer candidates were selected to move onto individual *in vitro* analysis. These aptamer candidates were deemed ASYN1, ASYN2, ASYN3, ASYN4, and ASYN5 while also retaining their names provided to them by AptaGUI. These names were 1LBiGJFJC, 1LBwAAjJ, GdJUhE, LTmUII, and JUeRc respectively.

The first aptamer candidate, ASYN1, was likely the result of a point mutation of the M5-15 aptamer with which the SELEX pool of round 2 was spiked. This point mutation likely occurred during PCR of SELEX round 3. This candidate scored four out of five points, losing a point for its abundance and enrichment in the round 4 counter fraction. This abundance is not repeated within the round 5 counter. Discrepancies also appear when ASYN1's appearance in the R4 negative-positive is compared to the odd lack of it in the round 5 negative-positive. This lends to a theory that the sequences strong enrichment in R4 pools was more a product of the sequence's conception via mutation than it was compatibility with the SELEX. Within round 4 this sequence appeared to a greater degree in the counter fraction than in the positive fraction. However, within round 5 this is reversed with ASYN1 demonstrating a strong affinity for the positive fraction without appearing to any degree in the counter fraction. This lack of appearance within the counter fraction of round 5 served as quite a surprise as ASYN1 holds such an overwhelming similarity to the established M5-15 which shows a relatively high affinity for larger aggregate formations prevalent in the denser counter fraction. When assessed by M-Fold, ASYN 1 generates an identical secondary structure to that of M5-15 as shown in Figure 19.

Table 7. Calculated values derived from MiSeq sequencing data for ASYN1. In the case of duplicate values, the lower row represents the round 4 MiSeq trial 1 which was deemed too low yield and too unbalanced to be a reliable source for analysis.

SCORE 4/5		NAME	ASYN1 (1LBiGJFJC)
		Random Region	GTATGGTACGGCGCGGTGGCGGGTGCGGGG
		Cluster ID	545813
➡	R5 Positive	Fraction	179.696868
		Enrichment	8.05656531
➡	R5 Counter	Fraction	0
		Enrichment	0
➡	R5 Negative	Fraction	10.8607861
		Enrichment	0.48693466
	R5 Negative (Positive)	Fraction	0
		Enrichment	0
➡	R4 Positive	Fraction	22.3044016
		Enrichment	NA
	R4 Positive	Fraction	0
		Enrichment	NA
	R4 Negative (Positive)	Fraction	8.41231091
		Enrichment	NA
	R4 Negative (Positive)	Fraction	0
		Enrichment	NA
➡	R4 Counter	Fraction	41.9426141
		Enrichment	NA
	R4 Counter	Fraction	0
		Enrichment	NA
	R2 Positive	Fraction	0
		Enrichment	NA
	R2 Positive	Fraction	0
		Enrichment	NA

The second aptamer candidate is ASYN2 (1LBwAAjJ). ASYN2 is a very interesting candidate as its origins are not entirely obvious due to the unusual degree of similarity to M5-15 coupled with a level of random region deviation at 43%. Of ASYN2's 30 base random region only 17 bases match those of M5-15 while the other 13 bases deviate. This 43% level of deviation is much higher that what was intended to be generated within the mutant pool which aimed for a target 30% level of deviation. Using a binomial distribution, the likely hood of a given sequence in the mutant pool generating this level of deviation from M5-15 is 8.45%. However, while possible it is also somewhat unlikely that ASYN2 with its 57% level of similarity to M5-15 originated within the novel pool. Of the $2.2x10^{15}$ different sequences introduced to SELEX round 1 in the novel pool, only about 126,000 of them possessed a 57% level of similarity to M5-15. Of those 126,000 sequences, ASYN2 had a 1 in 532 chance of being among them.

Of all the five final candidates, ASYN2 produced quantities within the various SELEX pools sequenced which agreed the most with the desired criteria. ASYN2, along with ASYN4 were the only candidates to demonstrate perfect 5/5 scores. In comparison to ASYN4, ASYN2 demonstrates better results when assessing the magnitude by which the enrichment scores used in the five criteria deviate from 1. In other words, ASYN2 demonstrates all the desired trends and demonstrates them all to an exceptional degree. ASYN2 was expressed 11.7 times more within the round 5 positive pool that it had within the round 4 positive pool. Between both rounds 4 and 5, ASYN2 was never detected in any counter selection pools (drawn from heavier gradient fractions), indicating an extremely limited affinity towards larger aggregate formations of alpha-synuclein. Of all the five final candidates, ASYN2 also demonstrated greatest presences within the round 5 negative-positive pool with respect to the round 5 negative-negative pool presence. As mentioned before, this "ON versus OFF rate" score provided candidates with special consideration outside of the five criteria score and represents a projected affinity of the aptamer candidate for alpha-synuclein monomer.

Table 8. Projected ON Versus OFF Measure for Special Consideration of Aptamer Candidates

Sequence	Enrichment in R5 Negative-Positive	Enrichment in R5 Negative-Negative	Projected ON Versus OFF Rate Score
ASYN1	0	0.4869	0
ASYN2	2.9636	0.6492	4.56464
ASYN3	0.329	0.325	1.014364
ASYN4	0.2195	0.1082	2.028722
ASYN5	1.482	0.649	2.282321

Table 9. Calculated values derived from MiSeq sequencing data for ASYN2. In the case of duplicate values, the lower row represents the round 4 MiSeq trial 1 which was deemed too low yield and too unbalanced to be a reliable source for analysis.

SCORE 5/5		NAME	ASYN2 (1LBwAAjJ)
		Random Region	GTAAGGAAACGCTACGGGGTGGGTACGGCA
		Cluster ID	554640
→	R5 Positive	Fraction	130.688631
		Enrichment	11.7186404
→	R5 Counter	Fraction	0
		Enrichment	0
→	R5 Negative	Fraction	7.24052405
		Enrichment	0.64924621
	R5 Negative (Positive)	Fraction	33.0503853
		Enrichment	2.96357517
→	R4 Positive	Fraction	11.1522008
		Enrichment	NA
	R4 Positive	Fraction	103.77104
		Enrichment	NA
	R4 Negative (Positive)	Fraction	8.41231091
		Enrichment	NA
	R4 Negative (Positive)	Fraction	0
		Enrichment	NA
→	R4 Counter	Fraction	0
		Enrichment	NA
	R4 Counter	Fraction	0
		Enrichment	NA
	R2 Positive	Fraction	0
		Enrichment	NA
	R2 Positive	Fraction	0
		Enrichment	NA

ASYN3 was a product of the mutant pool earned a score of 4/5. It possesses 33% variance in its random region with respect to M5-15. The only criteria within which it failed was the round 4 counter SELEX pool, in which it demonstrated an unusually strong presence. This presence was not reproduced when observing the round 5 counter SELEX pool. This discrepancy might imply some discrepancy between the large aggregate morphologies generated in the two SELEX rounds as a result of the shifted pH from 6.5 in round 4 to 7.2 in round 5. An alternative explanation might be that the capacity for ASYN3 to bind to large morphologies of alpha-synuclein might be pH dependant. A third explanation might be that the incubation of SELEX round 4 actually yielded a higher degree of aggregation shifting the distribution of binding sites towards larger aggregated morphologies.

Table 10. Calculated values derived from MiSeq sequencing data for ASYN3. In the case of duplicate values, the lower row represents the round 4 MiSeq trial 1 which was deemed too low yield and too unbalanced to be a reliable source for analysis.

SCORE 4/5		NAME	ASYN3 (GdJUhE)
		Random Region	GTATGAGATGGGGTGGTGACGTCAGCATGG
		Cluster ID	31665
→	R5 Positive	Fraction	130.6886
		Enrichment	5.85932
→	R5 Counter	Fraction	9.314239
		Enrichment	0.417596
→	R5 Negative	Fraction	7.240524
		Enrichment	0.324623
	R5 Negative (Positive)	Fraction	7.34453
		Enrichment	0.329286
→	R4 Positive	Fraction	22.3044
		Enrichment	NA
	R4 Positive	Fraction	51.88552
		Enrichment	NA
	R4 Negative (Positive)	Fraction	8.412311
		Enrichment	NA
	R4 Negative (Positive)	Fraction	0
		Enrichment	NA
⇨	R4 Counter	Fraction	41.94261
		Enrichment	NA
	R4 Counter	Fraction	0
		Enrichment	NA
	R2 Positive	Fraction	0
		Enrichment	NA
	R2 Positive	Fraction	0
		Enrichment	NA

ASYN4 was the second sequence to score a perfect score of 5/5 and originated from the mutant pool. It possesses 33% variance in its random region with respect to M5-15. Just as ASYN2, ASYN4 also produced an excellent presence within the positive fraction pools without any representation within the counter fraction pools. However, ASYN4 failed still underperformed in a couple regards. While many sequences such as ASYN2 demonstrated a strong presence in the round 4 positive pool through the original MiSeq trial for round 4, ASYN4 did not. While the original round 4 MiSeq trial yielded substantially less data than the following trial, it did often coordinate with the following trial and strengthen the choice of the final candidates. With regards to the scoring of each sequence using the five criteria outlined earlier, the data from the original round 4 MiSeq was excluded. ASYN4 also generated a projected ON verses OFF rate score of 2.03, significantly lower than the 4.56 generated by ASYN2.

Table 11. Calculated values derived from MiSeq sequencing data for ASYN4. In the case of duplicate values, the lower row represents the round 4 MiSeq trial 1 which was deemed too low yield and too unbalanced to be a reliable source for analysis.

SCORE 5/5		NAME	ASYN4 (LTmUII)
		Random Region	GAACGGAATGGCGCGGTGACCGGATAGTGT
		Cluster ID	13615
→	R5 Positive	Fraction	114.3526
		Enrichment	3.417937
→	R5 Counter	Fraction	0
		Enrichment	0
→	R5 Negative	Fraction	3.620262
		Enrichment	0.108208
	R5 Negative (Positive)	Fraction	7.34453
		Enrichment	0.219524
→	R4 Positive	Fraction	33.4566
		Enrichment	1.415564
	R4 Positive	Fraction	0
		Enrichment	0
	R4 Negative (Positive)	Fraction	16.82462
		Enrichment	0.711857
	R4 Negative (Positive)	Fraction	0
		Enrichment	0
→	R4 Counter	Fraction	0
		Enrichment	0
	R4 Counter	Fraction	0
		Enrichment	0
	R2 Positive	Fraction	23.63482
		Enrichment	NA
	R2 Positive	Fraction	0
		Enrichment	NA

Of all the final aptamer candidates, ASYN5 demonstrated the worst score at 3/5. Of all the five final aptamer candidates, ASYN5 also contains second the highest degree of similarity with respect to M5-15, with a degree of deviation of the random region at 27%. ASYN5 was primary chosen based on criteria outside of what is typically sought after within this SELEX. ASYN5 was chosen based on a strong degree of overrepresentation in both the light and heavy fractions. Within the light fractions ASYN5 showed a slightly reduced abundance within the round 5 negative-negative. Overall it expressed a flexible and likely strong affinity for alpha-synuclein. However, because of its reduced specificity and inability to demonstrate a capacity to prevent oligomerization of its bound monomer, ASYN5 might be better suited towards alternative applications such as detection or localization of alpha-synuclein. It is also worth noting that of the final aptamer candidates, ASYN5 produces the most energetically stable secondary structure as predicted by mfold analysis (mfold structures provides in Figures 19, 20, 21, 22, 23). However, mfold is unable to predict the formation of a G-quadruplex which can be quite stable and relevant to target binding.

In the future, steps could be taken towards selection of other aptamer candidates. The sequencing of the mutant pool might be a good place to start in the search for new candidates. The five final aptamer candidates selected within this work all likely came from the mutant pool or had strong associations with M5-15 at the very least. That is not to say that the novel pool did not generate strong aptamers. The candidates drawn from the novel pool were slightly out performed by five final candidates chosen. It should be noted however that the majority of top 100 contenders within the MiSeq sequencing results likely had origins within the mutant pool. Also, after the top 200 sequences, the prevalence of the mutant pool completely disappears, giving way to a vast series of sequences native to the novel pool. MiSeq analysis of the mutant pool would likely yield an entirely different set of strong candidates for analysis and vitro experimentation.

Table 12. Calculated values derived from MiSeq sequencing data for ASYN5. In the case of duplicate values, the lower row represents the round 4 MiSeq trial 1 which was deemed too low yield and too unbalanced to be a reliable source for analysis.

SCORE 3/5		NAME	ASYN5 (JUeRc)
		Random Region	GTATGATACAGTGAGGTGGCAGATGCATGC
		Cluster ID	567287
➡	R5 Positive	Fraction	81.68039
		Enrichment	3.662075
⇨	R5 Counter	Fraction	27.94272
		Enrichment	1.252789
➡	R5 Negative	Fraction	14.48105
		Enrichment	0.649246
	R5 Negative (Positive)	Fraction	33.05039
		Enrichment	1.481788
⇨	R4 Positive	Fraction	22.3044
		Enrichment	0.943709
	R4 Positive	Fraction	0
		Enrichment	0
	R4 Negative (Positive)	Fraction	25.23693
		Enrichment	1.067786
	R4 Negative (Positive)	Fraction	0
		Enrichment	0
➡	R4 Counter	Fraction	20.97131
		Enrichment	0.887305
	R4 Counter	Fraction	0
		Enrichment	0
	R2 Positive	Fraction	23.63482
		Enrichment	NA
	R2 Positive	Fraction	0
		Enrichment	NA

3.6 Sequence Analysis by Base Composition, Structure and G-Quadruplex Mapping

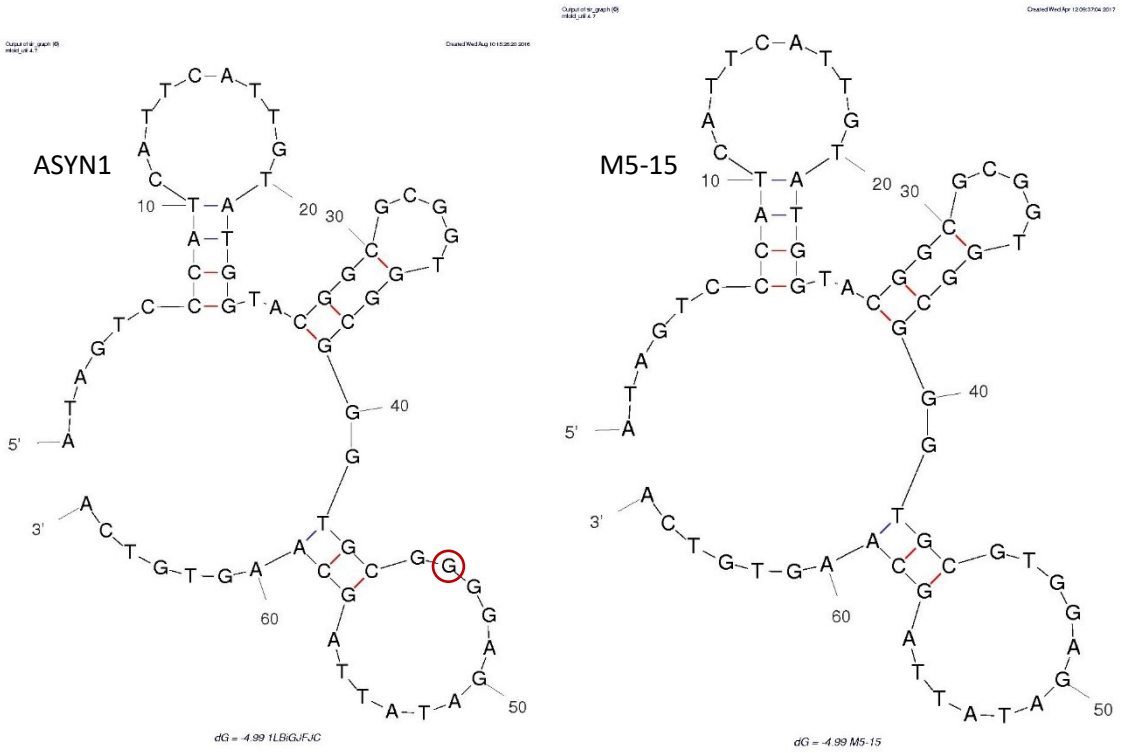

Figure 19. Predicted secondary structure of ASYN1 and M5-15 as generated by mfold (The RNA Institute of the University At Albany). Red circle indicates point of deviation of ASYN1 from the M5-15 sequence. dG=-4.99 kcal/mol for both structures.

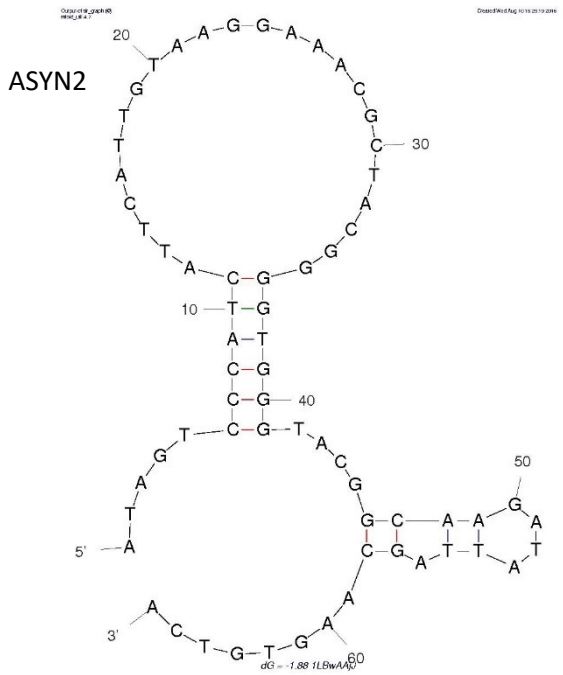

Figure 20. Predicted secondary structure of ASYN2 as generated by mfold (The RNA Institute of the University At Albany). dG=-1.88 kcal/mol

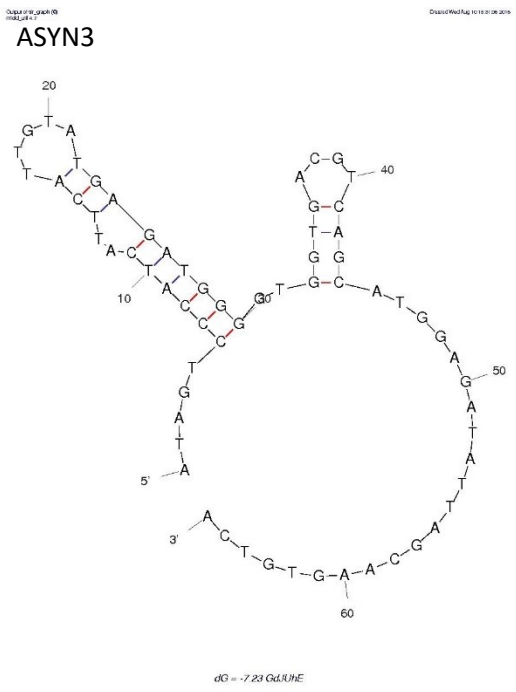

Figure 21. Predicted secondary structure of ASYN3 as generated by mfold (The RNA Institute of the University At Albany). dG=-7.23 kcal/mol

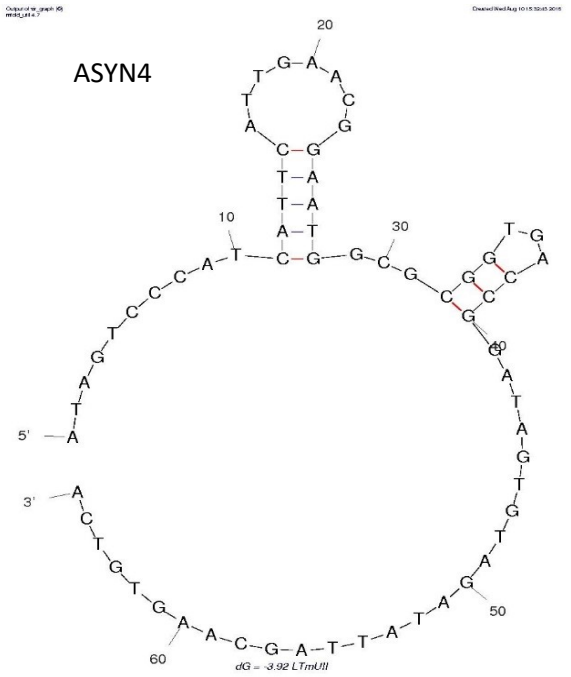

Figure 23. Predicted secondary structure of ASYN4 as generated by mfold (The RNA Institute of the University At Albany). dG= -3.92 kcal/mol

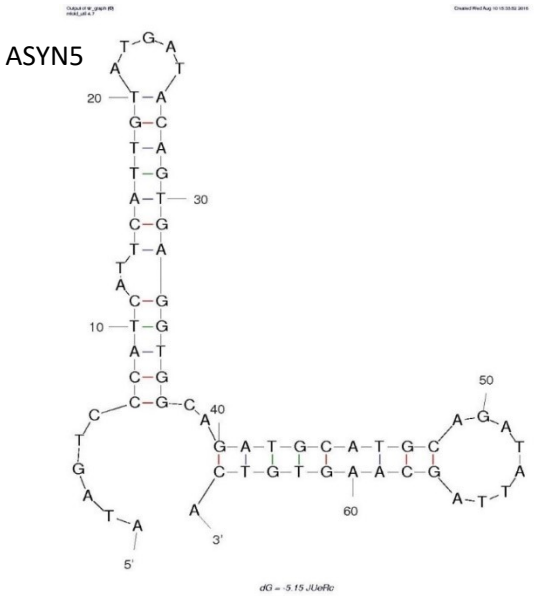

Figure 22. Predicted secondary structure of ASYN5 as generated by mfold (The RNA Institute of the University At Albany). dG=-5.15 kcal/mol

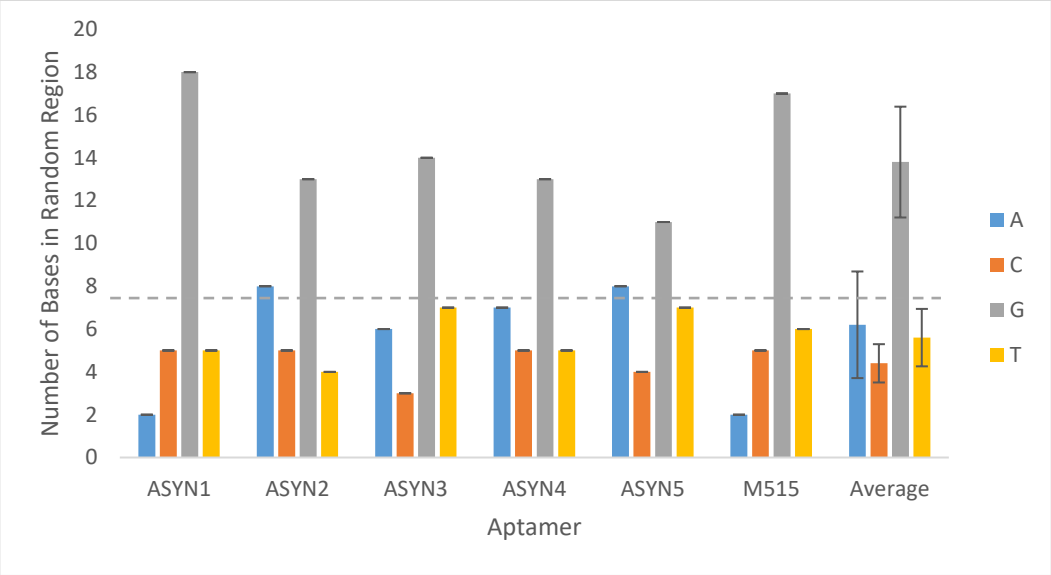

Figure 24. Base distribution of within the random region of the five final aptamer candidates and M5-15 aptamer. Average values do not incorporate M5-15 aptamer. Dashed line represents a base count of 7.5 (the count representing uniform base distrubtion).

Based on the average distribution of the four nucleotide bases (shown in Figure 24), the SELEX appears to have driven towards the overrepresentations of the adenine (A). This is apparent by the significant shift in its appearance within the random region of the candidate sequences with respect to their point of origin, M5-15. The average random domain of the five final candidates produces 6.2 adenine bases while the M5-15 aptamer only possesses 2 adenine bases within the random region.

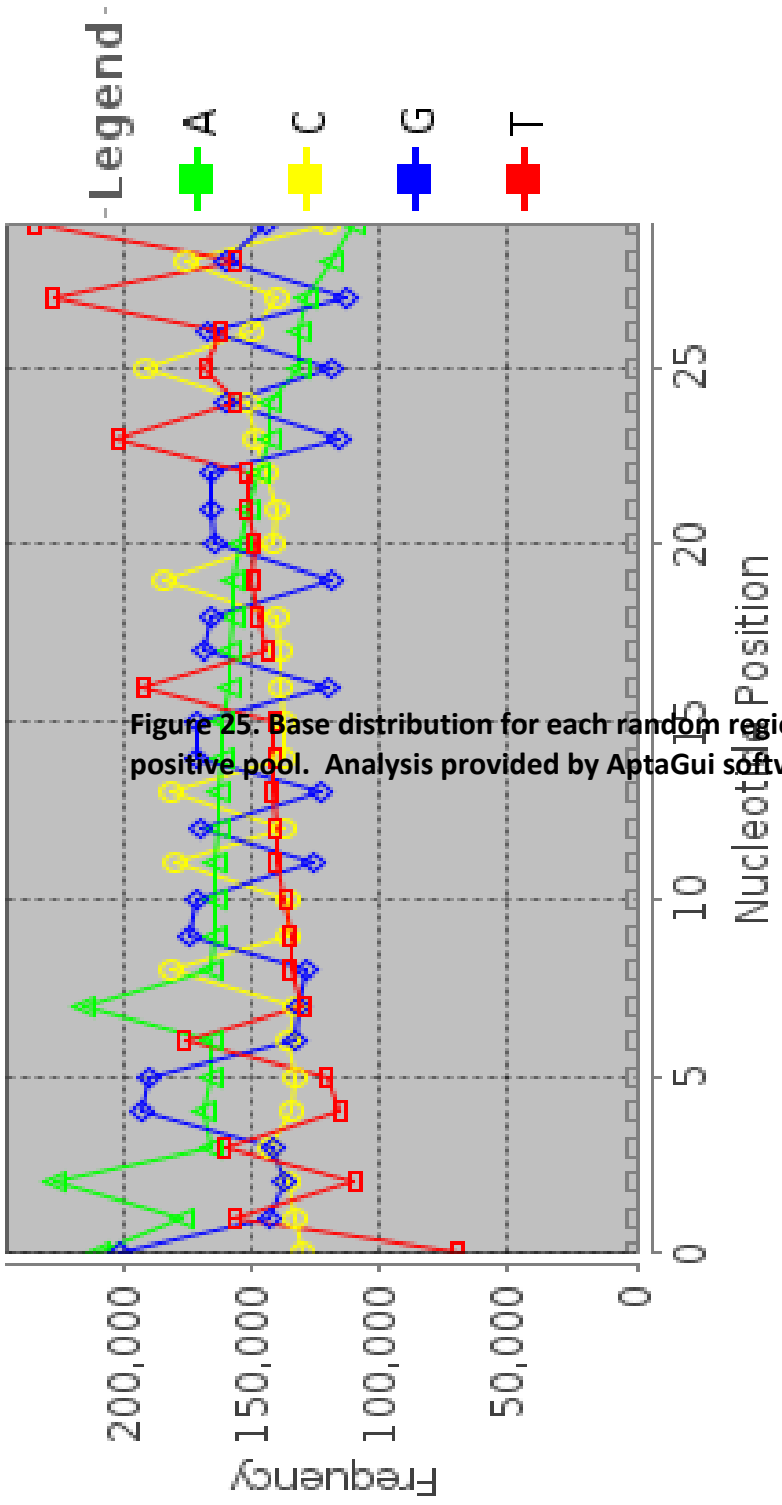

Figure 25. Base distribution for each random region position. This data pertains to the r positive pool. Analysis provided by AptaGui software.

Figure 25 demonstrates the distribution of bases for each of the thirty positions within the random region of all the sequences that made up the round 5 novel pool (spiked with M5-15 and mutant pool). Guanine bases are the most overrepresented within the random region, holding the highest representation within 14 of the 30 positions. This is a product of the spiking with the mutant pool and M5-15 aptamer to which the typical sequence illustrated by the data coordinates. However, it should also be noted that guanine also hold the greatest number of positions in which it is least represented at 10 of the 30. Another feature to note are that some trends exist between bases that occupy the same position. For instance, any time T or C appear as the most represented base of a position, G is always the least represented. While it is natural for the typical sequence illustrated in the data to coordinate to the bias imposed by the mutant pool, the sequence reflecting the least represented pool might be quite telling. While the mutant pool imposed a bias towards the G rich positions we see here (based on M5-15), it appears that G bases are being dramatically under expressed in the positions without a mutant G bias. This might represent that the SELEX process is actively removing the G rich nature of the average random region introduced by the mutant pool's bias. Because G bases are almost universally better at interacting with amino acids than the other three bases, this trend may imply that with continued rounds the pool is becoming less interested in affinity and more interested in selectivity.[78] Towards the end of the SELEX incubation phase, monomer becomes scarce and aggregate systems become common. Candidates which bind to protein and are non-specific for the monomeric morphology are more likely to find aggregates to bind and be removed from the pool in the counter fraction.

A 2012 paper outlined the apparent overrepresentation of G-quadruplex containing DNA sequences among aptamers selected *in vitro,* with an especially high number among those associated with protein targets.[79] This might suggest that G-quadruplex formations benefit aptamer affinity towards proteins. While improved aptamer affinity is largely something beneficial to an aptamer, it is possible that aptamer candidates which demonstrate a G-quadruplex might lose the crucial selectivity for the monomeric protein over aggregated morphologies.

Of all the five final aptamer candidates, ASYN5 contains the smallest number of guanine (G) bases within the random region indicating that it is the least likely to form a stable G-quadruplex. ASYN1 contains 18 G bases (60% of the 30 base domain) within its random region. ASYN2 and ASYN 4 each contain 13 G bases (43%). ASYN3 contains 14 bases (47%). ASYN5 contains 11 G bases (37%). The M5-15 aptamer itself contains 17 G bases (57%) within its random region. Using the QGRS Mapper by Ramapo College Bioinformatics, we can take the G-quadruplex (G-quad) assessment one step further. By providing the mapper with the five final aptamer candidate sequences, as well as M5-15, it is possible to measure the likelihood that a given sequence might generate a G-quadruplex, and within which domain it is most likely to appear. Table 13 provides the results generated by QGRS Mapper. G-quad domain position provides the most likely position within the sequence to generate a G-quadruplex. This position is expressed by counting from the 5-prime end of the sequence. All G-quadruplex domains generated by QGRS Mapper are all entirely within the random region of each sequence. The QGRS (Quadruplex forming G Rich Sequences) illustrated for each sequence is the identified G-quadruplex domain itself. The G-score is generated by assessing the groupings of G bases, their abundance within the domain, and the positioning of each G base. The number of G-quad variations predicted illustrates the number of possible orientation with which the mapper can generate a G-quadruplex within the domain.

Table 13. Predicted G-quadruplex regions within M5-15 and the five final aptamer candidates

Aptamer Candidate	Random region G base content	G-quad domain position	G-quad domain length	QGRS	G-Score	Number of G-quad variations predicted
M5-15	57%	23	18	GGTACGGCGCGGTGGCGG	20	25
ASYN1	60%	23	18	GGTACGGCGCGGTGGCGG	20	71
ASYN2	43%	34	13	GGGGTGGGTACGG	18	11
ASYN3	47%	28	21	GGGGTGGTGACGTCAGCATGG	9	1
ASYN4	43%	23	19	GGAATGGCGCGGTGACCGG	19	1
ASYN5	37%	-	-	-	-	0

Using the QGRS mapper a similar trend to what was predicted based on G base content emerges, though a couple exceptions exist. ASYN3, despite having a high G base content, generates a low G-score of 9. This draws from the fact that the 4 G base pairs which make up the quadruplex are spread out in a non-uniform manner and that the position of the fourth pair is a great distance from that of the third. ASYN5, which generated the lowest G content, fails to produce a viable G-quadruplex domain. This is due to the more uniform spread of the G bases within its random region. Ongoing work includes the continued analysis of potential G-quadruplex formation via melting point studies assessed by UV-vis spectroscopy.

3.7 Within SELEX Analysis of Established M5-15 Aptamer

From the very start of this work, the M5-15 aptamer was considered a launching point. Naturally, its potential as a therapeutic itself was a topic of interest as this SELEX experiment began. By running the M5-15 aptamer in parallel to SELEX round 2 it was possible to evaluate M5-15's capacity to prevent the aggregation of alpha-synuclein via TEM imaging. These images are provided in Figure 26.

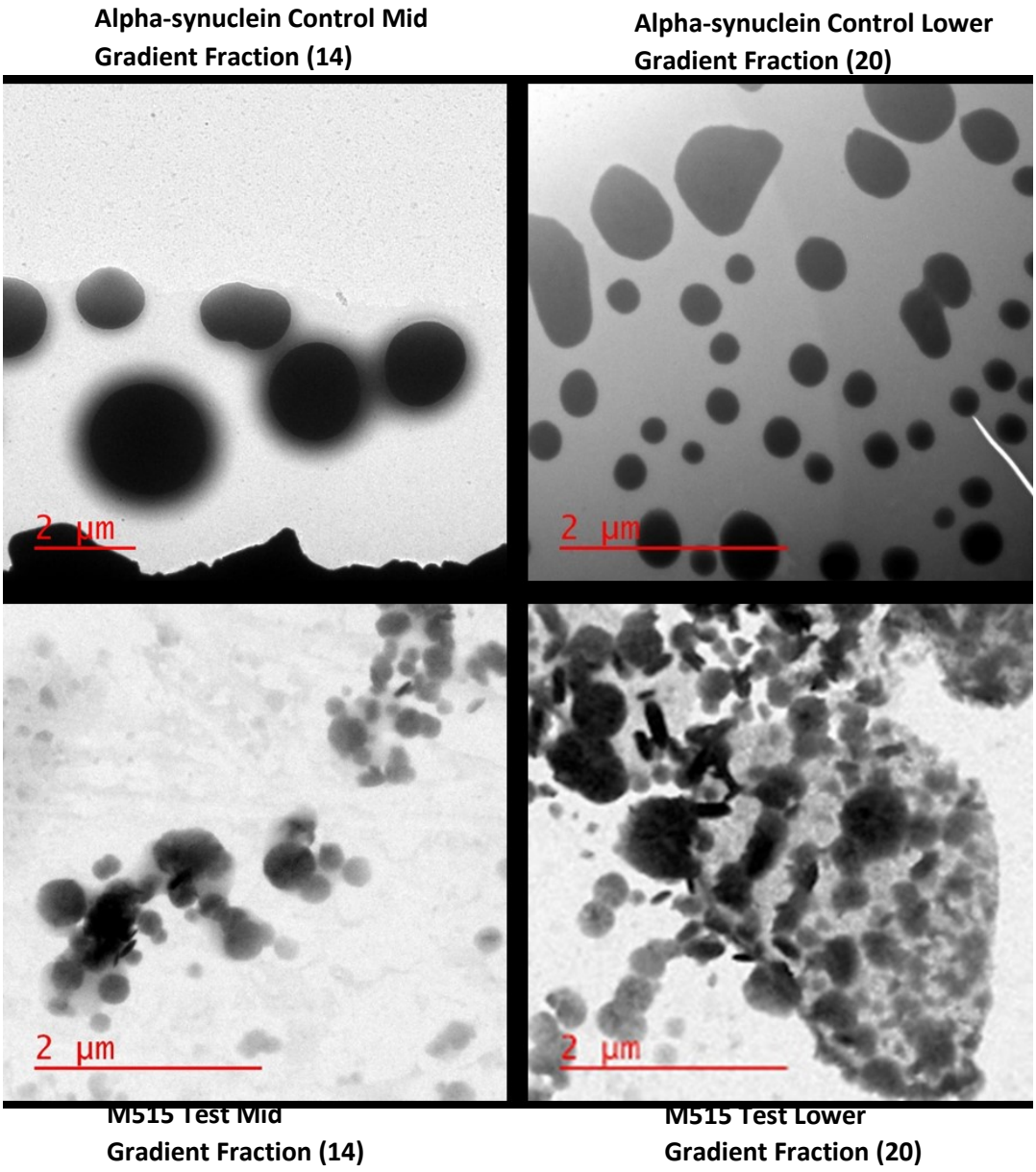

Figure 26. Representative TEM images for the M5-15 aggregation inhibition test's ultracentrifuge gradient fractions and corresponding alpha-synuclein control fractions.

Based on TEM analysis (Figure 26), M5-15 demonstrated very little capacity to prevent aggregation with respect to the alpha-synuclein control, and this capacity was matched by the mutant pool and potentially exceeded by the relatively undeveloped novel pool. Based on these results, M5-15 was ruled out for application as an aggregation preventing agent. Because it was during this round that

novel pool was spiked with M5-15 and mutant pool it allowed us to make more comprehensive evaluations on M5-15 later on via Miseq sequencing.

Through M5-15 spiking, several points have been yielded which help validate the SELEX method employed here. The first point is that M5-15 consistently showed a diminishing presence within the positive fractions with each progressive SELEX round. This trend is illustrated in Figure 27. While it is established that M5-15 undoubtedly binds to alpha-synuclein, this trend illustrates that despite this binding affinity, it is continually removed piece by piece from the SELEX as the rounds pass. This removal would suggest that it this SELEX method does not base retention and overrepresentation of candidates solely on alpha-synuclein affinity but on another factor as well. This second effect is likely the SELEX method's drive towards overrepresentation of candidates which are of inhibiting the aggregation of alpha-synuclein.

As was mentioned before, this SELEX method seeks to reduce the viable aptamer binding sites (alpha-synuclein monomer) to solely what individual sequences have prevented from undergoing aggregation. Simply binding to alpha-synuclein monomer without preventing aggregation of the monomer would likely result in the aptamer being pulled with the large aggregate morphologies into the heavier ultracentrifuge gradient (counter) fractions. If the oligomerization of the aptamer's bound alpha-synuclein monomer serves to displace the aptamer, or decrease their relative affinities, the aptamer would likely end up in the lighter ultracentrifuge gradient (negative) fractions. The result here is that aptamers located within the positive ultracentrifuge fractions would have to bind to a protein monomer and prevent it from aggregating to the point where the combined mass of the system would bring it to a mid-gradient fraction. In the case of M5-15, the decrease in its population would back up the TEM evidence which suggested M5-15 likely has little to no capacity to prevent aggregation.

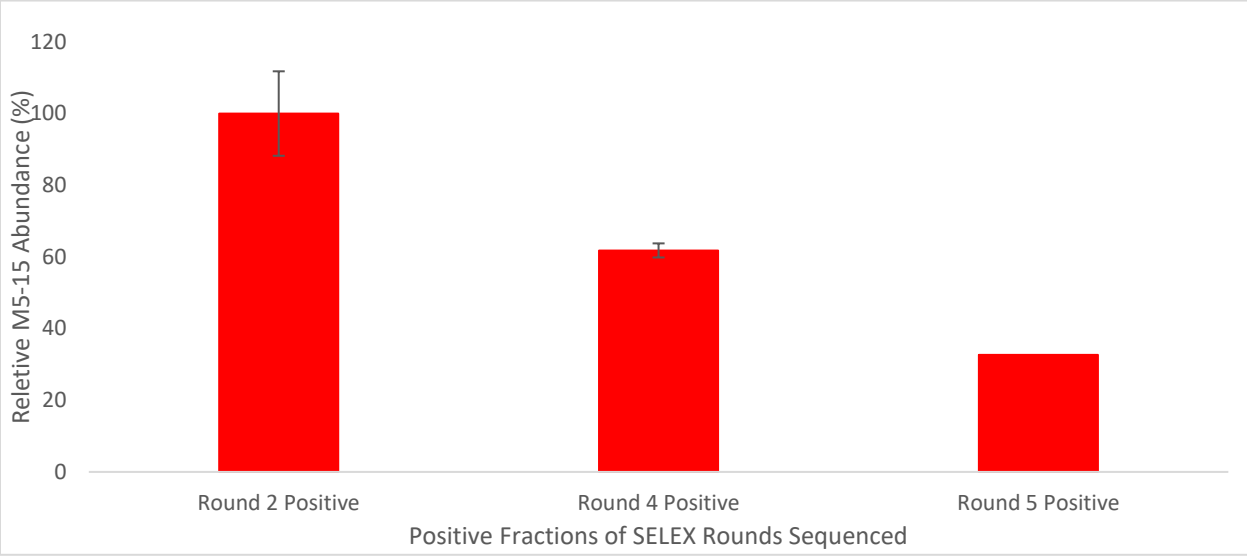

Figure 27. Diminishing M5-15 abundance with positive pools of each SELEX round sequenced. All values are corrected against the Round 2 Positive abundance (frequency) which is defined as 100%. Error bars provided within the Round 2 Positive and Round 4 Positive are the standard deviation of the scores generated by duplicate readings of the same pools.

The second point of M5-15's validation of this SELEX method derives from its abnormally high presence within the counter fractions of the rounds sequenced (illustrated in Figure 28). This would indicate that if the partitioning of protein morphologies by ultracentrifugation was functioning as intended, M5-15 would seem to have a higher affinity for oligomeric alpha-synuclein morphologies. This finding is exactly what the 2010 study by Tsukakoshi et al. published in their screening of the M5-15 aptamer.[64] This corroboration helps to validate this SELEX method's primary partitioning method, ultracentrifugation.

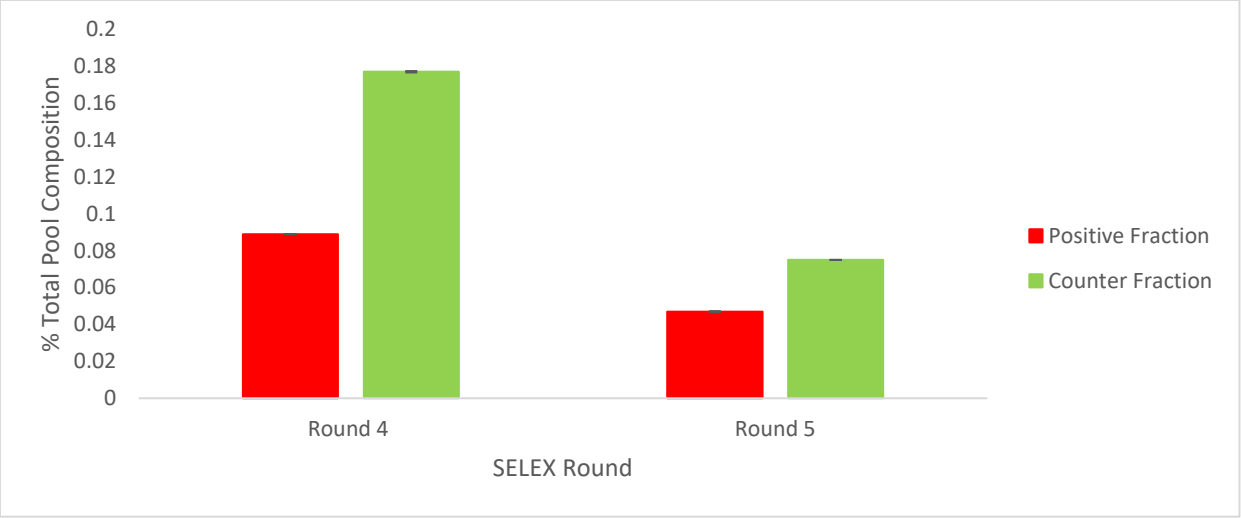

Figure 28. Relative abundance of spiked M5-15 aptamer between the positive and counter fractions of the rounds sequenced.

3.8 Alpha-Synuclein Aggregation Assay with Aptamer Candidates Under SELEX Conditions:

The alpha-aynuclein aggregation assay with aptamer candidates under SELEX conditions sought to place each of the five final aptamer candidates back into their SELEX conditions in order to assess their capacity to prevent aggregation individually rather than as components of a pool. This test served as an introduction for the aptamers into a wider scope of *in vitro* testing. Here, the inhibitory capacity of each sequence was measured by the average size of the alpha-synuclein morphologies generated within a larger positive ultracentrifuge fraction (1 mL). Broadening the positive ultracentrifuge fraction to 1 mL opened the TEM analysis to more diverse alpha-synuclein morphologies. In systems containing an aptamer with a strong capacity for the prevention of alpha-synuclein aggregation, a more uniform set of small morphologies were likely to be observed. In systems containing an aptamer with a weak capacity for the prevention of alpha-synuclein aggregation, a less uniform set of morphologies with a greater incidence of larger aggregated morphologies was likely. A control sample containing alpha-synuclein without aptamer was also run in parallel.

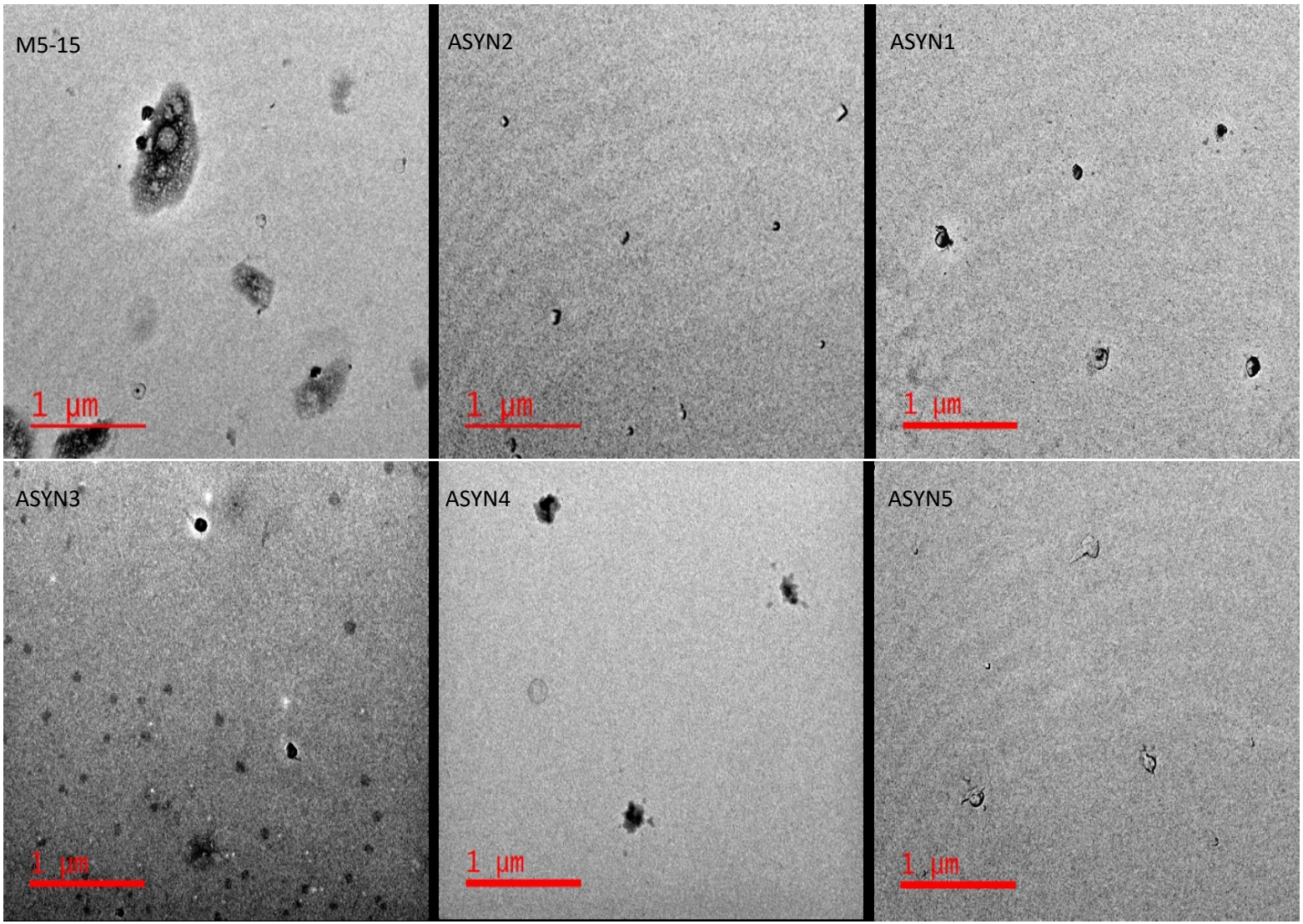

Figure 29. Representative TEM images for each aptamer from alpha-synuclein aggregation assay performed under SELEX conditions.

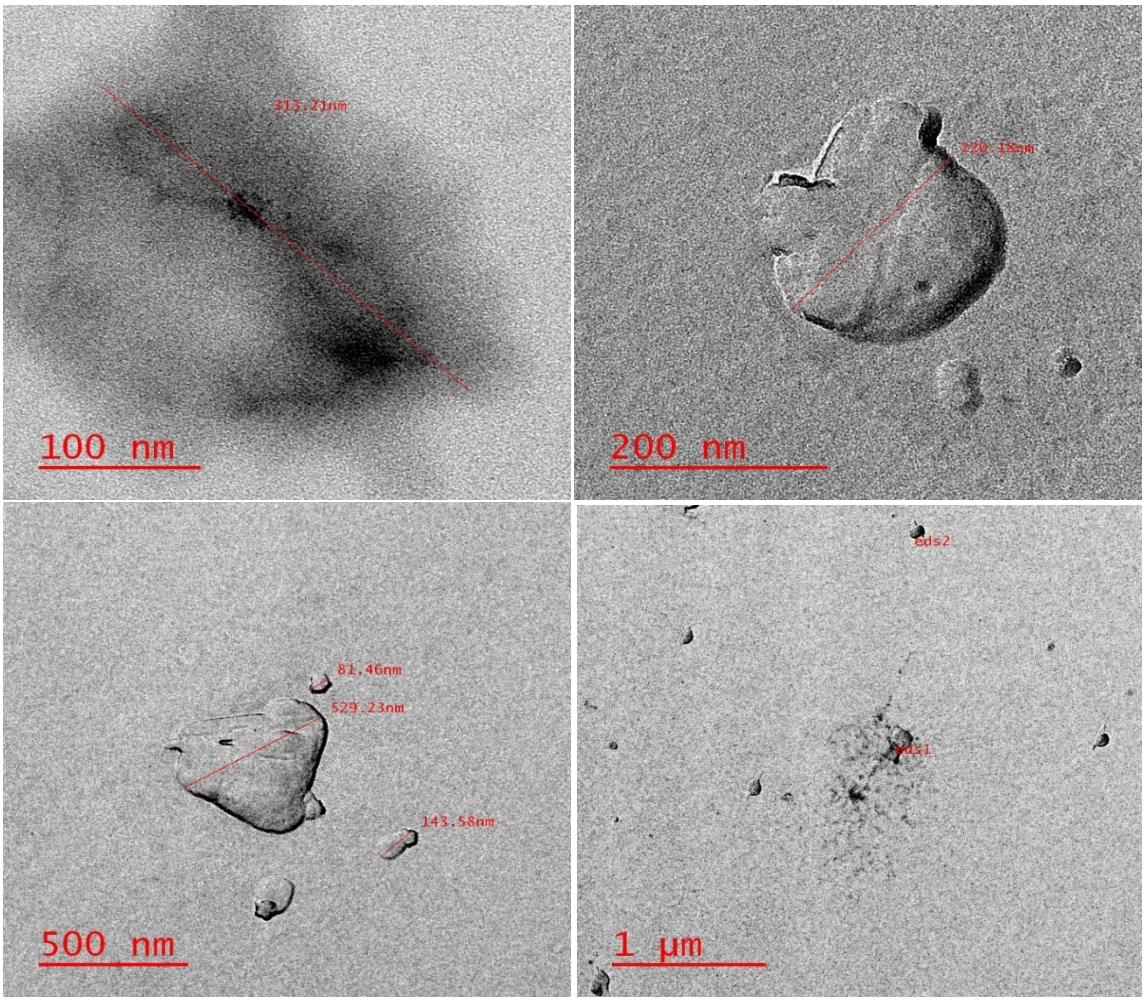

Figure 30. Representative TEM images for alpha-synuclein control from alpha-synuclein aggregation assay done under SELEX conditions.

Table 14. Sizes of alpha-synuclein morphologies present in TEM images from each aptamer candidate.

Aptamer Candidate	Average Size of Alpha-Synuclein Morphology Observed (±Standard Deviation) (nm)
ASYN1	176±128
ASYN2	87±34
ASYN3	94±67
ASYN4	156±68
ASYN5	98±38
M5-15	266±135
No Aptamer (Control)	242±220

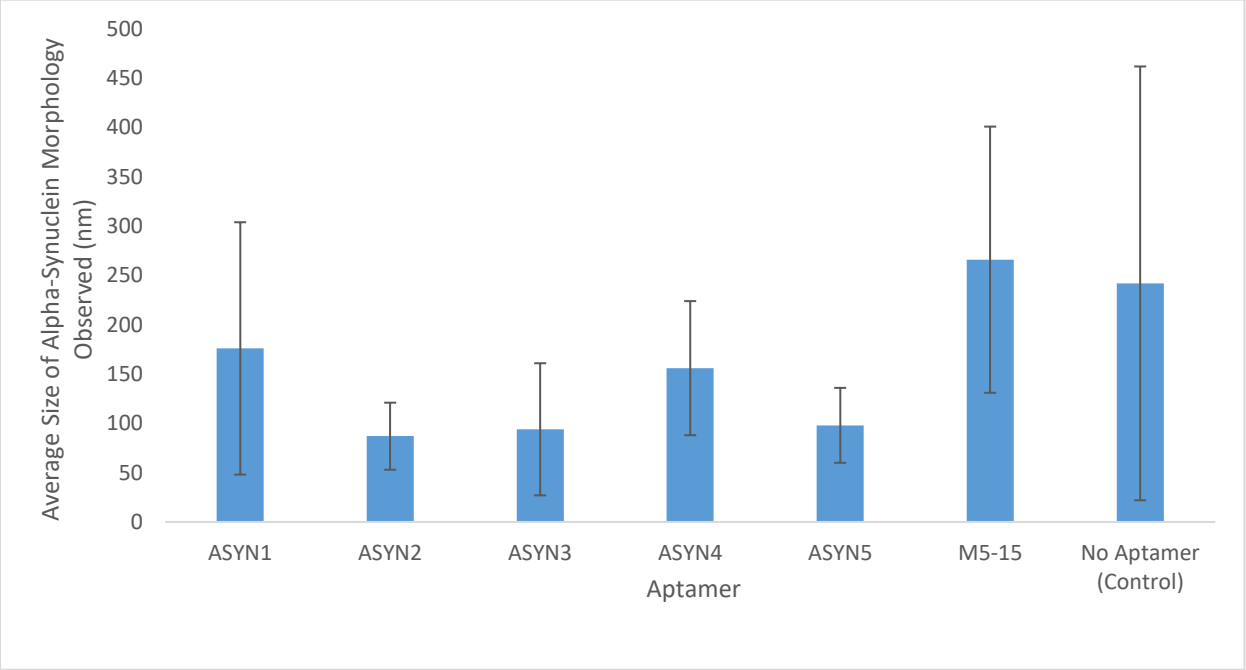

Figure 31. Sizes of alpha-synuclein morphologies present in TEM images from each aptamer candidate.

Based on these preliminary *in vitro* results (Figures 29, 30, and 31, as well as Table 14), the aptamer candidates appear to demonstrate variable but promising degrees of aggregation inhibition. As was seen in the analysis of M5-15's capacity to inhibit aggregation run in parallel to round 2, these results also indicate that M5-15 is relatively incapable of inhibiting aggregation as it appears to yield comparable results (266±135 nm) to those found within the control sample (242±220 nm). Based on these preliminary results, ASYN1 and ASYN4 appear to be underperforming in relation to the other aptamer candidates and the alpha-synuclein control with sizes of 176±128 nm and 156±68 nm respectively. ASYN2, ASYN3, and ASYN5 appear to yield comparable results with this preliminary data (87±34, 94±67, and 98±38 nm respectively). It should be noted that the standard deviation in morphology size might also be a strong indicator for aggregation. This would mean that reductions in standard deviation and the presence of more uniform morphologies might be a measure of interest when assessing aptamer candidates within this assay.

Beyond the varying affinity of five final aptamer candidates, the observed capacity for the aptamers to inhibit aggregation could be the result of differences in the mechanisms each given candidate employs towards this capacity. Several possible methods by which the selected aptamer may inhibit the aggregation of alpha-synuclein exist. One likely method is that the aptamer simply binds to the central domain of the misfolded protein necessary for the stacking and subsequent oligomerization of the protein, thereby impeding this activity. A second possible method is that the aptamer could serve to stabilize the correct folding of the protein. This would result in a drop in the misfolded protein concentration crucial to generate oligomer seeding and growth. Another less likely method is the potential for the aptamer to trigger a refolding of the misfolded protein through progressive binding originating from a highly stable aptamer-protein binding toehold. Other less likely methods include the potential for the aptamer to break down large oligomerized formation in an enzymatic manner, or the potential for the aptamer to induce protein stabilization of a less observed third or transitive folding state. Of these potential methods, the first is the method desired as it does not serve to interact with the properly folded protein which would have the potential to inhibit its desired biological functions. It also does not require the formation of larger oligomerized systems prior to action. Fortunately, mechanisms that involve the fragmenting of larger aggregate systems are likely under-expressed within the final candidate pool, as this mechanism would not mandate that the aptamer bind tightly to monomeric protein or end up within the retained ultracentrifuge fraction. The second method could be equally functional as a therapeutic by inducing stabilization through interactions with a non-active domain of the protein. The diversity of possible mechanisms which could have allowed a given sequence to progress within the SELEX is a potential weak point within the SELEX method employed. To remedy this potential, the final enriched pool could have been introduced to new SELEX which employed a truncated variant of the alpha-synuclein monomer. As the correct, functioning morphology of alpha-synuclein is stabilized the presence of the C-terminal of the protein, removing this domain or a large

portion of it would likely yield enhanced levels of misfolded protein.[15] In addition, removing the N-terminal of the protein to form a truncated SELEX target might serve to generate an enriched SELEX pool in which candidates whom exhibit the inhibition of aggregation via the desired mechanism would become overexpressed.[60] This effect might be enhanced through chemical modification of the target protein. While outside the scope of this project, introducing alternate or modified SELEX targets could be an approach to enhance aptamer functionality as a therapeutic in the future.

4 Conclusions

Designing and conducting a novel SELEX method centered around the selection of aptamers which act as inhibitors of protein aggregation, has yielded a handful of strong aptamer candidates and some promising preliminary results. The target of the SELEX, the slowed aggregation of alpha-synuclein, has the potential to compliment the current treatment arsenal for Parkinson's disease as a preventative therapeutic.

An *in vitro* test for the capacity for M5-15 to inhibit the aggregation of alpha-synuclein revealed an extremely limited capacity. This test was run in parallel to SELEX round 2, where inhibition of aggregation by the relatively undeveloped mutant and novel pools was shown to exceed that of M5-15. This result was corroborated by an alpha-synuclein aggregation assay with aptamer candidates under SELEX conditions, which demonstrated little difference between the degree of aggregation in the alpha-synuclein control and that of the sample containing M5-15.

Of the aptamer candidates presented by the MiSeq sequencing analysis, five final aptamer candidates were selected. Analysis of the sequence of their random regions showed high level of similarity with the established M5-15 aptamer. Base analysis revealed the five final aptamer candidates had significantly more adenine within their random regions than M5-15 possesses.

Based on the combination of sequencing data, G-quadruplex potential, and preliminary *in vitro* aggregation prevention assays, ASYN2 was selected as the introductory candidate for in *vivo* testing. ASYN2 outperformed the other aptamer candidates within the MiSeq results, yielding a near perfect set of scores. QGRS mapper predicted a promising G-score of 18, indicating a strong possibility of G-quadruplex formation. Within the preliminary *in vitro* alpha-synuclein aggregation inhibition assay, ASYN2 out-performed the other candidates by producing the smallest set of alpha-synuclein morphologies with the smallest diversity in sizes at 94±67 nm.

5 Contributions to Knowledge and Future Work

Current ongoing work in this project focusses on further *in vitro* testing of the five aptamer candidates, as well as, testing *in vivo* via mice based models for Parkinson's disease. Ongoing *in vitro* testing includes longitudinal TEM based assays without ultracentrifugation, as well as gel mobility shift assays. These mobility assays including both native protein systems and those incorporating aptamer to target chemical cross-linking. As mentioned before, ongoing work also includes the continued analysis of potential G-quadruplex formations via melting point studies assessed by UV-vis spectroscopy. Mice models for *in vivo* aptamer affinity testing are being conducted using mice possessing a genetic modification for the production of a mutant variant of human alpha-synuclein. This testing incorporates ASYN2 as a payload within a transferrin aptamer modified liposome delivery vector.

As more results develop from ongoing assays, the greater implications of the project will become more clear. If aptamer candidates continue to perform well, the novel SELEX method developed here will become further validated. This experiment could be directly recreated for any number of aggregating proteins such as amyloid beta, which is helps make up the protein masses found in Alzheimer disease.[80] In theory, this novel SELEX method, at its core, could be applied to the discovery of

aptamers which inhibit a wider range of chemical processes. The limitations only exist around the capacity for modern partitioning methods. In almost any scenario when Chemical A interacts with Chemical B to produce Chemical C, this method can apply to inhibit the production of Chemical C so long as a partitioning method exists which can accommodate the partitioning of an aptamer-Chemical A complex from all other constituents of the system. By letting all unbound, unprotected Chemical A undergo the reaction, the aptamers which retain Chemical A can be selectively retained. Another limitation would be that the chemical species or native interactions involved must not denature or destabilize the DNA aptamers candidates.

Within the scope of Parkinson's disease, mouse based *in vivo* assays are still underway. If aptamer candidates demonstrate a strong capacity for the inhibition of symptomology in the developed mouse method, though application via a transferrin aptamer mounted liposome delivery vector, this project may yield a therapeutic for Parkinson's disease that could see clinical testing. As a preventative therapeutic, an aptamer developed here might serve to complement the growing arsenal of Parkinson's disease treatment strategies.

6 References

1. Poewe, W. *et al.* Parkinson disease. *Nat. Rev. Dis. Prim.* **3,** 17013 (2017).
2. Schrag, A. What contributes to quality of life in patients with Parkinson's disease? *J. Neurol. Neurosurg. Psychiatry* **69,** 308–312 (2000).
3. Hely, M. A., Reid, W. G. J., Adena, M. A., Halliday, G. M. & Morris, J. G. L. The Sydney multicenter study of Parkinson's disease: The inevitability of dementia at 20 years. *Mov. Disord.* **23,** 837–844 (2008).
4. MAPPING CONNECTIONS AN UNDERSTANDING OF NEUROLOGICAL CONDITIONS IN CANADA. *Public Heal. Agency Canada Heatlth Canada* (2014).
5. Schrag, A., Sauerbier, A. & Chaudhuri, K. R. New clinical trials for nonmotor manifestations of Parkinson's disease. *Mov. Disord.* **30,** 1490–1504 (2015).
6. Twelves, D., Perkins, K. S. M. & Counsell, C. Systematic review of incidence studies of Parkinson's disease. *Mov. Disord.* **18,** 19–31 (2003).
7. Hirsch, L., Jette, N., Frolkis, A., Steeves, T. & Pringsheim, T. The Incidence of Parkinson's Disease: A Systematic Review and Meta-Analysis. *Neuroepidemiology* **46,** 292–300 (2016).
8. Dorsey, E. R. *et al.* Projected number of people with Parkinson disease in the most populous nations, 2005 through 2030. *Neurology* **68,** 384–386 (2007).
9. Wong, S., Gilmour, H. & Ramage-Morin, P. *Parkinson's disease: Prevalence, diagnosis and impact*. (2015).
10. The Burden of Neurological Diseases, Disorders and Injuries in Canada. *Can. Inst. Heal. Inf.* (2007).
11. Kim, W. S., Kågedal, K. & Halliday, G. M. Alpha-synuclein biology in Lewy body diseases. *Alzheimers. Res. Ther.* **6,** 73 (2014).
12. Goedert, M., Jakes, R. & Spillantini, M. G. The Synucleinopathies: Twenty Years On. *J. Parkinsons. Dis.* **7,** S51–S69 (2017).
13. Goedert, M. Alpha-synuclein and neurodegenerative diseases. *Nat. Rev. Neurosci.* **2,** 492–501 (2001).
14. *SNCA synuclein alpha [Homo sapiens (human)]*. *National Center for Biotechnology Information-Gene* (2017).
15. Emamzadeh, F. Alpha-synuclein structure, functions, and interactions. *J. Res. Med. Sci.* **21,** 29 (2016).
16. Bendor, J. T., Logan, T. P. & Edwards, R. H. The Function of α-Synuclein. *Neuron* **79,** 1044–1066 (2013).
17. Xilouri, M., Brekk, O. R. & Stefanis, L. α-Synuclein and protein degradation systems: a reciprocal relationship. *Mol. Neurobiol.* **47,** 537–51 (2013).

18. Jin, H. *et al.* α-Synuclein negatively regulates protein kinase Cδ expression to suppress apoptosis in dopaminergic neurons by reducing p300 histone acetyltransferase activity. *J. Neurosci.* **31,** 2035–51 (2011).

19. Geng, X. *et al.* -Synuclein binds the KATP channel at insulin-secretory granules and inhibits insulin secretion. *AJP Endocrinol. Metab.* **300,** E276–E286 (2011).

20. Martinez, J., Moeller, I., Erdjument-Bromage, H., Tempst, P. & Lauring, B. Parkinson's Disease-associated alpha -Synuclein Is a Calmodulin Substrate. *J. Biol. Chem.* **278,** 17379–17387 (2003).

21. Burré, J., Sharma, M. & Südhof, T. C. α-Synuclein assembles into higher-order multimers upon membrane binding to promote SNARE complex formation. *Proc. Natl. Acad. Sci.* **111,** E4274–E4283 (2014).

22. Scott, D. & Roy, S. -Synuclein Inhibits Intersynaptic Vesicle Mobility and Maintains Recycling-Pool Homeostasis. *J. Neurosci.* **32,** 10129–10135 (2012).

23. Peng, X. M. -Synuclein activation of protein phosphatase 2A reduces tyrosine hydroxylase phosphorylation in dopaminergic cells. *J. Cell Sci.* **118,** 3523–3530 (2005).

24. Witt, S. N. Molecular Chaperones, Alpha-Synuclein, and Neurodegeneration. *Mol. Neurobiol.* **47,** 552–560 (2013).

25. Ruipérez, V., Darios, F. & Davletov, B. Alpha-synuclein, lipids and Parkinson's disease. *Prog. Lipid Res.* **49,** 420–428 (2010).

26. Taneja, V., Verma, M. & Vats, A. Toxic species in amyloid disorders: Oligomers or mature fibrils. *Ann. Indian Acad. Neurol.* **18,** 138 (2015).

27. Halliday, G. M. & McCann, H. The progression of pathology in Parkinson's disease. *Ann. N. Y. Acad. Sci.* **1184,** 188–95 (2010).

28. Vekrellis, K., Xilouri, M., Emmanouilidou, E., Rideout, H. J. & Stefanis, L. Pathological roles of α-synuclein in neurological disorders. *Lancet Neurol.* **10,** 1015–1025 (2011).

29. Chermenina, M. *et al.* Single injection of small-molecule amyloid accelerator results in cell death of nigral dopamine neurons in mice. *npj Park. Dis.* **1,** 15024 (2015).

30. Chong, W., Jiménez, J., McIlvin, M., Saito, M. A. & Kwakye, G. F. α-Synuclein Enhances Cadmium Uptake and Neurotoxicity via Oxidative Stress and Caspase Activated Cell Death Mechanisms in a Dopaminergic Cell Model of Parkinson's Disease. *Neurotox. Res.* (2017). doi:10.1007/s12640-017-9725-x

31. Paillusson, S. *et al.* α-Synuclein binds to the ER-mitochondria tethering protein VAPB to disrupt Ca(2+) homeostasis and mitochondrial ATP production. *Acta Neuropathol.* (2017). doi:10.1007/s00401-017-1704-z

32. Chu, Y. & Kordower, J. H. Age-associated increases of alpha-synuclein in monkeys and humans are associated with nigrostriatal dopamine depletion: Is this the target for Parkinson's disease? *Neurobiol. Dis.* **25,** 134–49 (2007).

33. Lee, H.-J. *et al.* Dopamine promotes formation and secretion of non-fibrillar alpha-synuclein oligomers. *Exp. Mol. Med.* **43,** 216 (2011).

34. Mosharov, E. V. *et al.* Interplay between Cytosolic Dopamine, Calcium, and α-Synuclein Causes Selective Death of Substantia Nigra Neurons. *Neuron* **62,** 218–229 (2009).

35. Postuma, R. B. *et al.* MDS clinical diagnostic criteria for Parkinson's disease. *Mov. Disord.* **30,** 1591–1601 (2015).

36. Schmidauer, C. *et al.* Transcranial ultrasound shows nigral hypoechogenicity in restless legs syndrome. *Ann. Neurol.* **58,** 630–634 (2005).

37. Cenci, M. A. Presynaptic Mechanisms of l-DOPA-Induced Dyskinesia: The Findings, the Debate, and the Therapeutic Implications. *Front. Neurol.* **5,** (2014).

38. Poewe, W. & Antonini, A. Novel formulations and modes of delivery of levodopa. *Mov. Disord.* **30,** 114–120 (2015).

39. Ferreira, J. J. *et al.* Opicapone as an adjunct to levodopa in patients with Parkinson's disease and end-of-dose motor fluctuations: a randomised, double-blind, controlled trial. *Lancet. Neurol.* (2015). doi:10.1016/S1474-4422(15)00336-1

40. Schapira, A. H. V. Monoamine oxidase B inhibitors for the treatment of Parkinson's disease: a review of symptomatic and potential disease-modifying effects. *CNS Drugs* **25,** 1061–71 (2011).

41. Connolly, B. S. & Lang, A. E. Pharmacological Treatment of Parkinson Disease. *JAMA* **311,** 1670 (2014).

42. Voon, V., Mehta, A. R. & Hallett, M. Impulse control disorders in Parkinson's disease: recent advances. *Curr. Opin. Neurol.* **24,** 324–30 (2011).

43. Storch, A. *et al.* Nonmotor fluctuations in Parkinson disease: severity and correlation with motor complications. *Neurology* **80,** 800–9 (2013).

44. Fox, S. H. *et al.* The Movement Disorder Society Evidence-Based Medicine Review Update: Treatments for the motor symptoms of Parkinson's disease. *Mov. Disord.* **26,** S2–S41 (2011).

45. Deuschl, G. & Agid, Y. Subthalamic neurostimulation for Parkinson's disease with early fluctuations: balancing the risks and benefits. *Lancet Neurol.* **12,** 1025–1034 (2013).

46. Kefalopoulou, Z. *et al.* Long-term Clinical Outcome of Fetal Cell Transplantation for Parkinson Disease. *JAMA Neurol.* **71,** 83 (2014).

47. Grealish, S. *et al.* Human ESC-Derived Dopamine Neurons Show Similar Preclinical Efficacy and Potency to Fetal Neurons when Grafted in a Rat Model of Parkinson's Disease. *Cell Stem Cell* **15,** 653–665 (2014).

48. Schneeberger, A., Tierney, L. & Mandler, M. Active immunization therapies for Parkinson's disease and multiple system atrophy. *Mov. Disord.* **31,** 214–224 (2016).

49. Phase IB Follow-up Study to Assess a Second Boost Immunization With AFFITOPEÂ® PD01A in Those Who Participated in the AFF008 Program. *The Michael J. Fox Foundation - Funded Grants* (2015). Available at: https://www.michaeljfox.org/foundation/grant-detail.php?grant_id=1499.

50. Ascherio, A. & Schwarzschild, M. A. The epidemiology of Parkinson's disease: risk factors and prevention. *Lancet Neurol.* **15,** 1257–1272 (2016).

51. Ono, K., Hirohata, M. & Yamada, M. Anti-fibrillogenic and fibril-destabilizing activity of nicotine in

vitro: implications for the prevention and therapeutics of Lewy body diseases. *Exp. Neurol.* **205,** 414–24 (2007).

52. Ji, K. *et al.* Inhibition effects of tanshinone on the aggregation of α-synuclein. *Food Funct.* **7,** 409–16 (2016).

53. Gadad, B. S., Subramanya, P. K., Pullabhatla, S., Shantharam, I. S. & Rao, K. S. Curcumin-glucoside, a novel synthetic derivative of curcumin, inhibits α-synuclein oligomer formation: relevance to Parkinson's disease. *Curr. Pharm. Des.* **18,** 76–84 (2012).

54. Ono, K. *et al.* A chemical chaperone, sodium 4-phenylbutyric acid, attenuates the pathogenic potency in human alpha-synuclein A30P + A53T transgenic mice. *Parkinsonism Relat. Disord.* **15,** 649–54 (2009).

55. Sweeny, E. A. & Shorter, J. Mechanistic and Structural Insights into the Prion-Disaggregase Activity of Hsp104. *J. Mol. Biol.* **428,** 1870–85 (2016).

56. Jackrel, M. E. & Shorter, J. Reversing deleterious protein aggregation with re-engineered protein disaggregases. *Cell Cycle* **13,** 1379–83 (2014).

57. Qu, J. *et al.* Aptamer and its applications in neurodegenerative diseases. *Cell. Mol. Life Sci.* **74,** 683–695 (2017).

58. de Almeida, C. E. B., Alves, L. N., Rocha, H. F., Cabral-Neto, J. B. & Missailidis, S. Aptamer delivery of siRNA, radiopharmaceutics and chemotherapy agents in cancer. *Int. J. Pharm.* (2017). doi:10.1016/j.ijpharm.2017.03.086

59. Vieira, D. & Gamarra, L. Getting into the brain: liposome-based strategies for effective drug delivery across the blood–brain barrier. *Int. J. Nanomedicine* **Volume 11,** 5381–5414 (2016).

60. Keefe, A. D., Pai, S. & Ellington, A. Aptamers as therapeutics. *Nat. Rev. Drug Discov.* **9,** 537–550 (2010).

61. Bunka, D. H., Platonova, O. & Stockley, P. G. Development of aptamer therapeutics. *Curr. Opin. Pharmacol.* **10,** 557–562 (2010).

62. Jayasena, S. D. Aptamers: an emerging class of molecules that rival antibodies in diagnostics. *Clin. Chem.* **45,** 1628–50 (1999).

63. Lee, C. H. *et al.* Pharmacokinetics of a Cholesterol-conjugated Aptamer Against the Hepatitis C Virus (HCV) NS5B Protein. *Mol. Ther. - Nucleic Acids* **4,** e254 (2015).

64. Tsukakoshi, K., Harada, R., Sode, K. & Ikebukuro, K. Screening of DNA aptamer which binds to α-synuclein. *Biotechnol. Lett.* **32,** 643–648 (2010).

65. Tsukakoshi, K., Abe, K., Sode, K. & Ikebukuro, K. Selection of DNA Aptamers That Recognize α-Synuclein Oligomers Using a Competitive Screening Method. *Anal. Chem.* **84,** 5542–5547 (2012).

66. Liang, H. *et al.* Inhibition of BACE1 Activity by a DNA Aptamer in an Alzheimer's Disease Cell Model. *PLoS One* **10,** e0140733 (2015).

67. Rentmeister, A. RNA aptamers selectively modulate protein recruitment to the cytoplasmic domain of -secretase BACE1 in vitro. *RNA* **12,** 1650–1660 (2006).

68. Rahimi, F., Murakami, K., Summers, J. L., Chen, C.-H. B. & Bitan, G. RNA Aptamers Generated against Oligomeric Aβ40 Recognize Common Amyloid Aptatopes with Low Specificity but High Sensitivity. *PLoS One* **4,** e7694 (2009).

69. Rahimi, F. & Bitan, G. Selection of Aptamers for Amyloid β-Protein, the Causative Agent of Alzheimer's Disease. *J. Vis. Exp.* (2010). doi:10.3791/1955

70. Rhie, A. *et al.* Characterization of 2'-Fluoro-RNA Aptamers That Bind Preferentially to Disease-associated Conformations of Prion Protein and Inhibit Conversion. *J. Biol. Chem.* **278,** 39697–39705 (2003).

71. Skogen, M., Roth, J., Yerkes, S., Parekh-Olmedo, H. & Kmiec, E. Short G-rich oligonucleotides as a potential therapeutic for Huntington's Disease. *BMC Neurosci.* **7,** 65 (2006).

72. Hoinka, J., Dao, P. & Przytycka, T. M. AptaGUI-A Graphical User Interface for the Efficient Analysis of HT-SELEX Data. *Mol. Ther. Nucleic Acids* **4,** e257 (2015).

73. Hoinka, J., Berezhnoy, A., Sauna, Z. E., Gilboa, E. & Przytycka, T. M. AptaCluster - A Method to Cluster HT-SELEX Aptamer Pools and Lessons from its Application. *Res. Comput. Mol. Biol. ... Annu. Int. Conf. RECOMB ... proceedings. RECOMB (Conference 2005-)* **8394,** 115–128 (2014).

74. Bartels, T., Choi, J. G. & Selkoe, D. J. α-Synuclein occurs physiologically as a helically folded tetramer that resists aggregation. *Nature* **477,** 107–10 (2011).

75. Tsigelny, I. F., Sharikov, Y., Miller, M. A. & Masliah, E. Mechanism of alpha-synuclein oligomerization and membrane interaction: theoretical approach to unstructured proteins studies. *Nanomedicine Nanotechnology, Biol. Med.* **4,** 350–357 (2008).

76. An Introduction to Next-Generation Sequencing Technology. *Illumina-Marketing* (2016). Available at: https://www.illumina.com/content/dam/illumina-marketing/documents/products/illumina_sequencing_introduction.pdf.

77. Gopinath, S. C. B. Methods developed for SELEX. *Anal. Bioanal. Chem.* **387,** 171–182 (2006).

78. Hoffman, M. M. AANT: the Amino Acid-Nucleotide Interaction Database. *Nucleic Acids Res.* **32,** 174D–181 (2004).

79. O. Tucker, W., T. Shum, K. & A. Tanner, J. G-quadruplex DNA Aptamers and their Ligands: Structure, Function and Application. *Curr. Pharm. Des.* **18,** 2014–2026 (2012).

80. Murphy, M. P. & LeVine, H. Alzheimer's disease and the amyloid-beta peptide. *J. Alzheimers. Dis.* **19,** 311–23 (2010).

81. Mann, Brown, Owen, Baba & Iwatsubo. Amyloid beta protein (Abeta) deposition in dementia with Lewy bodies: predominance of Abeta42(43) and paucity of Abeta40 compared with sporadic Alzheimer's disease. *Neuropathol. Appl. Neurobiol.* **24,** 187–194 (1998).

Appendices

Appendix A

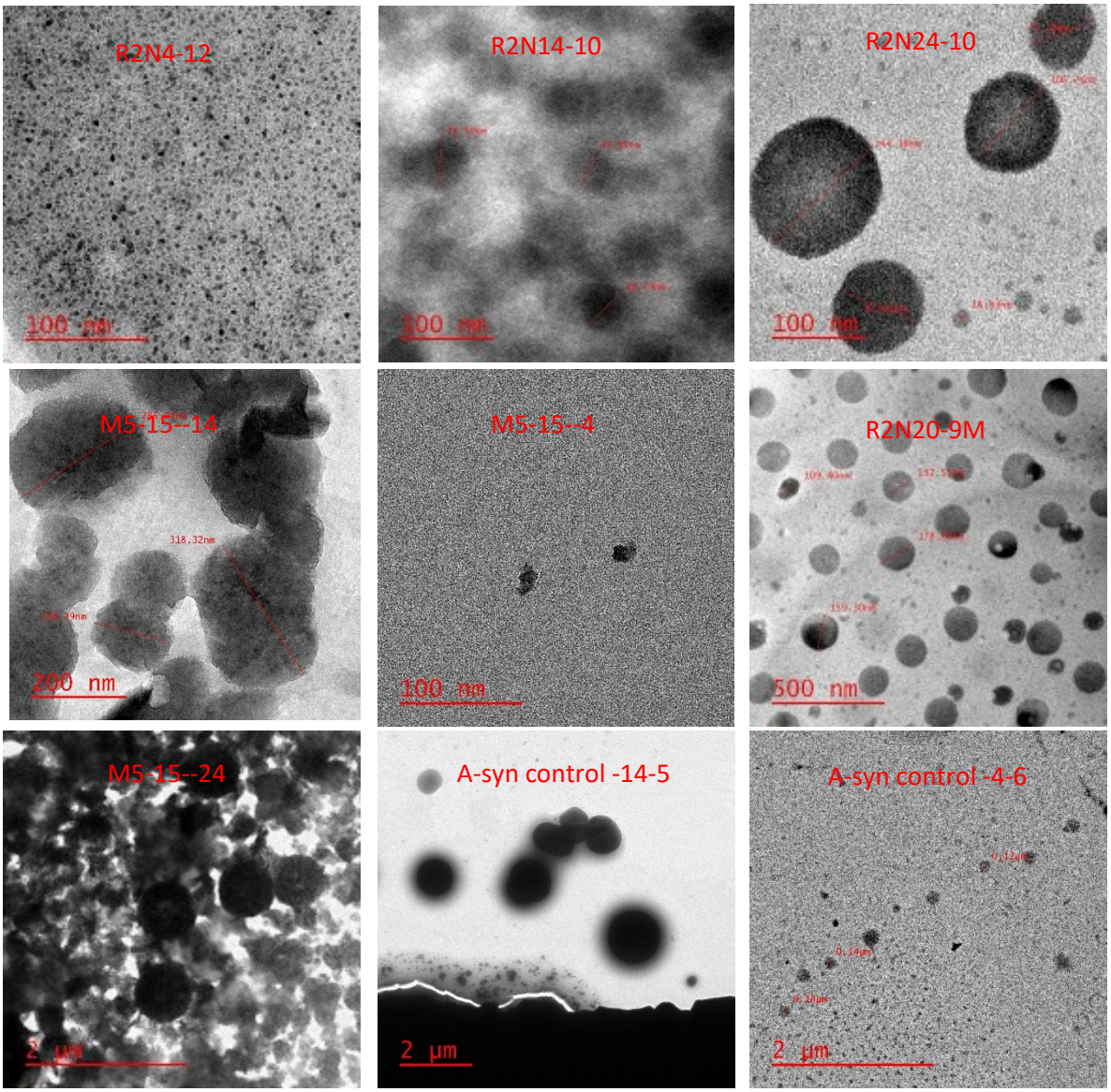

Figure 32 Continued…

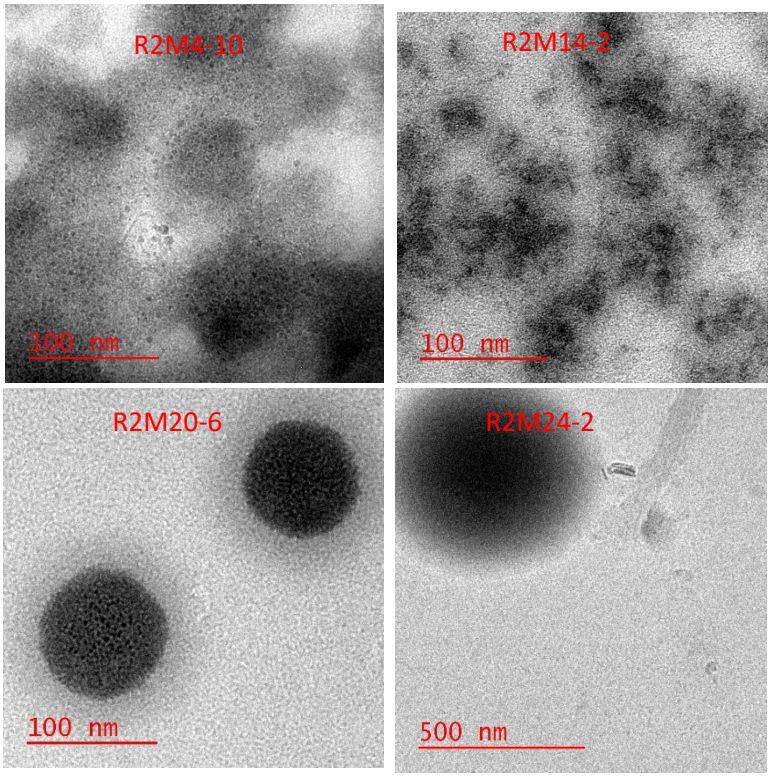

Figure 32. Extra TEM images for select density gradient fractions from SELEX round 2 and the M5-15 aggregation inhibition test run in parallel. Selected images are representative of the image lots from which they are drawn. Each sample had some degree of anomaly. Larger fractions often yielded some small amount of smaller morphologies, likely due to fragmentation.

Appendix B

Table 15. Raw counts generated by Illumina MiSEQ, compiled by Aptacluster, and sorted by AptaGUI.

** Denotes results generated by the original MiSeq of SELEX round 4 which yielded insufficient and unbalanced reads.*

Given Name	AptaGUI Name	R5 Positive Count	R5 Counter Count	R5 Negative (Negative) Count	R5 Negative (Positive) Count
ASYN1	1LBiGJFJC	11	0	3	0
ASYN2	1LBwAAjJ	8	0	2	9
ASYN3	GdJUhE	8	1	2	2
ASYN4	LTmUII	7	0	1	2
ASYN5	JUeRc	5	3	4	9

		R4 Positive Count	R4 Positive Count*	R5 Negative (Positive) Count	R5 Negative (Positive) Count*	R4 Counter Count	R4 Counter Count*
ASYN1	1LBiGJFJC	2	0	1	0	2	0
ASYN2	1LBwAAjJ	1	2	1	0	0	0
ASYN3	GdJUhE	2	1	1	0	2	0
ASYN4	LTmUII	3	0	2	0	0	0
ASYN5	JUeRc	2	0	3	0	1	0

		R2 Positive Count	R2 Positive Count*	R0 Count	R0 Count*
ASYN1	1LBiGJFJC	0	0	0	0
ASYN2	1LBwAAjJ	0	0	0	0
ASYN3	GdJUhE	0	0	0	0
ASYN4	LTmUII	2	0	0	0
ASYN5	JUeRc	2	0	0	0